Optimization Based Control and Estimation in Fed-Batch Processes

by

Javad Abdollahi

A thesis submitted in partial fulfillment of the requirements for the degree of

Doctor of Philosophy

in

Process Control

Department of Chemical and Materials Engineering

University of Alberta

Abstract

There are varieties of time-varying processes in chemical engineering industrial applications. These processes are abundant among lumped and distributed parameter systems and in batch systems they involve time-dependent change of parameters and/or geometry within lumped and/or distributed parameter systems settings. The focus of this thesis is on optimal state estimation and tracking regulation of two fed-batch processes with time-varying parameters and geometry. The first process is nonlinear time-varying microalgae growth and lipid production. An optimal reference trajectory is identified for maximum lipid production and moving horizon estimator along with model predictive control is realized for reference trajectory tracking of lipid production model. The second process is Czochralski crystal growth process which has moving boundary parabolic partial deferential equation describing heat transfer as dynamic model coupled with a lumped parameter model of pulling dynamics. Galerkin's method is used to reduce the distributed parameter model's order and an observer is developed to reconstruct temperature distribution evolution over the entire crystal domain during growth process. The performance of the observer is examined by implementing the observer on finite element model of the heat transfer in crystal. Furthermore, finite element model of the heat transfer along with finite element model of anisotropic thermal stresses in growing crystal are utilized to identify

an optimal trajectory and develop a model predictive reference trajectory tracking controller for temperature distribution in the Czochralski crystal growth process to maximize the crystal cooling while maintaining the thermally induced stresses below the critical value in order to improve the quality of the grown crystal.

Preface

Chapter 2 of this work is published as Abdollahi, J., Dubljevic, S., 2012. "Lipid production optimization and optimal control of heterotrophic microalgae fed-batch bioreactor", *Chemical Engineering Science* 84, 619-627". Stevan Dubljevic was the supervisory author and was involved with concept formation and manuscript composition.

Chapter 3 of this work is published as Abdollahi, J., Izadi, M., Dubljevic, S., 2014. "Temperature distribution reconstruction in Czochralski crystal growth process" *AIChE Journal*, DOI 10.1002/aic.14486. Mojtaba Izadi assisted with finite element analysis and Stevan Dubljevic was the supervisory author and was involved with concept formation and manuscript composition.

Chapter 4 of this work is submitted for publication as Abdollahi, J., Izadi M., Dubljevic, S., "Model predictive temperature tracking in Czochralski crystal growth process", *Computers and Chemical Engineering*. Mojtaba Izadi assisted with finite element analysis and Stevan Dubljevic was the supervisory author and was involved with concept formation and manuscript composition.

To my parents, for their love, encouragement and support.

Acknowledgements

I would like to express my special appreciation and thanks to my advisor Dr. Stevan Dubljevic for his appreciable inspiration and support during my PhD studies. I would not have been able to complete my research work without your guidance, support and helpful suggestions. Working under your supervision equipped me with skills that prepared me for my future life and career. I would like to express my gratitude to all those who help me in completion of this thesis. Especially, I would like to acknowledge my fellow graduate students in Distributed Parameter Systems Lab (DPS Lab) for their support and friendship. For last but not least, I would like to convey my gratitude to my mother and father for their continued, endless and unconditional support throughout of my life. This list would be deficient without expressing my deepest, heartfelt appreciation to my brothers.

Contents

List of Tables

List of Figures

Chapter 1

Introduction

1.1 Introduction

Batch processes are abundant in chemical engineering industry and are widely applied in modern industries to produce a large quantity of products with high consistency. Generally, a batch process is defined as a process that leads to the production of finite quantities of material by subjecting quantities of input materials to an ordered set of processing activities over a finite period of time using one or more pieces of equipment (Instrument Society of America, 1995). In batch process, due to cycle to cycle (non-continuous) operations, finite operation time and sensitivity to initial conditions and disturbances, there are fundamental control tasks to be accomplished such as to identify the optimal/desired set-point/trajectory, realize perfect tracking of the desired trajectory in each cycle, robustly track the desired trajectory as close as possible in the presence of uncertainties and comply with the process input and output constraints for implementation.

In most of the processes in industry, the dynamic models are assumed to be time-invariant and/or modeled by lumped parameters. However, neglecting time-varying and spatially distributed parameters in process models can decrease the modelling

accuracy and, consequently, the estimation and control efficiency. There are abundant processes in industry that can not be modelled as time-invariant and/or lumped parameter models and require different methodology rather than conventional methods to overcome the control and estimation challenges. This work provided strategies for control and estimation in two different categories of such processes.

Optimization, monitoring and controlling of industrial processes with time-varying parameters has recently gained increasing interest. Such processes exist in many industrial applications and cannot be handled by conventional control theory methods. This research is focused on developing a plausible framework to optimize, monitor and control the processes with time-varying parameters. Two specific applications are investigated and discussed, bio-fuel production from microalgae, and quality assurance of the single crystal production. The microalgae growth and bio-fuel production is governed by a nonlinear and time-varying model, where the crystal growth and temperature distribution model is a distributed parameter system with time-varying domain and parameters.

The first application is optimization and control of microalgae bioreactor. The motivation for extracting bio-fuel from microalgae is to find a sustainable and reliable replacement for the conventional fuels; however, due to the low production rate, bio-fuel produced from microalgae is not economically feasible. Optimal control of microalgae bioreactor is one of the large number of option to overcome the low lipid production rate, which can result in economic feasibility of microalgae bio-fuel production process. The process can be optimized by scheduling the nutrient feeding into the microalgae bioreactor. An optimal feeding strategy can be provided to maximize bio-fuel production from microalgae. The optimal strategy is enriched by monitoring and controlling strategies to ensure the performance of the bioreactor in realistic op-

erating conditions.

Off-line optimization and on-line Model Predictive Control (MPC) implementation are used to maximize and regulate lipid production in a fed-batch heterotrophic microalgae cultivation of *Auxenochlorella* protothecoides. A complex time-varying microalgae fed-batch growth and lipid production model, taken from De la Hoz Siegler et al. (2011), is used and a large-scale nonlinear programming optimization along with moving horizon estimator and model predictive control are applied to maximize, monitor and maintain the lipid concentration in the bioreactor. An optimal feeding strategy for lipid production is determined using the state-of-the-art interior point optimizer (IPOPT) solver. Moving horizon estimator (MHE) and MPC are used to estimate unmeasurable state (nitrogen concentration) and provide regulation of a highly nonlinear and time-varying microalgae growth process as a realizable real-time control strategy. In addition to the constrained large-scale optimization, naturally present input constraints (lower and upper bound on feed rates) and state constraints (lower bound on all concentration related states and upper bound on glucose concentration) are accounted for in explicit manner with moving horizon estimator and model predictive controller. The estimator and controller design is based on a set of linearized models in microalgae growth fed-batch process. A reliable and computationally efficient optimization, estimation and regulation procedure suitable for the real-time microalgae bioreactor operation is provided which accounts for constraints and measurement noises present in the realistic operation conditions (Abdollahi and Dubljevic, 2012).

The second application considered in thesis is silicon single crystal production by Czochralski process. Single crystals have unique mechanical, physical and electrical properties that justify their high demand in microelectronics and optoelectron-

ics(Sinno and Brown, 1999; Sinno et al., 2000). Temperature distribution in the crystal during the crystallization is the most important factor in dislocation density distribution and magnitude and residual stresses in the crystal which can alter the crystal's quality and physical properties significantly (Sinno et al., 2000; Gevelber, 1994). To assure the quality of the crystal, a potential solution is to maintain the temperature gradients and thermal stresses at a desirable level. The spatial temperature distribution, heat transfer between the solid-liquid interface, the coupled growth dynamics, time-varying domain and time-varying parameters make the existing control strategies inapplicable. On the other hand, the temperature distribution over the crystal domain is not directly measurable and a temperature distribution estimation is required for monitoring purposes and utilization of a full state feedback controller.

The coupled growth dynamics and heat transfer equations are derived and reduced to a low dimensional model (Abdollahi et al., 2014). A mechanical geometric crystal growth model is developed to describe the crystal length and radius evolution and a controller is synthesized by output-input linearization of the model to regulate and track crystal radius. This controller accounts for parametric uncertainty in the crystal growth rate. The associated parabolic PDE model of heat conduction is considered over the time-varying crystal domain and coupled with crystal growth dynamics. An infinite-dimensional representation of the thermal evolution is derived considering slow time-varying process effects and computational framework of the Galerkin's method is used for parabolic PDE order reduction and observer synthesis for temperature distribution reconstruction over the entire crystal domain. The proposed low-order observer is utilized to reconstruct temperature distribution from boundary temperature measurements. A finite element model of the process is developed to study the performance of the observer developed with geometric uncertainties

in the model.

After developing an estimation strategy for temperature distribution evolution, a model predictive temperature tracking control strategy is provided to track the reference trajectory. The controller is developed in order to maximize crystal cooling while maintaining the thermally induced stresses at a desirable level. The similar approach is taken as for the microalgae bioreactor control. An optimal trajectory is identified by off-line optimization and considering the constraints on temperature gradients and thermal stresses to avoid dislocation generation in crystal. Then the reference trajectory is used to implement model predictive tracking control in order to follow the desirable temperature distribution evolution. Finite element model of temperature distribution is used for model reduction and directly used as the temperature evolution model. Another finite element model is utilized to model the thermal stresses in the crystal, which is used to explicitly develop the constraints on thermal stresses during the crystallization process.

The organization of the thesis is as following: after the Introduction, optimization, control and estimation in microalgae bioreactor is provided in Chapter 2. Chapter 3 focuses on temperature distribution estimation in Czochralski crystal growth process and is followed by model predictive temperature distribution tracking of Czochralski crystal growth process in Chapter 4. Finally, Chapter 5 concludes the thesis and provides some ideas about possible future contributions.

1.2 References

Abdollahi, J., Dubljevic, S., 2012. Lipid production optimization and optimal control of heterotrophic microalgae fed-batch bioreactor. Chemical Engineering Sciencel 84, 619–627.

Abdollahi, J., Izadi, M., Dubljevic, S., 2014. Temperature distribution reconstruction in czochralski crystal growth process. AIChE Journal DOI 10.1002/aic.14486.

De la Hoz Siegler, H., Ben-Zvi, A., Burrell, R.E., Mccaffrey, W.C., 2011. The dynamics of heterotrophic algal cultures. Bioresource technology 102, 5764–5774.

Gevelber, M., 1994. Dynamics and control of the Czochralski process III. interface dynamics and control requirements. Journal of Crystal Growth 139, 271–285.

Instrument Society of America, 1995. Batch control. Part 1, models and terminology. ISA, Research Triangle Park.

Sinno, T., Brown, R., 1999. Modeling microdefect formation in Czochralski silicon. Journal of Electrochemical Society 146, 2300–2312.

Sinno, T., Dornberger, E., von Ammon, W., Brown, R., Dupret, F., 2000. Defect engineering of Czochralski single-crystal silicon. Materials Science and Engineering: R: Reports 28, 149 – 198.

Chapter 2

Lipid Production Optimization and Optimal Control of Heterotrophic Microalgae Fed-Batch Bioreactor

2.1 Introduction

Economic and population growth have steadily increased the global energy demand. It is expected that the world will need almost 60% more energy, if current policies for energy management are held (Patil et al., 2008). Due to finite resources of fossil fuels and the impact of their consumption on environment, they do not make sustainable and reliable sources of energy any longer (Chisti, 2007; Hoffert et al., 2002; Khan et al., 2009). Therefore, there is a need for development of new energy sources such as biofuels that are renewable and environmentally sustainable. Currently, biodiesel and bio-ethanol are produced on a large industrial scale. They are replacements for petroleum for internal combustion engines, and are derived from food crops, which results in food-fuel conflict (Patil et al., 2008). On the other hand, biomass resources in many cases require appropriate compensation (e.g. replanting), otherwise their use may give rise to a massive biomass deficit and serious environmental problems (e.g.

deforestation) (Patil et al., 2008).

In order to deal with the mentioned issues, one solution is to use heterotrophic microalgae as a substitute for the crops and other feedstock and consequently the produced biofuel can be used instead of traditional fuels. Heterotrophic microalgae cultivation requires less water and land compared to phototrophic microalgae, crops and other feedstock, it is productive throughout the year and is characterized by a high growth rate (Hoffert et al., 2002). However, biofuel production from microalgae is not commercially viable due to low performance of bioreactors.

In order to achieve good performance and efficiency, bioreactors require advanced regulation procedures to ensure performance and efficiency of bioprocesses. In general, a biological process is a network of complex biochemical reactions manipulated by enzymes (Mailleret et al., 2004; Farza et al., 1997). In fact, such kinetic networks give rise to highly complex and nonlinear dynamics of enzymes, nutrients and product concentrations in bioreactors. Modelling these dynamics with few states and parameters is a challenging task which may provide a relevant reduced order model of the process with usually time-varying and uncertain parameters. In addition to model uncertainties arising from complex biosystem dynamics, accurate and fast biochemical sensors are limited and difficult to realize in practice, which makes optimal bioreactor operation a challenging task. Therefore, in order to cope with such a complex biosystem, it is necessary to obtain sufficiently accurate and reliable information about the states and systems parameters to come to efficient monitoring and regulation (Farza et al., 1997).

State and parameter estimation methods are well developed techniques in the process system science whose purpose is to handle unknown states and uncertainties in a model. There are several studies confirming that parameter and state estimation

using linear and extended Kalman filter (EKF) fails or shows weak performance for the biological systems (Bastin and Dochain, 1990; Gonzalez et al., 2001; Selisteanu et al., 2007). Hence, using nonlinear observers for the state and parameter estimation of bioreactors has been successful and attracted much attention in recent years (Alcaraz-Gonzlez et al., 2005; Farza et al., 1998). In Alcaraz-Gonzlez et al. (2005), the state estimation scheme is designed based on an asymptotic observer with a tuneable convergence rate. This robust observer is verified numerically by simulation on the waste water treatment model. Farza et al. (1998) studied kinetic rates estimation in bioreactors and provided a theoretical framework for the kinetic rate estimation in bioreactors. Along the same line, Zhang and Guay (2002) used an adaptive nonlinear observer to estimate states and parameters of a microbial growth model. They used Lyapunov stability techniques and verified their approach by numerical simulations.

On the other hand, with respect to control synthesis, predictive control methodologies can be used with state estimation to solve the control problem while handling the governing constraints. Sendrescu et al. (2011), El Bahja et al. (2009) and Tebbani et al. (2010) used nonlinear model predictive control (NMPC) for state regulation. Sendrescu et al. (2011) used NMPC to regulate sates in a nonlinear bioprocess with known states and with no constraints present. Nonlinear model predictive control is used for unconstrained state regulation in a lipase production bioprocess, while states are estimated using Kalman Filter (El Bahja et al., 2009). Tebbani et al. (2010) converted a constrained bioprocess control problem to an unconstrained nonlinear programming, and solved the constrained control problem to maximize cultures of Escherichia coli.

One of the strategies to ensure that the efficiency of lipid production is guaranteed is to force the microalgae states to track a reliable predefined reference trajectory.

Using the growth model, the states and inputs evolution can be determined such that the maximum lipid density is achieved. Calculation of the optimal trajectory is a difficult task due to complexity of the model, constrained states and inputs and also due to the time scale of the optimization problem. For example, the lipid production optimization problem has been handled empirically by Hsieh and Wu (2009) and Doucha and Lvansky (2012) to find a strategy to maximize cell density based on experimental results. Wu and Shi (2007) optimized the cell density using a hybrid neural network model.

There are three main approaches for nonlinear constrained optimization. Sequential quadratic programming (SQP), Interior point and nested projection methods (Biegler, 2010). SQP algorithms are based on extension of Newton's method to quadratic problems and the computational expense of solution is limited to the quadratic problems solution. Active set selection and linear algebra used to solve KKT conditions determine the computational efficiency of the algorithm. These algorithms use few functions and derivative evaluations, but in the case of large-scale programs and large number of constraints they are computationally expensive due to necessity to choose an active set. Interior point or barrier methods are also based on the Newton's method but they do not use the active set and they deal with relaxed KKT conditions; therefore they can be used to handle large-scale programs. Nested projection methods are more efficient in the case of highly nonlinear objective function and constraints. They do not solve KKT conditions simultaneously, but decompose the problem and then use Newton's type methods, and as consequence they require more function evaluations (Biegler, 2010).

The Interior Point Optimizer (IPOPT) developed by Wachter and Biegler (2006), is a large-scale optimization solver for constrained nonlinear programs and can be

applied to the lipid production model. The solution provided by the IPOPT might not achieve global optimum solution. Theoretically, the solution for the IPOPT solver is not global, and there is also a proven example (Wachter and Biegler, 2000) that the interior point method fails to globally converge. However, practically, searching within an active set enforced by constraints, the possibility to achieve a global solution is more likely. In addition, multiple runs with different initial guesses over the search domain is helpful to avoid local optimums. IPOPT is used to optimize bioprocesses, for example Estrada et al. (2009) used IPOPT to solve a large-scale nonlinear program of algae growth in the water reservoir, and IPOPT is also used for optimal management of the water treatment bioreactor by Alvarez-Vzquez et al. (2010).

In this chapter, microalgae growth and lipid production model are used in a large-scale nonlinear programming format to obtain optimal feeding strategy and consequent state trajectories in the presence of physically relevant constraints. The large-scale constrained optimization solution realized by IPOPT uses perfect model and yields desired optimal input evolutions. However, the optimization can not account for the influence of possible disturbances in the feeds or bioreactor conditions, so that the obtained reference trajectory provides a desired state evolution to form a sequence of locally reduced and linearized models to synthesize control and estimation strategy for the regulation of lipid production rate. Subsequent linear time invariant models are used by the constrained moving horizon estimator (MHE) to construct full states of the process, since some of the states are not available for direct measurements (nitrogen concentration). With the real-time knowledge of the states, model predictive reference trajectory tracking is implemented to maintain optimal performance of the process.

This chapter is based on the experimental work of De la Hoz Siegler et al. (2012).

The contribution of the present chapter focuses on the predetermined optimal trajectory, simplicity for scaled-up implementation and also on handling constraints in estimation, control and optimization procedure. Tracking the predetermined optimal reference trajectory is a reliable way to maximize lipid concentration in a bioreactor, which maintains the efficiency of a single bioreactor at a desired level, and can be applied to different bioreactors to achieve the same properties of lipid. Using linear models for control and estimation guarantees the convexity of optimization in model predictive control, and therefore reduces the computational effort. In addition, linear models employed in algorithm simplify the algorithm implementation and realization on embedded controllers. Moreover, model predictive techniques used for control and estimation can handle constraints on inputs and states in explicit manner which is not common in conventional control algorithms.

In the ensuing sections we provide a description of the microalgae bioreactor model, with the microalgae mathematical model. The following three sections deal with feeding strategy optimization, formulation of moving horizon estimator (MHE) for the state estimation, and model predictive controller (MPC) for the reference trajectory tracking. Finally, we provide simulation results and biological interpretation of the results with the emphasis on possible presence of noise in the process regulation.

2.2 Microalgae growth and lipid production model

Microalgae growth takes place in a bioreactor vessel where microalgae cells grow in the presence of required nutrients and essential substances. Depending on the feeding strategy, different pathways of the growth and lipid production can be achieved by microalgae species (De la Hoz Siegler et al., 2011). These growth and lipid production pathways are governed by biochemical reactions in the microalgae cells. Detailed

modelling of all these reactions is not a feasible task at the moment. The most common approach to derive a mathematical model is to use a few most effective variables in the process. The mathematical model is based on the material balance applied to the bioreactor and is given in Eqs.2.1-2.6. The model parameters are identified using experimental data in De la Hoz Siegler et al. (2011):

$$\frac{dS_1}{dt} = -\rho x + s_1^i \frac{f_1^i}{V} - S_1 D \tag{2.1}$$

$$\frac{dS_2}{dt} = -\frac{1}{Y_{x/s}}\mu x - \frac{1}{Y_{p/s}}\pi x - k_m x + s_2^i \frac{f_2^i}{V} - S_2 D \tag{2.2}$$

$$\frac{dx}{dt} = \mu x - xD \tag{2.3}$$

$$\frac{dp}{dt} = \pi x - \frac{1}{Y_{x/p}}\mu x - pD \tag{2.4}$$

$$\frac{dq}{dt} = \rho x - \frac{1}{Y_{x/q}}\mu x - qD \tag{2.5}$$

$$\frac{dV}{dt} = VD - f^o \tag{2.6}$$

This model, given by Eqs.2.1-2.6, represents the heterotrophic growth and lipid production of *Auxenochlorella* protothecoides. The model is based on the assumption that algae cells are composed of three components, active biomass (x), lipid content (p), and nitrogen content (q). These three components can transfer to each other with constant rates ($Y_{i/j}$). Another important variable is glucose concentration (S_2), which is used to support cell growth and lipid production, while nitrogen (S_1) is taken into the cells and supports cell growth. μ is the growth rate, π is the lipid production rate and ρ is the nitrogen uptake rate into the cells, while s_1^i and s_2^i are the concentrations of nutrients in feeds, V is the volume of the bioreactor, while D is reserved for the dilution rate which is equal to $D = (f_1^i + f_2^i)/V$ and k_m is the maintenance factor. f_1^i and f_2^i are the feed rates of glycine and glucose as the sources of nitrogen and

glucose, respectively. These nutrient feed rates are available control inputs applied to the fed-batch process model. There is also an outflow (f^0) which is only used for the measurements and monitoring purposes.

Nonlinearities in the model description arise from the algae growth and nutrient consumption rate functions. The rate functions (μ, π, ρ) depend on the states of the system, which are given below:

$$\mu = \mu_m \frac{S_2}{K_\mu + S_2 + \frac{S_2^2}{K_{i2}}} \frac{\tilde{q}}{K_{\tilde{q}} + \tilde{q}} exp(-\frac{\frac{1}{t}\int_0^t \tilde{q} dt}{K_{i1}}) \tag{2.7}$$

$$\pi = \pi_m \frac{S_2}{K_\pi + S_2}(1 - \tilde{p}) \tag{2.8}$$

$$\rho = \rho_m \frac{S_1}{K_\rho + S_1} \tag{2.9}$$

where $\tilde{q}$ and $\tilde{p}$ are the mass fraction of nitrogen and lipid in the cells, respectively ($\tilde{q} = q/(x+p+q)$, $\tilde{p} = p(x+p+q)$). As it can be seen in Eq.2.7, the growth rate depends on glucose concentrations (S_2) and nitrogen content in the cells. This dependency is described as multiplication of Michaelis-Menten kinetics for glucose and nitrogen sources. The growth rate also depends on the history of nitrogen content in the cells. Lipid production and nitrogen uptake rates are also assumed to obey Michaelis-Menten kinetics. The parameters of the microalgae model are shown in Table 2.1. In the experimental realization of a microalgae bioreactor, which is done by Nadadoor et al. (2012), the same states are measured using laser Raman spectroscopy.

In general, the states of the growth model can be measured offline, while for the real-time online measurements, Raman spectroscopy can be utilized. In the microalgae bioreactor used in this chapter, the nitrogen concentration (S_1) in the bioreactor can not be detected directly by the Raman spectroscopy method and should be esti-

Table 2.1: Microalgae growth and lipid production model parameters

Parameter	Value	Unit
$Y_{x/s}$	0.55	-
$Y_{p/s}$	0.34	-
$Y_{x/q}$	56.67	-
$Y_{x/p}$	11.84	-
k_m	0.19	1/d
μ_m	14.18	1/d
K_μ	8.45	g/L
$K_{\tilde{q}}$	0.0041	-
ρ_m	0.93	1/d
K_ρ	0.14	g/L
π_m	0.50	1/d
K_π	0.09	g/L
K_{i2}	49.50	g/L
K_{i1}	0.016	-

mated on the basis of reliable real-time measurements for further regulation purposes.

2.3 Optimization, Estimation and Control methods

The main objective of this chapter is to demonstrate reliable lipid production maximization in the microalgae bioreactor by application of advanced optimization, estimation and control techniques. In general, the control strategy implementation requires both full knowledge of the state trough measurement or estimation, and a reliable reference trajectory. In this chapter, the reference trajectory is obtained by using the interior point optimizer (IPOPT), and the states are estimated using a moving horizon estimator; then, with full states available, a model predictive control based strategy is used to track a desired reference trajectory. As linear MPC and MHE are used, reliable linear models are required which are achieved by subsequent

process model linearization.

2.3.1 Feeding Strategy Optimization

Microalgae lipid concentration in the bioreactor can be manipulated by determining nutrient feed rates. Glucose and glycine feed rate profiles determine the growth and lipid production trajectories. In order to obtain an optimal trajectory in the sense of lipid production, the IPOPT optimization method is used to maximize lipid concentration in the bioreactor by manipulating nutrient input rates. The process dynamic is highly nonlinear and there are constraints on the states, process inputs and final bioreactor volume which induce model complexity that can be handled only by large-scale nonlinear optimization programs. In order to handle the nonlinearity and complexity of the model, the process model and the underlying optimization problem is formulated on the basis of the model given by Eqs.2.1-2.9 as a nonlinear program. The total process time is eight days and time discretization is accurate enough, with sampling time of 30 minutes and the total process time of eight days that induces 768 manipulating parameters in the program. In addition, the process discretization in time will produce over 6000 equality and inequality constraints. Therefore, the optimization problem is transformed to a large-scale nonlinear program with over 6000 constraints. Due to significant complexity, conventional numerical algorithms are not able to solve a large-scale nonlinear program with enough accuracy and within a reasonable time period, and cannot to be implemented in the on-line autonomous control and monitoring. The nonlinear program is formulated in Eqs.2.10-2.13 as

follows:

$$\xi^{k+1} = \xi^k + hf(\xi^k, u^k) \tag{2.10}$$

$$0 \leqslant u^k \leqslant u_{max} \tag{2.11}$$

$$0 \leqslant \xi^k \leqslant \xi_{max} \tag{2.12}$$

$$V^{t_f} = 2 \tag{2.13}$$

where $\xi = [S_1, S_2, x, p, q, V]$ is the state vector and ξ^k is the state vector at time k. The dynamic model of microalgae is realized with equality constraints given by Eqs.2.10-2.13 and inequality constraints given by Eqs.2.11-2.12, which yields nonlinear program to be solved. Table 2.2 shows the constraints used in the optimization of lipid production. Due to the model structure, Eqs.2.1-2.6, negative inputs are manifested as an increase in the lipid and biomass concentration, which means that the constraints on the inputs are necessary and will be active in the lipid production optimization by IPOPT. The other active constraint is the volume of the bioreactor which is finite. The maximum volume should not exceed 2 litres. In addition, there is also a constraint on the maximum nutrient concentration to prevent dehydration of the microalgae cells. Finally, the large-scale nonlinear program is solved using AMPL as interface and by utilization of the IPOPT solver. The resulted input feeds and state trajectories are used as reference state trajectories for the subsequent control and estimator design.

2.3.2 Model Linearization

Handling a nonlinear and time-varying system by successive approximations yielding linear models requires taking account of the physical process time relevant scales and

Table 2.2: List of constraints

Variable	Lower bound	Upper bound	Unit
Glucose concentration (S_2)	0	50	g/L
Nitrogen feed rate (f_1^i)	0	2	mL/h
Glucose feed rate (f_2^i)	0	10	mL/h
Nitrogen feed rate change (Δf_1^i)	-0.2	0.2	mL/h
Glucose feed rate change (Δf_2^i)	-1	1	mL/h
Bioreactor volume (V_{max})	-	2	$litres$

adequate and computationally reliable procedure that can be applied robustly in real-time. In particular, the microalgae process can not be approximated by a single linear model, as the single linearized model is not able to predict the system's behaviour through the entire bioreactor single cycle run. In this chapter we generate a set of linearized models along the optimal trajectories obtained by the IPOPT large-scale optimization. The algorithm linearizes the mathematical model based on the states at the current time along the reference state trajectory, so that MPC and MHE are designed based on these local linear models. Local linear models are obtained by replacing the time-varying integral term in Eq.2.7 by a constant parameter. This integral term depends only on the measurable states and it is numerically calculated by replacing a constant parameter, given by Eq.2.14, at each instance of the linearization process. Therefore we have:

$$\frac{1}{t}\int_0^t \tilde{q}(t)dt = \frac{1}{kT}\sum_{j=1}^{k} \tilde{q}(j)T \tag{2.14}$$

Linearized models are accurate enough for 40 sampling times and therefore, to reduce computational effort, local linear models are used for about 2 hours of the process time.

2.3.3 Moving Horizon Estimator (MHE)

Due to necessity to utilize the entire knowledge of the state in the regulation achieved by model predictive control algorithm, non measured bioreactor system's states (nitrogen concentration) need to be estimated accurately enough. One of suitable observers (estimators) in the presence of input and state constraints is a moving horizon estimator (MHE). As it can be inferred from the mathematical model Eqs.2.1-2.6, the origin is a single stable equilibrium of the dynamical model, and the states can not take negative values was this is imposed by a physical condition that the concentrations can not be negative. These physical restrictions associated with the model are manifested as restrictions on the states and inputs allowed signs specified in the observer design. In addition, the limit on glucose concentration available in the feed stream, which is considered as an input constraint, encourages the usage of an observer which can handle constraints.

State estimation by the moving horizon estimator is based on an idea similar to the synthesis of model predictive control. In the moving horizon state estimation approach, the state is estimated by solving an optimization problem in an iterative manner over the moving time horizon. In comparison with the model predictive controller, where future deviations of predictions from the reference value are minimized, the MHE minimizes past deviations of the trajectory from the output measured values. The MHE estimates all states and accounts for the noise in previous N steps (estimation horizon) by optimization based on online available measurements. At each step, previous states and noises will be reconstructed such that the error between the measured outputs and model predictions is minimized. Supposing that there is an initial guess about the states ($\bar{\xi}_{k-N-1}$) at the time $k-N-1$, the consequent states

can be calculated by Eqs.2.15-2.16 (Muske and Rawlings, 1993b):

$$\hat{\xi}_{k-N-1|k} = \bar{\xi}_{k-N-1|k-N} + \hat{\omega}_{k-N-1|k} \tag{2.15}$$

$$\hat{\xi}_{j+1|k} = A\hat{\xi}_{j|k} + Bu_j + \hat{\omega}_{j|k} \tag{2.16}$$

where $\hat{\xi}$ is the estimated state vector ($\xi = [S_1, S_2, x, p, q, V]^T$), $\hat{\omega}_j$ is noise estimate at the step j and $\hat{\omega}_{k-N-1|k-N}$ is reserved to modify uncertainties in the initial guess of the first state in the estimation window. The MHE problem is stated as a minimization problem of the objective function (Ψ_k) and is stated in Eq.2.17:

$$\begin{aligned} \min_{\{\hat{\omega}_{k-N-1|k},\cdots,\hat{\omega}_{k-1|k}\}} \Psi_k = \; & \hat{\omega}^T_{k-N-1|k} Q_0 \hat{\omega}_{k-N-1|k} \\ & + \sum_{j=k-N}^{k-1} \hat{\omega}^T_{j|k} Q \hat{\omega}_{j|k} + \sum_{j=k-N}^{k} \hat{e}^T_{j|k} R \hat{e}_{j|k} \end{aligned} \tag{2.17}$$

subject to:

$$\hat{\xi}_{k-N-1|k} = \bar{\xi}_{k-N-1|k} + \hat{\omega}_{k-N-1|k} \tag{2.18}$$

$$\hat{\xi}_{j+1|k} = A\hat{\xi}_{j|k} + Bu_j + \hat{\omega}_{j|k} \tag{2.19}$$

$$y_j = C\hat{\xi}_{j|k} + \hat{e}_{j|k} \tag{2.20}$$

where A, B, C are local linear matrices and $\hat{e}_{j/k}$ is the error between the measurements and predicted output ($\hat{e}_{j|k} = y_j - C\hat{\xi}_{j|k}$). The state estimation is subjected to the state constraints and chemically and/or biologically represented state variables can not take negative values in Eqs.2.1-2.6, which is enforced by:

$$\hat{\xi}_{j|k} > 0 \tag{2.21}$$

Substituting $\hat{e}_{j/k}$ from Eq.2.20 into Eq.2.17 results in a convex quadratic program which can be solved by MATLAB or any commercial optimization package. Then, Eqs.2.15-2.16 will be used to reconstruct the states.

2.3.4 Model Predictive Control (MPC)

Knowing the optimal reference trajectory and having the knowledge of all states, the MPC is designed to track the reference trajectory. Model predictive control uses the mathematical model of the process to predict future behaviour of the process and optimize the input actions in order to plan the best action to reach a desired objective. Usually, the MPC objective is to achieve regulation or trajectory tracking. The optimization objective with reference to the tracking problem is defined as (Muske and Rawlings, 1993a):

$$\min_{u_0 \cdots u_{N-1}} \Phi = \sum_{j=1}^{N} (y_j^r - C\xi_j)^T Q' (y_j^r - C\xi_j) + \sum_{j=0}^{N-1} (u_j - u_j^r)^T R' (u_j - u_j^r) \tag{2.22}$$

y_j^r and u_j^r are the reference trajectory and reference inputs at point j and $C\xi_j$ is the process output. Q' and R' are positive definite penalty matrices. The optimization is also subject to the process dynamics and the constraints given by Eqs.2.23-2.26.

$$\xi_{j+1} = A\xi_j + Bu_j \tag{2.23}$$

$$y_j = C\xi_j \tag{2.24}$$

$$0 \leqslant u_j \leqslant u_{max} \tag{2.25}$$

$$0 \leqslant \xi_j \leqslant \xi_{max} \tag{2.26}$$

The trajectory obtained from Eqs.2.10-2.13 is used as a reference trajectory and an MPC reference tracking controller is constructed to track the reference obtained as a solution of a nonlinear program, Eqs.2.10-2.13. The reference trajectory tracking control is formulated as Eqs.2.22-2.26 and inputs, $[u_0 \cdots u_{N-1}]$, are determined such that the objective function, Eq.2.22, is minimized. Once the sequence of optimal inputs from optimization problem is obtained, $[u_0 \cdots u_{N-1}]$, only the first input, $u^* = u_0$, is implemented and the process is iteratively repeated over a receding horizon.

The schematic of integrated estimation, control and optimization strategy is given in Fig.2.1. As it can be seen, the maximization process is carried out in two steps. In an off-line optimization step, the IPOPT solver is used to determine the optimal reference trajectory that has taken into account all the present constraints on the inputs and states. In an on-line step, providing the reference trajectory is in place, local linear models are used by MPC to track the predetermined optimal trajectory. At the same time, MHE provides full information of the states to MPC. Both MPC and MHE account for constraints used for off-line optimization.

2.4 Results and Discussion

Applying the above-mentioned procedure, obtained results are shown in Table 2.3 along with the results from previous work of De la Hoz Siegler et al. (2012). There are significant improvements in maximum lipid and biomass production using the suggested model predictive estimation, control and optimization strategies. Namely, the maximum magnitude of the lipid concentration achieved is 109 $gr/litre$ which is 36% higher than the reported value (De la Hoz Siegler et al., 2012) while the biomass concentration increased by 24%. The improvement in biomass and lipid production

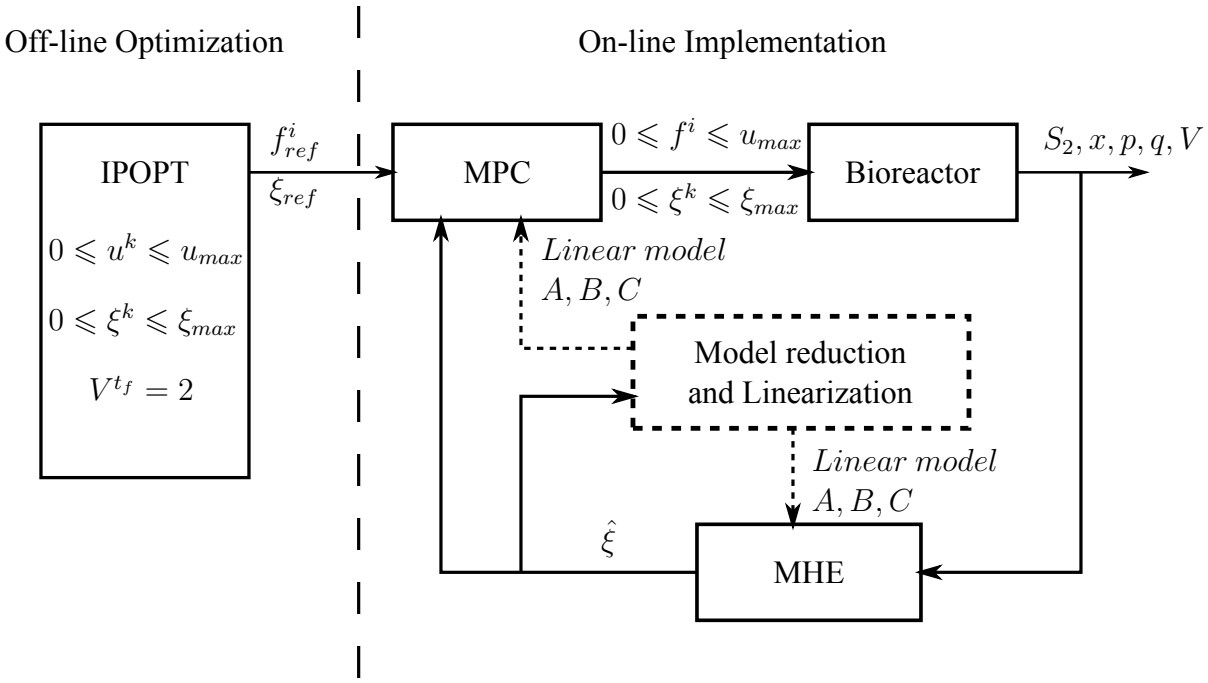

Figure 2.1: Schematic of optimization, estimation and control procedure in microalgae bioreactor.

Table 2.3: Oil production optimization results compared to (De la Hoz Siegler et al., 2012)

Parameter	De la Hoz Siegler et al. (2012)	Obtained by IPOPT optimization	unit
Biomass concentration	144	178	g/L
Lipid Concentration	80	109	g/L
Average lipid productivity	10.3	13.8	g/Ld
Maximum lipid productivity	20.1	21.3	g/Ld
Average Biomass productivity	15	23	g/Ld
Maximum lipid productivity	60	61.2	g/Ld
Oil content	60	62	%

is achieved taking into account all the constraints present in realistic real-time implementation. Maximum lipid and biomass productivity, which is reported in Table 2.3, occurs during the exponential growth and lipid accumulation period and is characteristic of microalgae cells growth process. These productivities are independent of the feeding strategies and can be seen as a measure of verification with respect to previous experimental work. The achieved values for maximum productivities are within an acceptable range, with a 2% and 6% difference with respect to the reported values in De la Hoz Siegler et al. (2012). The achieved oil content of microalgae cells also shows a slight difference compared to the previous work. The same oil content of cells shows that the improvement is achieved by a higher biomass production. In other words, higher biomass production rate and the same oil content mean higher lipid production rate. As it can be also seen in Table 2.3, the average biomass productivity is increased by 53% while the increase in average lipid productivity is about 34%.

Time evolution of the states and inputs is shown in Fig.2.2-2.9, dashed and solid lines are the reference trajectories and simulation results with MPC and MHE in the absence of measurement noise, respectively and dash-dotted lines represent results in the presence of measurement noise. Fig.2.2 shows the estimated nitrogen concentra-

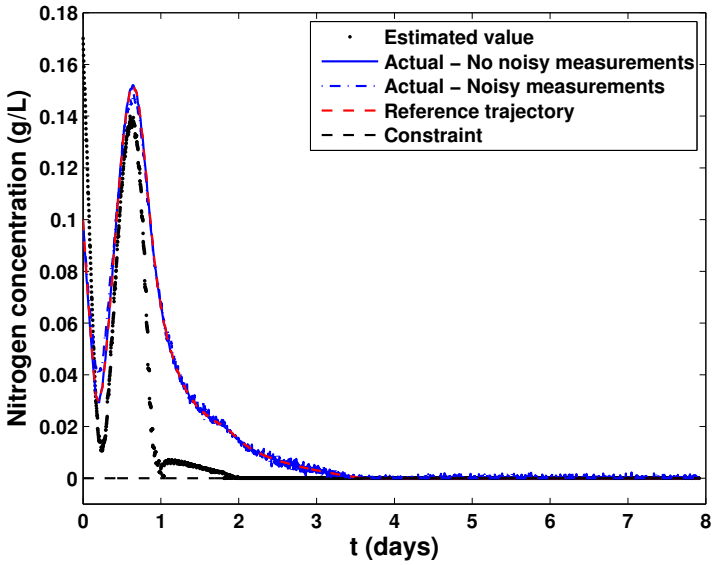

Figure 2.2: Actual and estimated nitrogen concentration in the bioreactor, S_1.

tion in the bioreactor compared to its actual value. The MHE tracks the changes in nitrogen concentration (S_1) and captures its rapid increases in the bioreactor. As the time elapses, the time-varying term in Eq.2.7 converges to 1 and consequently, as the time-varying term vanishes, the estimation performance becomes more efficient. The estimation error between days one and two directly affects the intracellular nitrogen concentration and as it can be seen in Fig.2.3, the intracellular nitrogen concentration weakly tracks the reference trajectory in this period. The error in the estimation of nitrogen concentration directly reflects in the nitrogen uptake rate (Eq.2.9), which determines how nitrogen is up-taken into microalgae cells.

The active biomass and lipid concentration in the bioreactor is shown in Fig.2.4 and 2.5 and despite relatively poor performance of the state estimation in the first to the second day-period, the optimal control strategy tracks the reference trajectory with high efficiency. Finally, Fig.2.6 shows the oil content in microalgae cells. The oil content of microalgae cells decreases during the first day due to high growth rate,

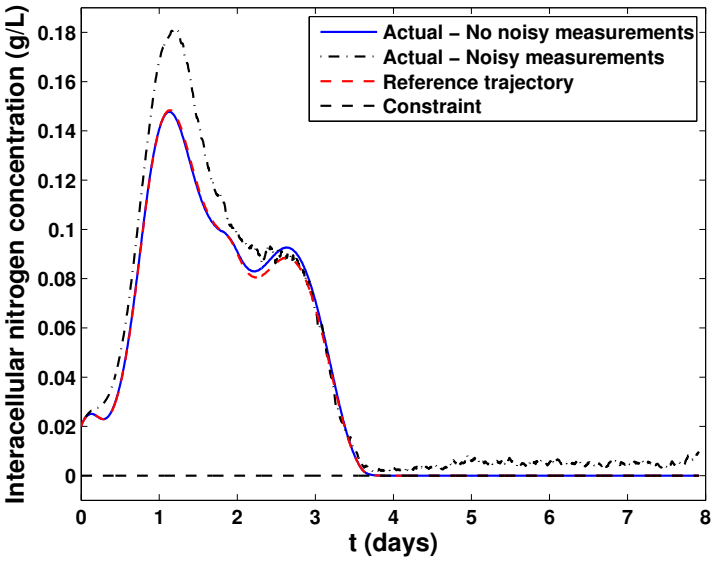

Figure 2.3: Intracellular nitrogen concentration, q.

but starts to grow afterward when glucose is present and nitrogen concentration is limited.

Under an optimized feeding strategy, microalgae cells behave as expected. At low concentration of glucose and nitrogen, microalgae tend to store glucose as lipids to continue surviving in the absence of glucose. Glucose is completely consumed after the second day (Fig.2.7) and it is then that the nutrition-starvation cycle starts to accumulate lipids in the cells. The optimum control strategy, as it can be seen from Fig.2.2, 2.7, 2.8 and 2.9, is to feed microalgae to grow to as high biomass concentration as possible, when due to the craving for nitrogen, microalgae start to produce lipid.

Nutrient feed rates (inputs) are shown in Fig.2.8-2.9. Nitrogen is fed to the bioreactor only during the first three days to supports algae growth and thereafter nitrogen fed is stopped to create nitrogen limited condition which is favourable condition for lipid accumulation (Fig.2.8). The nitrogen feed rate is determined by constraints, namely upper and lower limits on nitrogen feed rate and feed rate change

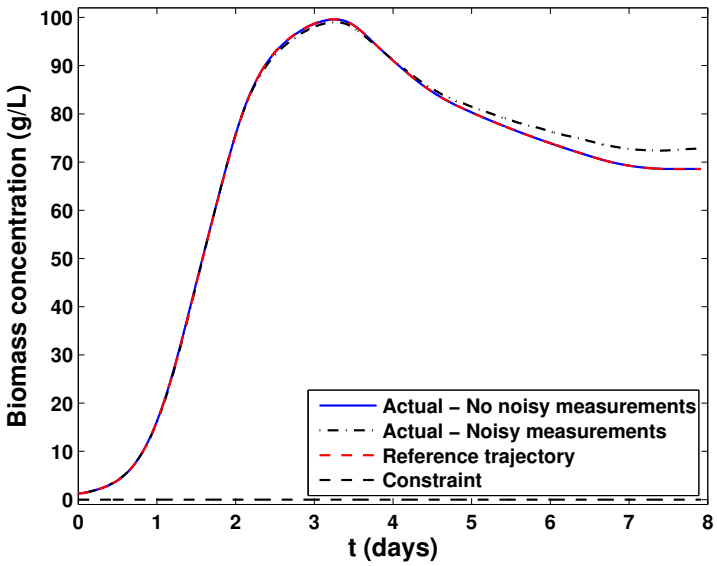

Figure 2.4: Active biomass concentration in the bioreactor, x.

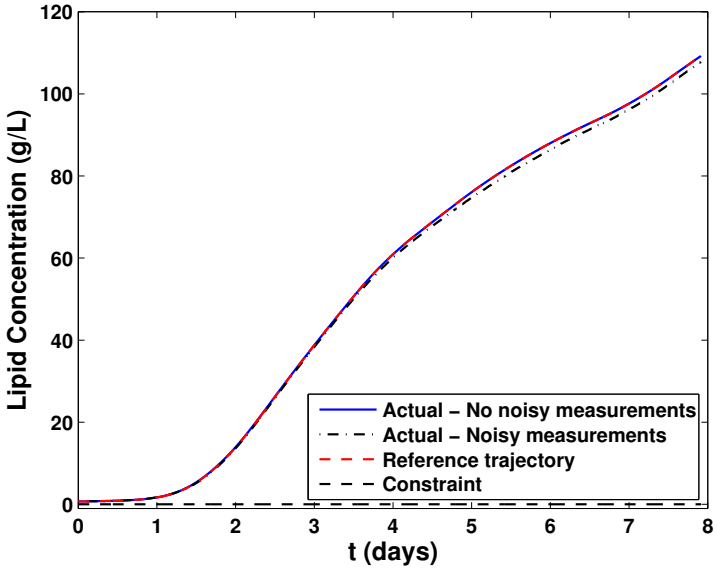

Figure 2.5: Lipid concentration in the bioreactor, p, and optimal lipid concentration reference trajectory.

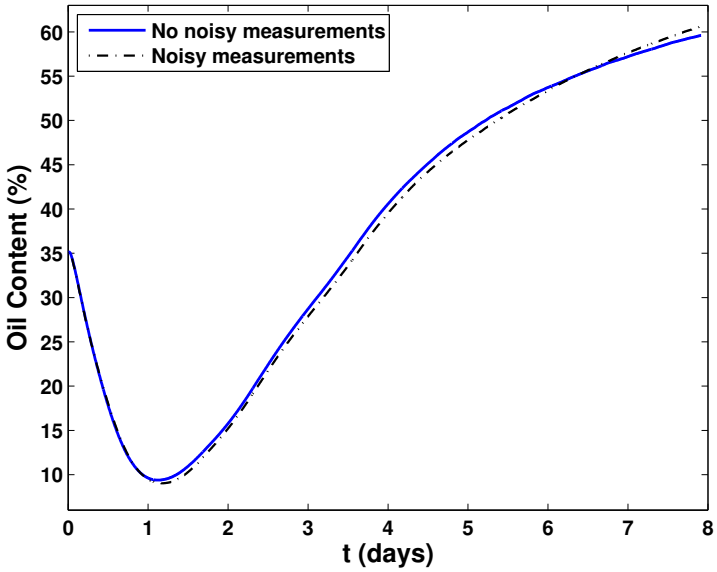

Figure 2.6: Oil content in the microalgae cells.

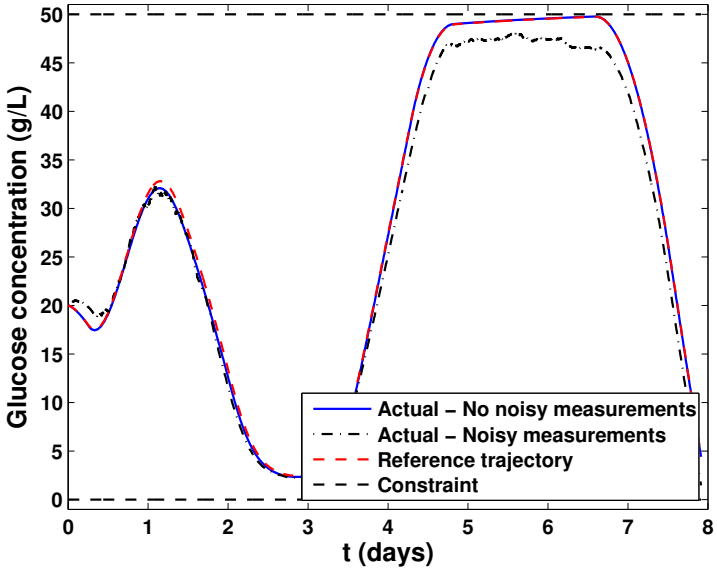

Figure 2.7: Glucose concentration in the bioreactor, S_2.

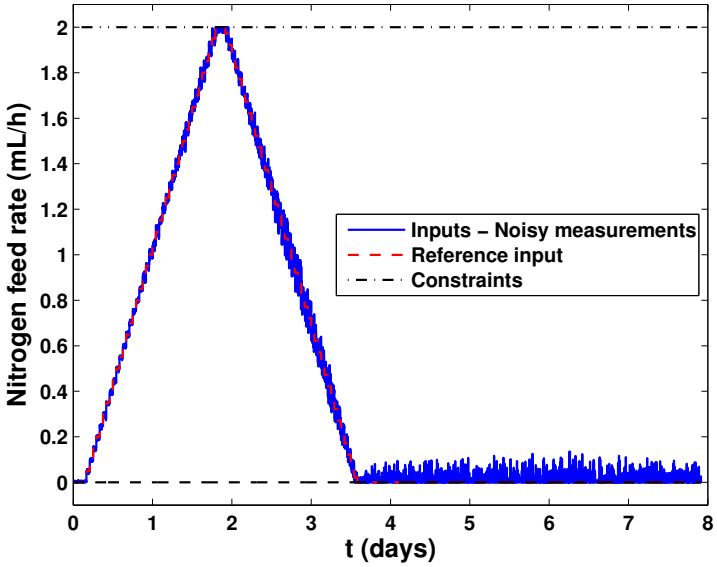

Figure 2.8: Glycine feed rate (nitrogen source).

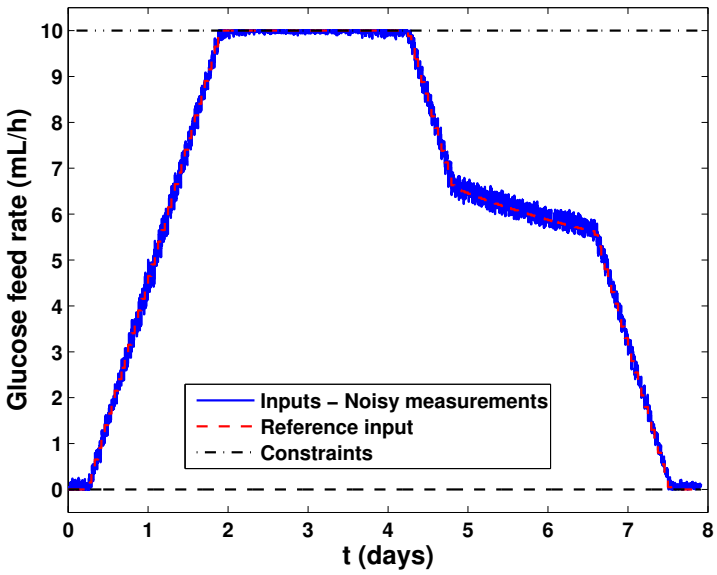

Figure 2.9: Glucose feed rate (carbon source).

($\Delta f_1^i < 0.2\,mL/h$ and $f_1^i < 2\,mL/h$). The glucose feed rate is governed by the present input and state constraints. During the first five days of operation, the glucose feed rate is governed by the constraints on the glucose feed rate change ($\Delta f_2^i < 1\,mL/h$) and upper limit for the glucose feed rate ($f_2^i < 10\,mL/h$). The upper limit constraint on the glucose concentration in the bioreactor (S_2) can be seen as an input constraint between days five and seven (see Fig.2.7 and 2.9).

Under realistic operating conditions, the measurements of biological properties are highly noisy, so that the presence of noise must be considered in the estimator and controller synthesis. The simulations are repeated for the case with noisy measurements. A uniform random noise of magnitude 20% of nominal values of the states is added to the measurements. The achieved results are shown in Figs.2.2-2.9 as dash-dotted lines. It can be seen that even with noisy measurements, the MPC tracks the reference trajectory. The feed rates in the presence of noise differ from reference inputs due to quadratic optimization which tries to track the reference lipid production trajectory. The resulted lipid concentration in the bioreactor is slightly lower than the maximum possible lipid concentration obtained from IPOPT. Due to the noisy measurement, the reference trajectories and the inputs are not optimal and as a result, new feed rates determined by MPC cause a change in the optimal solution which then leads to a slight violation of constraint associated with the bioreactor volume (Fig.2.10). However, the constraints on inputs and other states are not violated. There is an error in tracking of nitrogen (S_1) and intracellular nitrogen (q) between days one and two. The low efficiency of tracking is due to an estimation error for the nitrogen concentration (Fig.2.2 and 2.3). The glucose concentration (S_2) has also tracking error between days four and seven (Fig.2.7). The noisy measurements and the reference trajectory close to the glucose constraint give rise to an error in reference

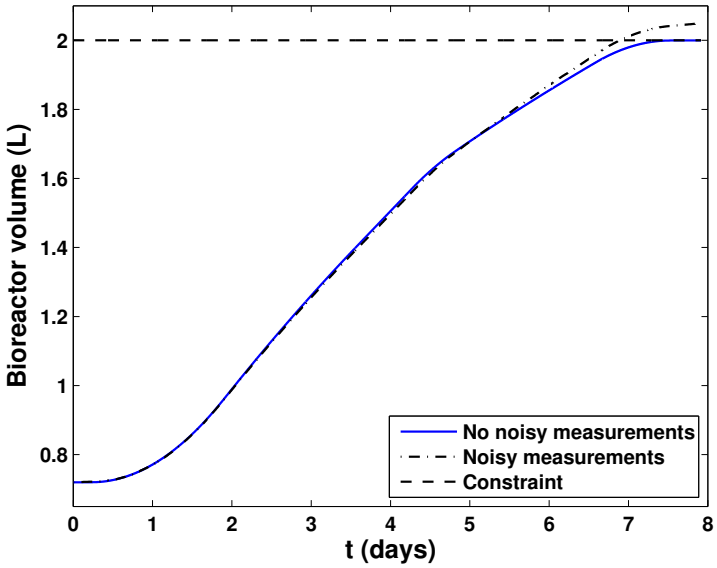

Figure 2.10: Bioreactor volume, V.

trajectory tracking of glucose concentration during the mentioned time interval(Fig 2.9).

Choosing sampling time has direct effect on the accuracy of linear models and computational effort of MPC and MHE. Shorter sampling time will make simulations more accurate, but on the other hand, for specified control and estimation horizons, smaller sampling time implies more time steps in the horizon which induces larger matrices for the evaluation of quadratic programming algorithms. Thus, there is a trade off between accuracy and computational effort. In this chapter, the sampling time is chosen to be 3 minutes, while control and estimation horizons are 5 and 2 hours, respectively.

There is a difference between trajectory tracking and simple maximizing of lipid production. The former is a reliable optimal control method which can be simply implemented to an experimental bioreactor. In the model predictive trajectory tracking, the optimization problem is convex and can be handled and implemented on

the online realization of a bioreactor with inaccurate measurements. In the optimal trajectory tracking, the presence of measurement noises can be tolerated by MPC by tuning the penalty matrices. However, in the case of direct maximization of lipids, the lack of the reference trajectory will likely decrease the controller efficiency.

If the initial states of the bioreactor are known and are the same as the initial states of the optimal trajectory, the open loop implementation will result in similar lipid production, however the states of the bioreactor are unknown and the tracking strategy is necessary in order to manipulate the production trajectory towards the optimal trajectory. In addition, tracking control will compensate for present disturbances and uncertainties.

The faster biomass and lipid production results in low saturated fatty acid content and induces lower cold filter plugging point (CFPP) (De la Hoz Siegler et al., 2012) which is an indication of the fuel's ability to flow through a filter. Another advantage of using reference tracking is that the maintaining of the lipid production along the specified trajectory will guarantee the same lipid quality for different fed batch runs. In addition, the same quality of lipid for different fed-batch runs will reduce the cost of lipid to biofuel conversion.

2.5 Conclusion

Lipid production rate of the *Auxenochlorella* protothecoides microalgae bioreactor is maximized by using the IPOPT solver for constrained large-scale nonlinear program formulation. The microalgae bioreactor process dynamics model is reduced and linearized to a set of linear and time invariant models. Then by using the constrained moving horizon estimator and the set of linear models, nitrogen concentration is es-

timated. Finally, model predictive control is used to track the obtained reference trajectory. The optimization results show 36% increase in lipid concentration in the microalgae bioreactor. Also, The implemented MHE based state estimation and MPC reference trajectory tracking regulator not only maintain the functionality as monitoring and regulation devices in the presence of measurement noise, but show reliable performance as well.

2.6 References

Alcaraz-Gonzlez, V., Salazar-Pea, R., Gonzlez-lvarez, V., Gouz, J., Steyer, J., 2005. A tunable multivariable nonlinear robust observer for biological systems. Comptes Rendus - Biologies 328, 317–325.

Alvarez-Vzquez, L.J., Fernndez, F.J., Martnez, A., 2010. Optimal management of a bioreactor for eutrophicated water treatment: A numerical approach. Journal of Scientific Computing 43, 67–91.

Bastin, G., Dochain, D., 1990. On-line estimation and adaptive control of bioreactors. Process measurement and control, Elsevier.

Biegler, L., 2010. Nonlinear Programming: Concepts, Algorithms, and Applications to Chemical Processes. Mos-siam Series on Optimization, Society for Industrial and Applied Mathematics.

Chisti, Y., 2007. Biodiesel from microalgae. Biotechnology Advances 25, 294–306.

De la Hoz Siegler, H., Ben-Zvi, A., Burrell, R.E., Mccaffrey, W.C., 2011. The dynamics of heterotrophic algal cultures. Bioresource technology 102, 5764–5774.

De la Hoz Siegler, H., McCaffrey, W.C., Burrell, R.E., Ben-Zvi, A., 2012. Optimization of microalgal productivity using an adaptive, non-linear model based strategy. Bioresource technology 104, 537–546.

Doucha, J., Lvansky, K., 2012. Production of high-density chlorella culture grown in fermenters. Journal of Applied Phycology 24, 35–43.

El Bahja, H., Vega, P., Bakka, O., Mesquine, F., 2009. Non linear gpc of a nutrient removal biological plant, in: ETFA 2009 - 2009 IEEE Conference on Emerging Technologies and Factory Automation, pp. 1–7.

Estrada, V., Parodi, E.R., Diaz, M.S., 2009. Addressing the control problem of algae growth in water reservoirs with advanced dynamic optimization approaches. Computers and Chemical Engineering 33, 2063–2074.

Farza, M., Busawon, K., Hammouri, H., 1998. Simple nonlinear observers for on-line estimation of kinetic rates in bioreactors. Automatica 34, 301–318.

Farza, M., Hammouri, H., Othman, S., Busawon, K., 1997. Nonlinear observers for parameter estimation in bioprocesses. Chemical Engineering Science 52, 4251–4267.

Gonzalez, J., Fernandez, G., Aguilar, R., Barron, M., Alvarez-Ramirez, J., 2001. Sliding mode observer-based control for a class of bioreactors. Chemical Engineering Journal 83, 25–32.

Hoffert, M.I., Caldeira, K., Benford, G., Criswell, D.R., Green, C., Herzog, H., Jain, A.K., Kheshgi, H.S., Lackner, K.S., Lewis, J.S., Lightfoot, H.D., Manheimer, W., Mankins, J.C., Mauel, M.E., Perkins, L.J., Schlesinger, M.E., Volk, T., Wigley, T.M.L., 2002. Engineering: Advanced technology paths to global climate stability: Energy for a greenhouse planet. Science 298, 981–987.

Hsieh, C., Wu, W., 2009. Cultivation of microalgae for oil production with a cultivation strategy of urea limitation. Bioresource technology 100, 3921–3926.

Khan, S.A., Rashmi, Hussain, M.Z., Prasad, S., Banerjee, U.C., 2009. Prospects of biodiesel production from microalgae in India. Renewable and Sustainable Energy Reviews 13, 2361–2372.

Mailleret, L., Bernard, O., Steyer, J., 2004. Nonlinear adaptive control for bioreactors with unknown kinetics. Automatica 40, 1379–1385.

Muske, K.R., Rawlings, J.B., 1993a. Model predictive control with linear models. AIChE Journal 39, 262–287.

Muske, K.R., Rawlings, J.B., 1993b. Receding horizon recursive state estimation, in: American Control Conference, pp. 900–904.

Nadadoor, V.R., De la Hoz Siegler, H., Shah, S.L., McCaffrey, W.C., Ben-Zvi, A., 2012. Online sensor for monitoring a microalgal bioreactor system using support vector regression. Chemometrics and Intelligent Laboratory Systems 110, 38–48.

Patil, V., Tran, K., Giselrd, H.R., 2008. Towards sustainable production of biofuels from microalgae. International Journal of Molecular Sciences 9, 1188–1195.

Selisteanu, D., Petre, E., Rasvan, V.B., 2007. Sliding mode and adaptive sliding-mode control of a class of nonlinear bioprocesses. International Journal of Adaptive Control and Signal Processing 21, 795–822.

Sendrescu, D., Popescu, D., Petre, E., Bobasu, E., Selisteanu, D., 2011. Nonlinear model predictive control of a lipase production bioprocess, in: Proceedings of the 2011 12th International Carpathian Control Conference, ICCC'2011, pp. 337–341.

Tebbani, S., Dumur, D., Hafidi, G., vande Wouwer, A., 2010. Nonlinear predictive control of fed-batch cultures of escherichia coli. Chemical Engineering and Technology 33, 1112–1124.

Wachter, A., Biegler, L.T., 2000. Failure of global convergence for a class of interior point methods for nonlinear programming. Mathematical Programming 88, 565–574.

Wachter, A., Biegler, L.T., 2006. On the implementation of an interior-point filter line-search algorithm for large-scale nonlinear programming. Mathematical Programming 106, 25–57.

Wu, Z., Shi, X., 2007. Optimization for high-density cultivation of heterotrophic chlorella based on a hybrid neural network model. Letters in applied microbiology 44, 13–18.

Zhang, T., Guay, M., 2002. Adaptive nonlinear observers of microbial growth processes. Journal of Process Control 12, 633–643.

Chapter 3

Temperature Distribution Reconstruction in Czochralski Crystal Growth Process

3.1 Introduction

The Czochralski (Cz) crystal growth process is a well-known crystallization process to grow and produce single crystals. The process starts with inserting a small crystal seed into heated melt and the crystal seed is slowly drawn out of the crucible, with heated melt of crystal material, allowing the melt to solidify and grow at the melt-crystal interface. Due to continuous and unbroken crystal lattice in single crystals, produced crystals have unique mechanical, physical and electrical properties, which speaks for high demand for quality grown single crystals in microelectronics and opto-electronics, as well as demand for structurally robust and high temperature resistant materials (Derby and Brown, 1987; Szabo, 1985; Gevelber and Stephanopoulos, 1987).

Due to the nature of high-tech applications reflecting in high quality of a grown crystal and high energy and time consuming growth process, there are manufacturing concerns that should be addressed in the Cz process. In particular, crystal shape and

geometry, as well as crystal quality, are among the most important manufacturing concerns. The former is usually addressed by producing the crystal with constant diameter to minimize machining waste. Along the consideration of the crystal geometry from the standpoint of manufacturing, the crystal quality is also defined by physical properties of the produced crystal. Uniform composition, dopant concentration, defects density and residual stresses in crystal are the most important properties that should be considered in a crystallization process, see Szabo (1985); Gevelber and Stephanopoulos (1987); Brown (1988); Winkler et al. (2010a).

In the Cz crystal growth process, the presence of solid and liquid phases, melt fluid flow, thermal and heat transfer phenomena, solid-liquid interface and pulling dynamics make the modelling and control of the Cz process a challenging task (Derby and Brown, 1986a,b). Due to the crystal growth and phase transition between solid and liquid phases, the crystal spatial domain undergoes time-varying changes which brings complexity to the process regulation. There are studies focusing on modelling and simulation of coupled phenomena together (Cao et al., 2011; Demina and Kalaev, 2011). However, for control and estimation purposes and specially for model based control/estimation, reduced order models are required. Reduced order models are used for both radius and temperature control purposes. For example, reduced order models are developed and used by Irizarry-Rivera et al. for coupled radius and melt temperature control in the Cz crystal growth process (Irizarry-Rivera and Seider, 1997a,b). In general, to achieve a simpler model description, one can apply suitable assumptions to decouple the thermal phenomena in the solid crystal and the melt for the purpose of temperature observation/control in the grown solid crystal. In particular, in this chapter, the temperature control and/or estimation in a solid grown crystal is formulated as a heat transfer model with interface phenomena modelled as

a Dirichlet boundary condition at the melt-solid interface (Ng and Dubljevic, 2012; Ng et al., 2013; Armaou and Christofides, 2001a) (for details see Eqs.3.25-3.27).

Real-time knowledge of temperature distribution evolution in crystal and its interfaces is necessary for monitoring and control purposes. The temperature distribution and gradients in crystal determine and influence residual stresses, crystal oxygen and dopant concentration and grown crystal defects concentration (Gevelber and Stephanopoulos, 1987; Gevelber et al., 1988). However, temperature measurements over the entire domain are not directly available and can not be realized in practice. In particular, possibly available and realizable temperature measurement is carried out at the grown crystal boundary but can not be used to construct the temperature and temperature gradients directly. Moreover, all the boundary temperatures are not available for direct sensor applied measurements, namely bottom boundary is the melt-crystal interface and the top is used for installing pulling devices. Usually, the only available temperature measurement is at the cylindrical surface of the crystal, and in order to reconstruct temperature profile over the entire domain and boundaries, an estimation strategy is required.

A boundary and in-domain state estimation/reconstruction and control strategies for parabolic partial differential equation (PDE) systems are well developed and make an active research area, see Curtain and Zwart (1995); Bensoussan et al. (2007); Krstic and Smyshlyaev (2008). For example, there are several contributions on control problems with fixed spatial domain for linear PDEs (Ito, 1990; Bensoussan et al., 2007; Curtain and Zwart, 1995), nonlinear PDEs (Fard and Sagatun, 2001; Dunbar et al., 2003; Rudolph et al.), problems with spatially distributed actuation (Ito, 1990; Balas, 1986; Bensoussan et al., 2007) and boundary control problems (Fard and Sagatun, 2001; Dunbar et al., 2003; Liu and Krstic, 2000). Despite distributed parameter con-

trol strategies, state estimation algorithms for parabolic PDEs are less developed and are of interest in the context of temperature estimation in the crystal growth process. In particular, Xu et al. (1995) provide a simple observer for dissipative bilinear systems with weak error convergence to zero. The Luenberger observer synthesis is used by both Vries et al. (2010) for state estimation of the Sturm-Liouville systems, and Li and Xu (2011) for a higher order PDE describing the rotating body-beam system. Harkort and Deutscher (2011) have developed an observer based controller framework for Riesz-spectral systems. Along the same line, Hagen and Mezic (2003) have studied the observer and control design using spillover analysis for a class of partial differential equations with periodic boundary conditions. State estimation of the systems governed by parabolic PDEs on a fixed domain are well developed, however there are limited contributions on parabolic PDEs with a moving boundary setting.

Moving boundaries and time-varying parameters bring complexity to the system that needs to be addressed in the control and estimation framework. There are several works focusing on controller design for time-varying parabolic PDEs. For example, Armaou *et al.* have reduced a 2-D heat transfer model in the Cz crystal growth process to a 1-D model, and then synthesized a controller to regulate temperature distribution in the crystal (Armaou and Christofides, 2001a). They also provided a non optimal stabilizing robust control law for moving boundary crystal growth problem (Armaou and Christofides, 2001b). Wang studied various optimal controller synthesis for stabilization and control of distributed systems with time-dependent spatial domains, see Wang (1990, 1995), while Ng and Dubljevic contributed on optimal boundary control of the Cz crystal growth process with time-varying spatial domain coupled with pulling dynamics, see Ng and Dubljevic (2012, 2011). In the former contributions, the developed control laws require full state knowledge of the

process which motivates this contribution to reconstruct the entire temperature field in the Cz process from the boundary measurement.

In the Cz process, the boundary movement is the result of the crystal growth in both radial and axial directions. The time evolution of the solid crystal determines the crystal shape and consequently, the spatial domain of the governing temperature evolution equations. The radius regulation and estimation in the Cz process have attracted several researchers. There are early works on radius regulation, for example, Gross and Kresten (Gross and Kersten, 1972) worked on the crystal radius control and Jordan et al. (1983) used the crystal weight signal as a measurement for control purposes. Recently, Winkler et al. (2010a,b) revisited the radius control and estimation problem, provided a modelling approach based on capillary forces and a nonlinear approach combined with a conventional PI controller to estimate and regulate the crystal radius. Neubert and Winkler (2012) introduced parameters such as thermal conductivity, latent heat, average axial thermal gradients and actual growth rate to refine the scheduling of a PI controller for better performance. Hence, one concludes that the growth dynamics and the temperature distribution evolution in the crystal are coupled in the Cz process, however this coupling is not taken into account in the aforementioned works.

In this chapter, a mechanical-geometric crystal growth model is developed based on the constant crystal growth rate, then assuming a large parametric uncertainty in the growth rate, a robust controller synthesis is provided using the input-output linearization for crystal diameter tracking. Time-varying radius and crystal length evolution, obtained from a nonlinear mechanical-geometric radius evolution model, determine the spatial domain of the underlying heat transfer model which leads to the time-varying boundary parabolic partial differential equation (PDE) model of

the temperature distribution evolution which can be expressed with operators and embedded in an infinite–dimensional PDE setting. The governing temperature evolution is approximated by a time-varying parabolic PDE model on a rectangular domain and a finite dimensional representation of the PDE model is derived using Galerkin's method. The effect of time-varying domain is investigated and is taken into account in order to obtain the low dimensional model. An observer is synthesized using a reduced finite dimensional model to reconstruct the entire temperature distribution by using physically realizable temperature measurements. The separation principle is examined and shown to hold in order to utilize the proposed observer in the output feedback control synthesis. In addition, a Finite Element Method (FEM) model of the crystal growth process is used to numerically simulate the temperature evolution in the solid crystal on the non-trivial and time-varying domain. The developed FEM model is used as the actual process to evaluate and verify the performance and efficiency of the temperature distribution reconstruction.

The temperature distribution evolution in the crystal affects the crystal quality in two ways. The first is through influencing the formation, diffusion and aggregation of point defects and atomic oxygen in the crystal (Sinno and Brown, 1999). The second is through the residual stresses in the crystal that occur during crystal cooling. An accurate dynamic model of the point defects in the crystal requires the knowledge of temperature distribution over the crystal. This chapter focuses on the temperature estimation and it is a basis for control and optimization of residual stresses and point defects through manipulating the temperature distribution. The temperature control can be done to minimize the formation, diffusion or aggregation of point defects and also to optimally control the cooling process to avoid residual stresses in the crystal.

The provided methodology for the temperature reconstruction from boundary

measurements can be extended to other chemical engineering processes with time-varying domain and especially with moving front and other material processing applications with same governing equations such as Bridgman crystal growth process and/or steel slab annealing (Brown, 1988; Ng et al., 2011). This chapter is focused on Czochralski crystallization process in order to cover more issues in practical implementation. Furthermore, the observer synthesis is developed based on reduced order Galerkin' model and finite element model realization is provided to verify both the reduced order model and the observer. Hence that, finite element realization is shown to be a suitable numerical approach for modelling and simulation of the Czochralski crystal growth process by comparing and validation of FEM results with experimental and/or numerical data carried out by different contributors (Thomas et al., 1989; Derby et al., 1987, 1989; Sackinger et al., 1989).

The organization of the chapter is as follow: after the Introduction, in Section 3.2, translational mechanical-geometric dynamic model for the Cz process is derived and the controller synthesis is presented to maintain constant crystal diameter in the presence of parametric uncertainty. In Section 3.3, the solid crystal heat transfer model is presented and the boundary conditions are defined. The infinite dimensional PDE model representation with defined spatial operators is developed along with the model reduction using Galerkin's method and the influence of time-varying effects is described. Section 3.4 provides the observer design, FEM model and the implementation of the estimation strategy. Numerical simulation results are presented in Section 3.5.

3.2 Crystal growth model and radius regulation

In the Cz crystal growth process, the crystal is slowly pulled out of the melt, allowing solidification of crystal at the crystal-melt interface. Mechanical pulling rate influences the crystal profile and determines the shape of the crystal. The crystal radius and growth can be regulated by a conventional PID controller (Gevelber and Stephanopoulos, 1987; Gevelber et al., 1988; Gevelber, 1994a,b), however, for more precise control, model-based approaches can be utilized. Model-based control approaches have attracted more attention recently, for example, Winkler, Neubert and Rudolph focused on nonlinear model-based control and estimation of the Cz process (Winkler et al., 2010a,b; Neubert and Winkler, 2012). As for the model-based control, a sophisticated process model is required to achieve desired performance. In this chapter, a new approach is used for radius regulation. The influence of temperature distribution and heat transfer phenomena on crystal growth are seen as an uncertainty in the crystal growth rate. Then control synthesis is provided to compensate for large parametric uncertainty in the growth rate. The crystal growth model is derived assuming that the crystallization rate is constant, the deviation from the nominal growth rate is considered as parametric uncertainty and then the control synthesis is provided.

3.2.1 First principal crystal growth model

The translational movement has direct influence on the crystal surface profile and affects the crystal radius (Winkler et al., 2010a). Crystal growth is modelled based on conservation of mass and Newton's second law. The schematic of the crystal pulling dynamics along with the notations are presented in Fig.3.1. In deriving a dynamic

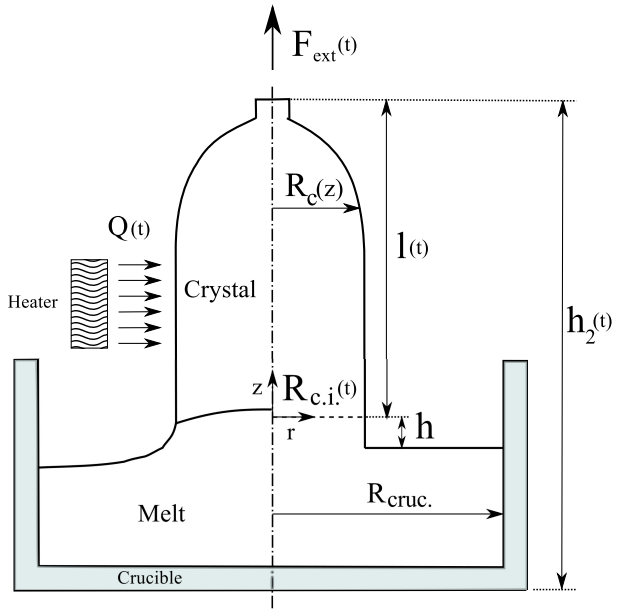

Figure 3.1: Schematic of the Cz crystal growth process with the realistic geometry of the process given in the left figure side, and geometric simplifications and parameters given in the right figure side.

model, the melt-solid interface is assumed to be a horizontal plane (Abdollahi and Dubljevic, 2013).

Assuming the same density for both the solid crystal and melt, the total volume (V_t) is constant during the process, that is:

$$V_t = V_c + V_m + V_l \tag{3.1}$$

where V_c is the volume of the solid crystal, V_l is the melt volume and V_m is the meniscus' volume. Eq.3.1 can be written as:

$$V_t = \int_0^t \pi R_{c.i.}(\tau)^2 \dot{l}(\tau) d\tau + V_m + \pi R_{cruc.}^2 (h_2(t) - l(t) - h(t)) \tag{3.2}$$

where $V_c = \int_0^t \pi R_{c.i.}^2 \dot{l} dt$ and $V_l = \pi R_{cruc.}^2 (h_2(t) - l(t) - h(t))$. The schematic of the crystal and crucible is shown in Fig.3.1. Total mass is constant and assuming a constant volume for the meniscus, then $\dot{V}_t = 0$ and mass conservation can be written as follows:

$$\dot{h}_2(t) = \dot{l}(t)(1 - \frac{R_{c.i.}^2}{R_{cruc.}^2}) \tag{3.3}$$

where $R_{c.i.}(t)$ is the crystal radius at the interface. On the other hand, the total mass subjected to motion is the crystal mass which is given as follows:

$$M_c = \rho_c V_c = \rho_c \int_0^t \pi R_{c.i.}(\tau)^2 \dot{l}(\tau) d\tau \tag{3.4}$$

and the crystal velocity is the average of the velocity at two crystal ends and is given as:

$$v_c = \dot{h}_2(t) - \dot{l}(t)/2 = \dot{l}(t)(\frac{1}{2} - \frac{R_{c.i.}(t)^2}{R_{cruc.}^2}) \tag{3.5}$$

applying the conservation of linear momentum (Newton's second law),

$$\frac{d(M_c v_c)}{dt} = F_{ext}(t) \tag{3.6}$$

and substituting Eqs.3.4-3.5 into Eq.3.6 results in:

$$\rho_c V_c(t) \ddot{l}(t)(\frac{1}{2} - \frac{R_{c.i.}(t)^2}{R_{cruc.}^2}) + \rho_c V_c(t) \dot{l}(t)(\frac{-2R_{c.i.}(t)\dot{R}_{c.i.}(t)}{R_{cruc.}^2}) + \rho_c \dot{l}(t)(\frac{1}{2} - \frac{R_{c.i.}(t)^2}{R_{cruc.}^2}) \dot{V}_c(t) = F_{ext}(t) \tag{3.7}$$

The crystal growth rate can be formulated as a function of heat fluxes in the solid-liquid interface as following (Duffar, 2010):

$$\dot{l}(t) = \frac{\Phi_s - \Phi_l}{\pi R_{c.i.}^2 \rho_c \Delta H} \tag{3.8}$$

Considering the constant heat flux at the interface,

$$\dot{l}(t) = \frac{C_{growth}}{R_{c.i.}(t)^2} \tag{3.9}$$

where

$$C_{growth} = \frac{\Phi_s - \Phi_l}{\pi \rho_c \Delta H} \tag{3.10}$$

C_{growth} depends on the heat fluxes and material characteristics at the interface. Substituting Eq.3.9 into Eq.3.7 results in:

$$\frac{\rho_c V_c(t)}{2}\ddot{l}(t) + \rho_c \pi C_{growth}(\frac{1}{2} - \frac{R_{c.i.}(t)^2}{R_{cruc.}^2})\dot{l}(t) = F_{ext}(t) \tag{3.11}$$

Finally, in the state space form, we denote $x_1(t) = l(t)$, $x_2(t) = \dot{l}(t)$ and $x_3(t) = V_c(t)$, so the model is given as:

$$\begin{aligned}
\dot{x}_1(t) &= x_2(t) \\
\dot{x}_2(t) &= \frac{2}{\rho_c x_3(t)}[F_{ext}(t) - \rho_c \pi C_{growth}(\frac{x_2(t)}{2} - \frac{C_{growth}}{R_{cruc.}^2})] \\
\dot{x}_3(t) &= \pi C_{growth}
\end{aligned} \tag{3.12}$$

and the crystal radius, $R_{c.i.}$, as the output is given as:

$$R_{c.i.}(t) = \sqrt{\frac{C_{growth}}{x_2(t)}} = \sqrt{\frac{C_{growth}}{\dot{l}(t)}} \tag{3.13}$$

The crystal growth process starts with inserting seed crystal into the melt and therefore the initial condition for Eqs.3.12-3.13 are the initial dimensions of the seed crystal. Specifically, the initial crystal volume is denoted by $x_3(0) = V_{c0}$.

Remark: In the Cz crystal growth process, the Young-Laplace force acts on the solid crystal. In the above derivation of the growth dynamics of the Cz crystal growth, the Young-Laplace force is neglected. This force is usually approximated by hydrostatic force (first term) and the vertical component of the surface tension (second term) (Duffar, 2010), is described as below:

$$F_{Y.L.} = \pi g \rho_l R_{c.i.}^2 h + \pi g \rho_l a^2 R_{c.i.} \cos(\alpha_0 + \alpha_c) \tag{3.14}$$

where, a is the Laplace constant, α_0 and α_c are the growth and capillary angles, ρ_l is the liquid density and g is the gravitational constant. In this chapter, the meniscus shape is considered to be constant, therefore, the Young-Laplace force can be calculated and incorporated into the system as a known disturbance. The crystal radius, $R_{c.i.}$, and meniscus height, h, are measured and the capillary angle can be calculated from the Young-Laplace equation (Irizarry-Rivera and Seider, 1997a):

$$h = a\sqrt{\frac{1 - \sin(\alpha_0 + \alpha_c)}{1 + a/(\sqrt{2}R_{c.i.})}} \tag{3.15}$$

3.2.2 Growth control

An important objective in the Cz process is to regulate the crystal radius at a constant value along the crystal length during the process. In order to achieve this goal, a controller is designed based on the input-output linearization of the growth model to regulate the radius at the desired pre-specified crystal radius. Assuming the pulling force as an input to the growth model and the radius of the crystal as an output, the

input-output relation is obtained as:

$$\frac{dR_{c.i.}}{dt} = \frac{R_{c.i.}}{2(t + V_{c0}/\pi C_{growth})} - \frac{R_{c.i.}^3}{\rho_c \pi C_{growth}^2 (t + V_{c0}/\pi C_{growth})} F(t) \tag{3.16}$$

where $R_{c.i.}$, the crystal's radius, is the process output, $F(t) = F_{ext}(t) + \frac{\rho_c \pi C_{growth}^2}{R_{cruc.}^2}$ is the input to the growth model, V_{c0} is the crystal's initial volume. Using the input-output linearization and defining $F(t)$ as:

$$F(t) = \frac{\rho \pi C_{growth}^2}{2R_{c.i.}^2} - \frac{\rho \pi C_{growth}^2 (t + V_{c0}/\pi C_{growth})}{R_{c.i.}^3} u_{mech.}(t) \tag{3.17}$$

Eq.3.16 is transformed into $\dot{r}(t) = u_{mech.}(t)$. As it can be seen, the radius can be manipulated directly by $u_{mech.}(t)$. In order to regulate the radius at a pre-specified desired constant value R_d, the control law is chosen to be $u_{mech.}(t) = -K(R_{c.i.} - R_d)$, where K is a positive number. Therefore, the following control action is derived to stabilize the process at the constant radius R_d.

$$F_{ext}(t) = \rho_c \pi C_{growth}^2 \left(\frac{1}{2R_{c.i.}(t)^2} - \frac{1}{R_{cruc.}^2}\right) + K\rho\pi C_{growth}^2 \left(t + \frac{V_{c0}}{\pi C_{growth}}\right) \frac{R_{c.i.}(t) - R_d}{R_{c.i.}(t)^3} \tag{3.18}$$

where K is the controller gain determined in the ensuing section to compensate the parametric uncertainty in the crystal growth rate.

3.2.3 Modelling uncertainties and disturbance rejection

The main assumption in the mechanical modelling in the previous section is that the heat flux at the solid-melt interface is constant. However, the heat flux across the solid-melt interface changes during the process and the dominant heat transfer is

the melt heat loss through the solid-melt interface. Therefore, in this subsection, we account for this assumption by considering a parametric uncertainty to the dynamic model given by Eq.3.12. The deviation of heat flux at the solid-melt interface is considered as heat fluctuations and is defined as $d(t)$, where:

$$\frac{\Phi_s - \Phi_l}{\pi \rho_c \Delta H} = C_{growth} + d(t) \tag{3.19}$$

The controller synthesis is based on constant heat fluxes and the deviation from this constant value results in a process model with a similar structure as given by Eq.3.12. The resulting model is given as follows:

$$\begin{aligned}
\dot{x}_1(t) &= x_2(t) \\
\dot{x}_2(t) &= \frac{2}{\rho_c x_3(t)}[F_{ext}(t) - \rho_c \pi (C_{growth} + d(t))(\frac{x_2(t)}{2} - \frac{C_{growth} + d(t)}{R^2_{cruc.}})] \\
\dot{x}_3(t) &= \pi (C_{growth} + d(t)) \qquad (3.20) \\
R_{c.i.}(t) &= \sqrt{(C_{growth} + d(t))/x_2(t)} \qquad (3.21)
\end{aligned}$$

Applying the control law given by Eq.3.18 to the model, Eqs. 3.20-3.21, result in the following relation:

$$\dot{R}_{c.i.}(t) = \frac{\epsilon \ R_{c.i.}(t)}{2(t + V_{c0}/\pi (C_{growth} + d(t)))} - K(1-\epsilon)(R_{c.i.}(t) - R_d) \tag{3.22}$$

where $\epsilon = 1 - \frac{C^2_{growth}}{(C_{growth}+d(t))^2}$ and $d(t)$ is the deviation from the nominal value of C_{growth}. The crystal growth rate is assumed to vary from no crystallization to fast crystallization rates and then it can be concluded that $d(t) \in (-C_{growth}, \infty)$, while ϵ in Eq.3.22 is $\epsilon \in (-\infty, 1)$. The second term in Eq.3.22 is negative for all ϵ and the

first term is negative for $\epsilon \in (-\infty, 0)$. For $\epsilon \in (0, 1)$, the stability of the controller is guaranteed by defining K in order to have $\dot{R}_{c.i.} = -\mu(K)(R_{c.i.} - R_d(t))$. K is calculated as:

$$K > \frac{\pi}{2V_{c0}C_{growth}^2} D(C_{growth} + D)(2C_{growth} + D) \tag{3.23}$$

where D is an upper limit for disturbance $d(t)$, $-C_{growth} < d(t) < D$.

The control law, despite the uncertainty in the crystal growth rate, stabilizes the crystal radius at the desired value. The lower bound on parametric uncertainty, $d(t)$, is $-C_{growth}$ which corresponds to no solidification in the process and it is assumed that no crystal melting happens during the process. As long as the crystallization rate is positive ($D > -C_{growth}$), the robustness of the control law suffices for regular process operation (where no melting happens). The advantage of the proposed controller is that the controller stabilizes the crystal diameter despite the uncertainty in nonmodeled thermal dynamics and effects at the crystal-melt interface. In other words, the radius control synthesis is decoupled from the phenomena that can adversely affect the crystallization rate and the radius growth.

Remark: The crystal growth model and control strategy provided in this section is a simple and effective representation of the crystal growth dynamics used to demonstrate time-varying effects and coupling between the crystal growth and temperature distribution. However, more complex models (e.g. considering capillary forces, the meniscus dynamics, etc.) can be realized and replaced with presented model.

3.3 Heat transfer model

A comprehensive model of the Cz crystal growth process concerning heat conduction, fluid flow in the crucible, capillary forces at the crystal-melt interface, heat radia-

tion and mechanical pulling dynamics can be found in literature (Derby and Brown, 1987; Brown, 1988; Derby and Brown, 1986a,b). This chapter is concerned with the temperature distribution and heat transfer time evolution in a solid crystal as a foundation for the full state feedback control synthesis, and therefore domain geometry of a grown crystal is of paramount importance in modelling efforts.

The crystal domain evolution is determined by the crystal radius and length evolution during the process and is provided in Section 3.2. In the Cz crystal growth process, the heat transfer within the solid crystal is described by the conduction-convection PDE model given by Eq.3.24 where convective terms are manifested by the growth velocity of boundaries. Fig.3.2 shows the process domain with simplifications made on the crystal domain along with boundary conditions. For modelling purposes, the crystal domain is assumed to be rectangular and heat transfer equations are written over the rectangular domain. Two-dimensional Cz growth process' temperature dynamics is described by the following PDE, see Derby and Brown (1987); Ng and Dubljevic (2012):

$$Pe\frac{\partial x(r,z,t)}{\partial t} = \nabla \cdot (k_r \nabla x(r,z,t)) - Pe\mathbf{V}(r,z,t) \cdot \nabla x(r,z,t) \tag{3.24}$$

where $x(r,z,t)$ is the temperature field and ∇ is the spatial gradient operator in the cylindrical coordinate system, $Pe = \rho_c C_p v_0 R_{cruc.}/k_s$ is the Peclet number, and v_0, $R_{cruc.}$, k_s and k_r are the nominal growth rate, crucible radius, regional thermal conductivity and conductivity ratio, respectively and $\mathbf{V}(r,z,t)$ is the velocity vector field over the entire crystal domain. The PDE is written as an appropriately scaled time-varying moving boundary temperature model dynamics with neglected boundary velocity along the radial direction. Therefore, the temperature evolution is given by

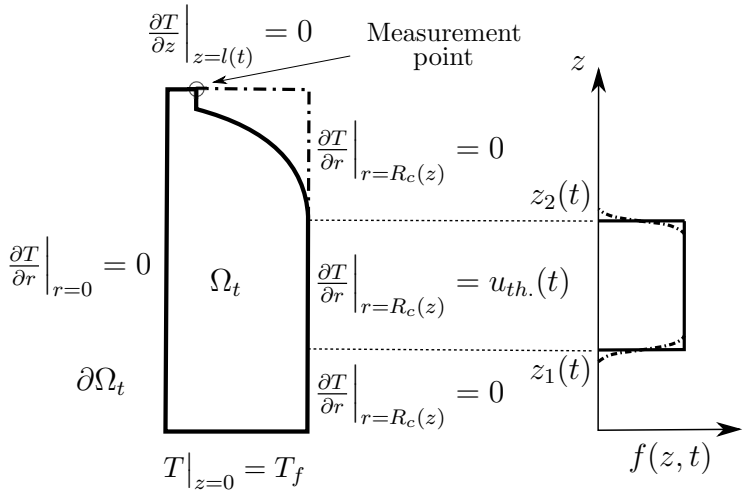

Figure 3.2: Geometric approximation along with the boundary conditions are given in left figure side, and the actuation profile function, $f(z,t)$ in Eq.3.39, is given in right figure side.

the PDE given as follows:

$$\frac{\partial x}{\partial t} = \frac{1}{r}\frac{\partial}{\partial r}\left(k_0 r \frac{\partial x}{\partial r}\right) + k_0 \frac{\partial^2 x}{\partial z^2} - V_z(t)\frac{\partial x}{\partial z} \tag{3.25}$$

where $k_0 = 1/Pe$ and $V_z(t)$ is the bulk movement velocity along the axial direction. The thermal conductivity ratio is equal to one for the crystal, $k_r = k_s/k_s = 1$.

The boundary conditions along with the boundary actuation are shown in Fig.3.2. The control actuation is placed at the crystal boundary and assumed to be at a fixed height from the crucible, which means that the actuation location changes with respect to the crystal as it grows. Solidification happens at the melt-solid interface and the temperature is assumed to be the solidification temperature at this boundary. Hence that this boundary condition at the interface decouples the heat transfer in the crystal and the melt. Moreover, the process is axisymmetric (no flux at $r = 0$) and at all other boundaries, the zero flux condition is assumed. The boundary conditions

are given as:

$$x\Big|_{z=0} = 0\,; \qquad \frac{\partial x}{\partial z}\Big|_{z=l(t)} = 0\,; \qquad \frac{\partial x}{\partial r}\Big|_{r=0} = 0 \tag{3.26}$$

$$\frac{\partial x}{\partial r}\Big|_{r=R_c(z),\, z<z_1(t)} = 0\,; \; \frac{\partial x}{\partial r}\Big|_{r=R_c(z),\, z>z_2(t)} = 0\,; \; \frac{\partial x}{\partial r}\Big|_{r=R_c(z),\, z_1(t)<z<z_2(t)} = \frac{Q(t)}{Pe} = u_{th.}(t) \tag{3.27}$$

where $R_c(z)$ and $l(t)$ are the crystal radius and length, respectively; $Q(t)$ is the heat flux from heaters; $z_1(t)$ and $z_2(t)$ indicate the spatial interval where the heater is placed, and $R_c(z)$, $l(t)$, $z_1(t)$ and $z_2(t)$ are determined from the crystal growth dynamics given by Eq.3.12 and the height of the melt in crucible is given by Eq.3.3. The Dirichlet boundary condition at the melt/solid interface to decouple the heat transfer in the solid crystal from the melt temperature(Ng and Dubljevic, 2012; Ng et al., 2013; Armaou and Christofides, 2001a). The initial condition for temperature distribution $x(r, z, 0)$ is the equilibrium temperature distribution over the crystal. The temperature evolution model of the grown crystal consist of a parabolic PDE model (Eq.3.25) along with boundary conditions (Eqs.3.26-3.27).

For temperature estimation or control purposes, one needs to consider coupled ODE-PDE equations given by Eqs.3.12 and 3.25-3.27. The coupling between ODE and PDE systems is through the PDE's spatial domain which is determined by the crystal's radius and length evolution.

3.3.1 Parabolic PDE model representation

Parabolic PDEs can be modelled and numerically solved by the Finite Difference Method (FDM) and/or Finite Element Method (FEM) (Reddy, 2004). Despite the accuracy of numerical solutions by FDM and FEM, due to the large scale numerical re-

alizations of these methods, they are not suitable for model based control/estimation purposes. Spectral methods (e.g. Galerkin's method) allow parabolic PDEs to be reduced to a low-order dynamic system representation which can be easily used for control synthesis (Curtain and Zwart, 1995). In order to obtain a low-order model, we utilize a general operator representation of the parabolic PDE system. In particular, the infinite-dimensional representation of a parabolic PDE on the time invariant domain can serve as basis for appropriately defined approximations on the time-varying domain within parabolic PDE representation setting. However, the use of the operators and defining Hilbert space needs to be carefully considered. The idea is to utilize already existing methods and formulations of parabolic PDEs for fixed domains, and to assure that we can consider a slow grown crystal domain evolution as a large set of well defined fixed domains that can take standard form of well defined Hilbert spaces. In particular, let $\Omega_t \in \mathbb{R}^2$ be the spatial domain of the crystal at time instance $t \in [0, T]$, and $\partial\Omega_t$ be the boundary of the domain Ω_t (rectangular boundary as shown in Fig.3.2). In order to define the appropriate basis, we define Ω as the union of all possible domains in $t \in [0, T]$ given as (Ng et al., 2013):

$$\Omega = \bigcup_{t\in[0,T]} \Omega_t \times \{t\} \tag{3.28}$$

Note that, Ω is a fixed open set in $\mathbb{R}^2$ with smooth boundary $\partial\Omega$ such that $\Omega_t \subset \Omega$ for all $t \in [0, T]$. Assume $\{\phi_i(\xi, t)\}$ is a family of orthonormal functions defined on a subset Ω_t for every $t \in [0, T]$ and forms a basis of $L^2(\Omega_t)$. In order to define a set of eigenfunctions for Ω, we define the complement of Ω_t as Ω_t^c in the fixed domain Ω,

the functions $\{\phi_i(t)\}$ can be extended to the fixed domain Ω as follow:

$$\phi(\xi,t) = \begin{cases} \phi(\xi) & \text{for } \xi \in \Omega_t \ , \\ 0 & \text{for } \xi \in \Omega_t^c \end{cases} \tag{3.29}$$

where Ω_t^c is the complement of Ω_t in Ω. The inner product on $L^2(\Omega)$, is defined as:

$$\langle \phi(t), \psi(t) \rangle_{L^2(\Omega)} = \int_\Omega \phi(\xi,t)\psi(\xi,t)d\xi = \int_{\Omega_t} \phi(\xi)\psi(\xi)d\xi = \langle \phi(t), \psi(t) \rangle_{L^2(\Omega_t)} \tag{3.30}$$

Implementing the formulation given by Eqs.3.28-3.30, the parabolic PDE model, given by Eq.3.25, along with boundary conditions, given by Eqs.3.26-3.27, is written in the state space formulation following the formulation given by Curtain and Zwart (1995) as:

$$\frac{\partial x(t)}{\partial t} = \mathfrak{A}(t)x(t) \tag{3.31}$$

$$\mathfrak{B}(t)x(t) = [0, u_{th.}(t), 0]^T \tag{3.32}$$

where $x(t) \in L^2(\Omega)$ is the state of the system. The operator $\mathfrak{A}(t)$ is given by:

$$\mathfrak{A}(t) = \frac{1}{r}\frac{\partial}{\partial r}\left(k_0 r \frac{\partial}{\partial r}\right) + k_0 \frac{\partial^2}{\partial z^2} - V_z(t)\frac{\partial}{\partial z} \tag{3.33}$$

with the domain:

$$\begin{aligned} D(\mathfrak{A}(\mathfrak{t})) = \{\phi \in L^2(\Omega) : \phi, \frac{\partial \phi}{\partial z}, \frac{\partial \phi}{\partial r} \ \ are \ \ a.c. \ \ and \ \mathfrak{A}(t)\phi \in L^2(\Omega) \\ \phi(0,z,t) = 0, \ \frac{\partial \phi}{\partial r}(r,0,t) = 0, \frac{\partial \phi}{\partial r}(r,l(t),t) = 0\} \end{aligned} \tag{3.34}$$

where a.c. means absolutely continuous, $l(t)$ and $R_c(z)$ are the crystal length and radius, respectively. The boundary operator $\mathfrak{B}(t) : L^2(\Omega) \rightarrow \mathbb{R}^3$ represents the boundary conditions in Eq.3.27 and is given by:

$$\mathfrak{B}(t)\phi = \begin{bmatrix} \frac{\partial \phi}{\partial r}\Big|_{r=R_c(z),\, z<z_1(t)} \\ \frac{\partial \phi}{\partial r}\Big|_{r=R_c(z),\, z>z_2(t)} \\ \frac{\partial \phi}{\partial r}\Big|_{r=R_c(z),\, z_1(t)<z<z_2(t)} \end{bmatrix} \tag{3.35}$$

The transformation, $p(t) = x(t) - b(r, z, t)u_{th.}(t)$, with function $b(r, z, t)$ satisfying,

$$\mathfrak{B}(t)b(r, z, t)u_{th.}(t) = [0, u_{th.}(t), 0]^T \tag{3.36}$$

transfers the PDE model, Eqs.3.25-3.27, to the following PDE with in-domain actuation:

$$\frac{dp(t)}{dt} = \mathcal{A}p(t) + \mathcal{A}b(t)u_{th.}(t) - b(t)\dot{u}_{th.}(t) - \dot{b}(t)u_{th.}(t) \tag{3.37}$$

where the new $\mathcal{A}(t)$ operator is defined as:

$$\mathcal{A}(t) = \frac{1}{r}\frac{\partial}{\partial r}\left(k_0 r \frac{\partial}{\partial r}\right) + k_0 \frac{\partial^2}{\partial z^2} - V_z(t)\frac{\partial}{\partial z} \tag{3.38}$$

with the domain $D(\mathcal{A}(t)) = D(\mathfrak{A}(t)) \bigcap \ker\ \mathfrak{B}(t)$.

The spatial actuation profile function $b(r, z, t)$ satisfying Eq.3.36 is not unique and it only requires to satisfy Eq.3.36. In this chapter, $b(r, z, t)$ is considered as the following function:

$$b(r, z, t) = \frac{r^2}{2R_{c.i.}(t)} f(z, t) + \frac{z^2 - 2l(t)z}{l(t)^2} \tag{3.39}$$

In Eq.3.39, $R_{c.i.}(t)$ and $l(t)$ are time-varying and are determined by the growth dynamics, from Eqs.3.12, while $f(z,t)$ is the actuation profile at the boundary in axial direction, which indicates the interval that reflects input flux to the system (see Fig.3.2).

3.3.2 Low dimensional model

The PDE represented by Eq.3.25 along with boundary conditions in Eqs.3.26-3.27 is transformed into Eq.3.37 using the transformation $x(t) = p(t) + b(r,z,t)u_{th.}(t)$. In order to reduce the infinite-dimensional representation of the process to a finite-dimensional model, Galerkin's method is used where only a finite number of eigenfunctions is used to describe the PDE state.

The eigenvalue problem, $\mathcal{A}(t)\Phi = \lambda(t)\Phi$, is considered with homogenous boundary conditions:

$$\Phi(0,r,t) = 0\,; \qquad \frac{\partial \Phi}{\partial z}\Big|_{z=l(t)} = 0$$
$$\frac{\partial \Phi}{\partial r}\Big|_{r=0} = 0\,; \qquad \frac{\partial \Phi}{\partial r}\Big|_{r=Rc(t)} = 0$$

Solving the eigenvalue problem for the radial and axial directions yield to a family of time-parametrized eigenfunctions, $\phi_m(z,t), \psi_n(r,t)$:

$$\phi_m(z,t) = \left(\frac{l(t)}{2} - \frac{\sin\left(2\alpha_m l(t)\right)}{4\alpha_m}\right) e^{\frac{V_z(t)z}{2k_0}} \sin(\alpha_m z) \tag{3.40}$$

where α_m is the m-th root of the transcendental equation:

$$\tan(\alpha_m l(t)) = -\frac{2k_0}{V_z}\alpha_m \tag{3.41}$$

and,

$$\psi_n(r,t) = \frac{\sqrt{2}}{Rc(t)J_0(\beta_n)} J_0(\beta_n r/Rc(t)) \tag{3.42}$$

where $J_0(r)$ is the Bessel function of the first kind and zero order, and β_n is the n-th root of the $J_1(\beta_n) = 0$. The corresponding eigenvalues are:

$$\lambda_{mn}(t) = -k_0(\alpha_m^2 + \beta_n^2) - \frac{1}{2}k_0^{-1}\frac{V_z(t)^2}{2} \tag{3.43}$$

with corresponding functions:

$$\Phi_{mn}(r,z,t) = \phi_m(z,t)\psi_n(r,t) \tag{3.44}$$

The weighted norm over the spatial domain is defined as:

$$\langle \phi_i, \psi_j \rangle_\sigma = \int_\Omega \phi_i(z,t)\psi_j(r,t)\sigma(r,z,t)d\Omega \tag{3.45}$$

where $\sigma(r,z,t)$ is defined as:

$$\sigma(r,z,t) = \sigma_r(r)\sigma_z(z) = re^{-\frac{V_z(t)}{k}z} \tag{3.46}$$

such that the operator is self-adjoint with respect to $\sigma(r,z,t)$.

Then, from Eq.3.37, we can obtain an extended state space system, with state $p^e(t) = [u_{th.}(t), p(t)^T]^T$, on the extended Hilbert space, $H^e = H \bigoplus R$ which leads to the following time-varying boundary control problem:

$$\frac{dp^e(t)}{dt} = \begin{bmatrix} 0 & 0 \\ \mathcal{A}(t)b(t) - \dot{b}(t) & \Lambda(t) + \Delta(t) \end{bmatrix} \begin{bmatrix} u_{th.}(t) \\ p(t) \end{bmatrix} + \begin{bmatrix} 1 \\ -b(t) \end{bmatrix} \tilde{u}_{th.}(t) \tag{3.47}$$

$$= A^e(t)p^e(t) + B^e(t)\tilde{u}_{th.}(t)$$

$$y = T(r,z,t) = C^e(t)p^e \tag{3.48}$$

where $p^e = [u_{th.}(t) \quad p^T]^T$ is the extended state, $\tilde{u}_{th.}(t) = \dot{u}_{th.}(t)$, $\Lambda(t)$ is associated with the eigenvalues of $\mathcal{A}(t)$ and $\Delta(t)$ is associated with the time-varying effects of the eigenfunctions. $y = T(r,z,t)$ is the system output, where $C^e(t)$ is the output operator which denotes the output measurements. $\Delta(t)$ is expressed as follows:

$$\Delta(i,j) = \langle \Phi_i, \frac{\partial \Phi_j}{\partial t} \rangle_\sigma \tag{3.49}$$

Eq.3.47 is the infinite-dimensional representation of the parabolic PDE of Eq.3.37, accounting for the time-varying domain geometry. The process model in Eq.3.47 has eigenvalues given by the $\Lambda(t)$ which may be perturbed by $\Delta(t)$ terms evolution. Therefore, the time-varying domain effects, $\Delta(t)$, can influence diagonal matrix $\Lambda(t)$. In the next section, it is demonstrated that the matrix $\Delta(t)$ is diagonal with negative entries implying that the time-varying domain will not destabilize the system. From Eq.3.47, one concludes that the process is driven by the derivative of input and through the boundary actuation transformation $b(t)$.

3.3.3 Effect of time-varying domain

It can be shown that the effects of the time-varying domain result in off-diagonal terms evolution given in Eqs.3.47-3.49. Careful inspection of the inner product in Eq.3.49 reveals that after a finite time passed, the off-diagonal terms will vanish. In order to calculate $\langle \Phi_i, \frac{\partial \Phi_j}{\partial t} \rangle_\sigma$, assume, $\Phi_i(r,z,t) = \phi_m(z,t)\psi_n(r,t)$ and $\Phi_j(r,z,t) = \phi_q(z,t)\psi_s(r,t)$, where m,n,q,s are integer numbers according to Eq.3.44. $\Delta(i,j)$

given by Eq.3.47 is written as:

$$\Delta(i,j) = \langle \Phi_i, \frac{\partial \Phi_j}{\partial t} \rangle_\sigma = \langle \phi_m, \phi_q \rangle_{\sigma_z} \langle \psi_n, \frac{\partial \psi_s}{\partial t} \rangle_{\sigma_r} + \langle \phi_m, \frac{\partial \phi_q}{\partial t} \rangle_{\sigma_z} \langle \psi_n, \psi_s \rangle_{\sigma_r} \tag{3.50}$$

The eigenfunctions in each direction (radial or axial) are orthonormal and then the inner product in Eq.3.50 can be written as:

$$\Delta(i,j) = \begin{cases} 0 & \text{if} \quad m \neq q \ \ \& \ \ n \neq s \\ \langle \psi_n, \frac{\partial \psi_s}{\partial t} \rangle_{\sigma_r} & \text{if} \quad m = q \ \ \& \ \ n \neq s \\ \langle \phi_m, \frac{\partial \phi_q}{\partial t} \rangle_{\sigma_z} & \text{if} \quad m \neq q \ \ \& \ \ n = s \\ \langle \phi_m, \frac{\partial \phi_q}{\partial t} \rangle_{\sigma_z} + \langle \psi_n, \frac{\partial \psi_s}{\partial t} \rangle_{\sigma_r} & \text{if} \quad m = q \ \ \& \ \ n = s \end{cases} \tag{3.51}$$

In order to explore the influence of the terms contained in $\Delta(t)$ on the model dynamics given by Eq.3.47, the eigenfunctions are investigated. Namely, in the case when the radius controller provided in Eq.3.18 stabilizes the crystal at a desired constant radius such that it can be assumed that $\dot{R}_{c.i.}(t) \to 0$, and which leads according to Eq.3.13, to the constant crystal growth rate $\dot{l}(t)$. Consequently, the constant crystal radius in Eq.3.42 results in time-invariant eigenfunctions in radial direction such that:

$$\langle \psi_n, \frac{\partial \psi_s}{\partial t} \rangle_{\sigma_r} = 0 \tag{3.52}$$

In order to calculate the remaining terms in Eq.3.51, the roots of Eq.3.41 are approximated by $\alpha_m = \frac{1}{l(t)}(m\pi - \frac{\pi}{2})$ (see Fig.3.3). The eigenfunctions in Eq.3.40 can then be simplified as:

$$\phi_m(z,t) = \frac{l(t)}{2} e^{\frac{V_z(t) z}{2k_0}} \sin(\alpha_m z) \tag{3.53}$$

and the remaining term in Eq.3.51, $\langle \phi_m, \frac{\partial \phi_q}{\partial t} \rangle_{\sigma_z}$, is calculated analytically as follows:

$$\langle \phi_m, \frac{\partial \phi_q}{\partial t} \rangle_{\sigma^z} = \frac{1}{2} V_z(t) \int_0^{l(t)} sin(\alpha_m z) sin(\alpha_q z) dz + \frac{1}{2} l(t) \dot{\alpha}_q(t) \int_0^{l(t)} sin(\alpha_m z) cos(\alpha_q z) z dz \tag{3.54}$$

which leads o:

$$\langle \phi_m, \frac{\partial \phi_q}{\partial t} \rangle_{\sigma_r} = -\frac{V_z(t) l(t)}{8} \delta_{mq} \tag{3.55}$$

where, $l(t)$ and $V_z(t)$ are crystal length and pulling velocity, respectively and δ_{mq} is the Kronecker delta. The time-varying effect represented by $\Delta(i, j)$ is reduced to a diagonal matrix using Eqs.3.51-3.55 and the eigenvalues of the system represented in Eq.3.47, $\lambda_i^e(t)$ are expressed as $\lambda_i^e(t) = \lambda_i(t) - \frac{V_z(t) l(t)}{8}$. This diagonal form of the infinite dimensional representation of temperature dynamics allows for decoupling between slow and fast modal states and provides a basis for model reduction of dissipative systems represented by parabolic PDEs. In other words, a few slow modes can be chosen to model the temperature dynamics with high accuracy.

3.4 Observer design and temperature estimation

The finite dimensional representation of the temperature dynamics, given by Eq.3.47, is used for temperature estimation. Temperature measurements are available at crystal boundaries and can be used to reconstruct the temperature field over the entire domain using a few most dominant and slow modes.

It can be shown that point temperature measurements at boundary with the Neumann boundary condition is enough for the entire temperature profile reconstruction. Assume the measurements are carried out at point (r^*, z^*). Then the temperature

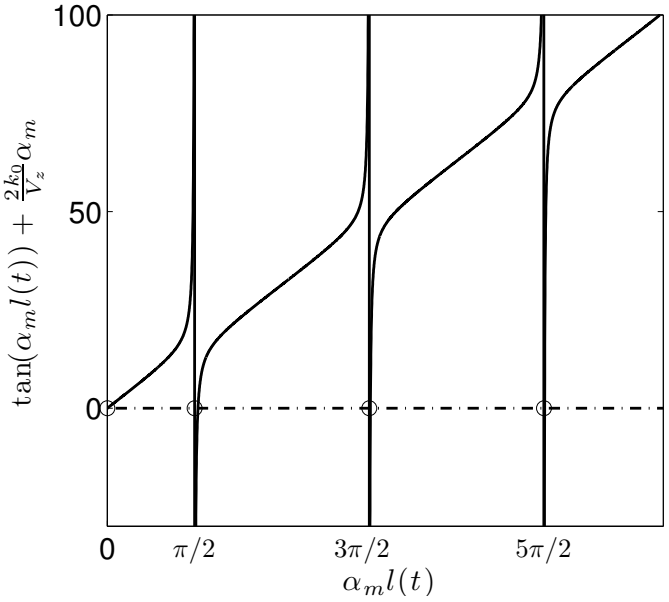

Figure 3.3: Roots of Eq.3.41 are shown to be approximated by $m\pi - \frac{\pi}{2}$.

measurement, $x(r^*, z^*, t)$, can be written as follows:

$$x(r^*, z^*, t) = b(r^*, z^*, t)u_{th.}(t) + \sum_{i=1}^{\infty} p_i \Phi_i(r^*, z^*, t) = C^e(t)p^e(t) \tag{3.56}$$

where $b(r^*, z^*, t)$ is the boundary transformation function in Eq.3.39, $u_{th.}(t)$ is the heat flux input, p_i is the i-th mode, $\Phi_i(r^*, z^*, t)$ is the i-th eigenfunction evaluated at the measurement point, $p^e(t)$ is the extended state vector and $C^e(t)$ is the output operator defined as follow:

$$C^e(t) = [b(r^*, z^*, t), \quad \Phi_1(r^*, z^*, t), \quad \Phi_2(r^*, z^*, t), \ldots] \tag{3.57}$$

Since the input $u_{th.}(t)$ is known, the approximate observability matrix, $\mathcal{O}^{N+1} = [C^{eT}, A^{eT}C^{eT}, ...]^T$, for the system given by Eq.3.47, for the first N modes is reduced and can be expressed as Eq.3.58. Note that, as $u_{th.}(t)$ is known and measurable,

$rank(\mathcal{O}^{N+1}) = rank(\mathcal{O}^N) + 1.$

$$\mathcal{O}^N = [C^T, A^T C^T, ..., A^{N-1^T} C^T]^T \tag{3.58}$$

where $C = [\Phi_1, \quad \Phi_2, \ldots, \quad \Phi_N]_{(r^*,z^*,t)}$ and $A = \Lambda(t) - \frac{V_z(t)l(t)}{8} I$. Using a linear transformation, the matrix $\mathcal{O}^N$ can be transformed into $[C^T, \Lambda^T C^T, ..., \Lambda^{N-1^T} C^T]^T$ which has the same rank as $\mathcal{O}^N$:

$$rank(\mathcal{O}^N) = rank \begin{pmatrix} \Phi_1 & \Phi_2 & \ldots & \Phi_N \\ \lambda_1\Phi_1 & \lambda_2\Phi_2 & \ldots & \lambda_1\Phi_N \\ \vdots & \vdots & \ddots & \vdots \\ \lambda_1^{N-1}\Phi_1 & \lambda_2^{N-1}\Phi_2 & \ldots & \lambda_1^{N-1}\Phi_N \end{pmatrix}_{(r^*,z^*,t)}$$

The observability matrix is full rank if the eigenvalues do not vanish at the measurement point. Therefore, a single measurement at the boundary with the Neumann condition will suffice to satisfy the approximate observability condition. Note that the observability matrix for the parabolic PDE with time-varying domain reduces to the standard approximate observability matrix (see Ray (1981)).

In order to accomplish model order reduction, modal decomposition is used to model the parabolic PDE, given by Eq.3.24, and reduce the temperature evolution to a low dimensional ODE. As expected in the case of parabolic PDEs, the few most dominant modes of the system can reconstruct the temperature profile with high accuracy. Furthermore, a Luenberger observer is used to estimate the most dominant modes and to reconstruct the temperature profile. In order to make relevant comparison with our findings, we also develop a high fidelity FEM model of the crystal growth PDE as our plant. The FEM model is constructed on the realistic and non-cylindrical

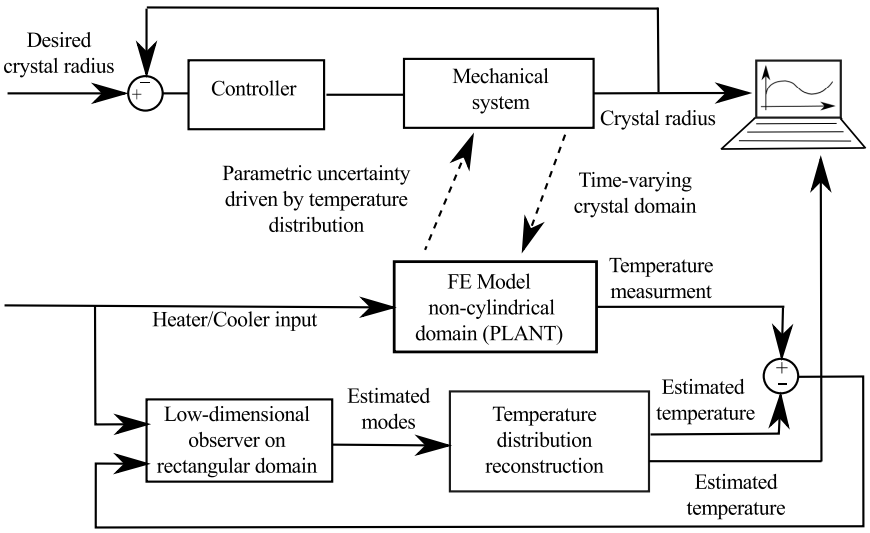

Figure 3.4: Temperature distribution reconstruction algorithm and the coupling between crystal growth and temperature dynamics.

crystal geometry with boundary actuation. A mesh moving scheme is utilized to discretize the time-varying domain to develop the FEM model of the process. A point measurement is used for the state reconstruction and is taken at the crystal boundary (shown in Fig.3.2). In our simulation studies and analysis temperature measurement from the FEM model is fed back to the observer and the temperature distribution is reconstructed. The estimation strategy is shown in Fig.3.4. The Luenberger observer is utilized given as follow:

$$\frac{d\hat{p}^e(t)}{dt} = A^e(t)\hat{p}^e(t) + B^e(t)\tilde{u}_{th.}(t) + L(t)\big(y(t) - \hat{y}(t)\big) \tag{3.59}$$

where $A^e(t)$, $B^e(t)$ are given in Eq.3.47. $L(t)$ is the observer gain and is evaluated at each time step in order to place the eigenvalues of the error dynamics, $A^e(t) - L(t)C^e(t)$, at pre-specified values.

The proposed observer estimates the temperature distribution evolution in grown

crystal and in order to utilize the reconstructed temperature distribution for feedback control purposes, we need to explore the separation principle to ensure the stability of the closed loop process when output regulation -which includes the gain based feedback and observer- is employed. We assume that there exists a stabilizing control law $u_{th.}(t) = -Fp(t)$ for the temperature distribution model, given by:

$$\frac{d}{dt}\begin{pmatrix} u_{th.}(t) \\ p(t) \end{pmatrix} = \begin{pmatrix} 0 & 0 \\ \mathfrak{A}(t)\mathcal{B}(t) & \mathcal{A}(t) \end{pmatrix}\begin{pmatrix} u_{th.}(t) \\ p(t) \end{pmatrix} + \begin{pmatrix} I \\ -\mathcal{B}(t) \end{pmatrix}\tilde{u}_{th.}(t) \tag{3.60}$$

$$y = T(r,z,t) = \Big(\mathcal{C}(t)\mathcal{B}(t)\ \ \mathcal{C}(t)\Big)\begin{pmatrix} u_{th.}(t) \\ p(t) \end{pmatrix} \tag{3.61}$$

where $\mathfrak{A}(t)$, $\mathcal{A}(t)$, $\mathcal{B}(t)$ and $\mathcal{C}(t)$ are the operators introduced in Section 3.3.1. The proposed temperature estimation in Eq.3.59 is written as:

$$\frac{d\hat{p}(t)}{dt} = \mathcal{A}\hat{p}(t) + \mathfrak{A}\mathcal{B}u_{th.}(t) - \mathcal{B}\tilde{u}_{th.}(t) + L(t)\Big(y(t) - \mathcal{C}\hat{p}(t) - \mathcal{C}\mathcal{B}u_{th.}(t)\Big) \tag{3.62}$$

the time notation is not shown for a simpler representation. Substituting $u_{th.}(t) = -F\hat{p}(t)$, the actual and estimated modes are given by:

$$\frac{dp(t)}{dt} = \mathcal{A}p(t) - \mathfrak{A}\mathcal{B}F\hat{p}(t) + \mathcal{B}F\dot{\hat{p}}(t) \tag{3.63}$$

$$\frac{d\hat{p}(t)}{dt} = \mathcal{A}\hat{p}(t) - \mathfrak{A}\mathcal{B}F\hat{p}(t) + \mathcal{B}F\dot{\hat{p}}(t) + L\mathcal{C}(p(t) - \hat{p}(t)) \tag{3.64}$$

Assuming the error $e(t) = p(t) - \hat{p}(t)$, Eqs.3.63-3.64 can be written as:

$$\big[I - BF\big]\dot{\hat{p}}(t) = \big[\mathcal{A} - \mathfrak{A}\mathcal{B}F\big]\hat{p}(t) + L\mathcal{C}e(t)$$
$$\dot{e}(t) = \big[\mathcal{A} - L\mathcal{C}\big]e(t)$$

or alternatively as:

$$\dot{p}(t) = \Gamma^{-1}\Big[\mathcal{A} - \mathfrak{A}\mathcal{B}F\Big]p(t) + \Big[\big(I - \Gamma^{-1}\big)\big(\mathcal{A} - L\mathcal{C}\big) + \Gamma^{-1}\mathfrak{A}\mathcal{B}F\Big]e(t)$$
$$\dot{e}(t) = \Big[\mathcal{A} - L\mathcal{C}\Big]e(t)$$

where $\Gamma = (I - \mathcal{B}F)$. The unified closed loop system is given by:

$$\begin{pmatrix}\dot{p}(t)\\ \dot{e}(t)\end{pmatrix} = \begin{pmatrix}\Gamma^{-1}\big(\mathcal{A} - \mathfrak{A}\mathcal{B}F\big) & \big(I - \Gamma^{-1}\big)\big(\mathcal{A} - L\mathcal{C}\big) + \Gamma^{-1}\mathfrak{A}\mathcal{B}F\\ 0 & \mathcal{A} - L\mathcal{C}\end{pmatrix}\begin{pmatrix}p(t)\\ e(t)\end{pmatrix} \tag{3.65}$$

The operators $\mathcal{A}$ and $\mathfrak{A}$ are identical operators with different domains, however, $D(\mathcal{A}) \subset D(\mathfrak{A})$ and Eq.3.65 can be written as:

$$\begin{pmatrix}\dot{p}(t)\\ \dot{e}(t)\end{pmatrix} = \begin{pmatrix}\Gamma^{-1}\mathcal{A}\Gamma & \big(I - \Gamma^{-1}\big)\big(\mathcal{A} - L\mathcal{C}\big) + \Gamma^{-1}\mathfrak{A}\mathcal{B}F\\ 0 & \mathcal{A} - L\mathcal{C}\end{pmatrix}\begin{pmatrix}p(t)\\ e(t)\end{pmatrix} = \mathbb{A}\begin{pmatrix}p(t)\\ e(t)\end{pmatrix} \tag{3.66}$$

where the eigenvalues of the unified system, $\mathbb{A}$, are given as $\sigma(\mathbb{A}) = \sigma(\Gamma^{-1}\mathcal{A}\Gamma) \cup \sigma(\mathcal{A} - L\mathcal{C})$. Γ is assumed to be invertible and therefore $\sigma(\mathbb{A}) = \sigma(\mathcal{A}) \cup \sigma(\mathcal{A} - L\mathcal{C})$. Since the operator $\mathcal{A}$ is stable and the eigenvalues of $\mathcal{A} - L\mathcal{C}$ are placed at pre-specified locations, the unified closed loop system of control and state estimation, Eq.3.66, is stable and the separation principle holds. It is concluded that the proposed observer

can be utilized for state reconstruction in output feedback regulation frameworks.

3.5 Numerical simulation results

The proposed radius control and temperature reconstruction is simulated numerically and is validated by implementing on a FEM model of the process (see Fig.3.4). The considerations regarding numerical implementation and results of radius control and temperature reconstruction are explained in the following paragraphs. The parameters used for numerical simulation are presented in Table 3.1.

The FEM model of heat conduction in the crystal with non-cylindrical and time-varying domain is utilized as the plant in numerical simulations. The crystal domain movement is obtained from crystal radius and length evolution dynamics, Eqs.3.20-3.21, and a mesh moving scheme is utilized to discretize the time-varying geometry of the domain in developing the finite element model of the process. Due

Table 3.1: Physical and numerical parameters.

Parameter	Value	Dimensionless value
Solidification temperature, T_s	1430 ^oC	0
Crystal density, ρ_c	2420 kg/m^3	-
Scaled conductivity, k_0	-	0.025
Peclet number, Pe	-	0.1
Time scale	87 min	1
Sampling time	1 samples/min	0.01
Spatial discretization	-	40,100
Nominal crystal growth rate	5 cm/hour	-
ODE controller gain, K	0.005	-
Crucible radius, $R_{cruc.}$	7.3 cm	1
Initial crystal radius	3.5 cm	0.48
Desired crystal radius	5 cm	0.68
Initial crystal length	7.3 cm	1

to the fact that the evolution of the crystal domain is known from the crystal growth dynamics, the Arbitrary Lagrangian Eulerian (ALE) method (Reddy, 2004) is used to spatially discretize the domain of interest as shown in Fig.3.5a. The finite element mesh consists of 10×20 two-dimensional linear 4-node elements which discretizes spatial geometry to 220 degrees of freedom. The evolution of the time-dependent set of ordinary differential equations obtained from the finite element model is realized by first-order implicit time integration with the time step $dt = 0.01$.

The parabolic PDE, Eq.3.25, is represented by a finite dimensional model, Eq.3.37, using computational framework of the Galerkin's method. The Galerkin's method on a fixed domain is a well known method for order reduction of parabolic PDE equations, but in the case of a time-varying domain, few considerations should be taken into account. Temperature distribution evolution in growing crystal is represented by evolution of both the spectral modes, $p(t)$, and the basis eigenfunctions, $\Phi_i(r, z, t)$. Hence, due to the time-varying nature of the process, the basis eigenfunctions, obtained from eigenvalue problem, will be also time-varying. In order to integrate the modes in time and calculate the modes and temperature distribution evolution, the modes evolution are calculated on a fixed domain and then the resulting temperature distribution is mapped into the time evolved new geometry; then the modes are recalculated by simple projection on the new evolved geometry configuration. The algorithm used for numerical implementation of the Galerkin's method on the time-varying domain is given by Table 3.2. The geometry and temperature mappings between different domain configurations are carried out using a property preserving transformation which preserves the total thermal energy over the domain (see Fig.3.5b). The domain configuration is obtained from the crystal radius and length evolution. For a slow time-varying process, the geometry mapping between

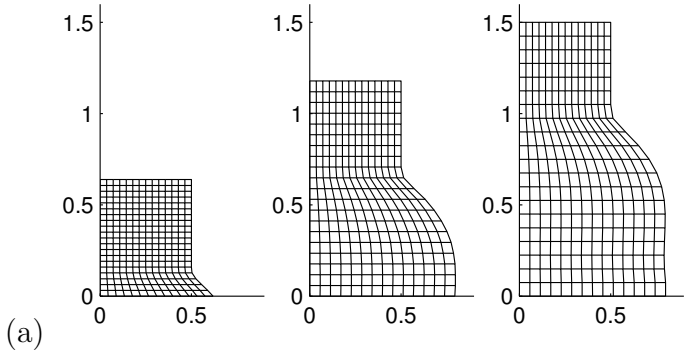

(a)

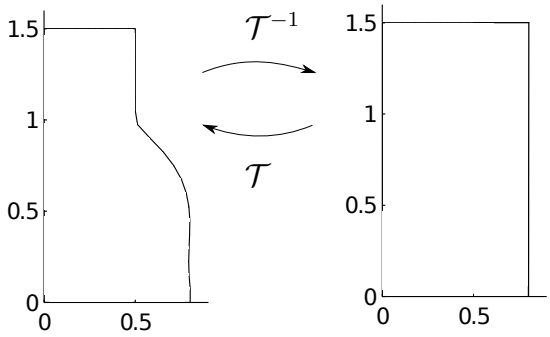

(b)

Figure 3.5: (a) Moving mesh used for FE analysis. (b) Galerkin's method and estimation performed on rectangular domain and the temperature distribution is mapped to the domain obtained from FEM.

different domain configurations, $\mathcal{T} : (r, z) \in \Omega_{t_0} \rightarrow (\hat{r}, \hat{z}) \in \Omega_t$, is assumed to be smooth and invertible and consequently, the temperature transformation is given as, $T_{\Omega_t}(r, z) = J^{-1} T_{\Omega_{t_0}}(r, z)$, where J^{-1} is the determinant of the inverse of the Jacobian matrix, $J = \partial(r, z)/\partial(\hat{r}, \hat{z})$.(Izadi and Dubljevic, 2013)

Since the heat flux is provided through an interval on the boundary, the actuation structure is described by a step function in the z direction, see Fig.3.2. This function is smoothed out using the sigmoid function to avoid discontinuity when transforming the temperature profile using the transformation $x(t) = p(t) + b(r, z, t)u_t h(t)$. Using the step-like function for actuation and boundary conditions, avoids the Neumann and Dirichlet boundary condition mismatch at corner points. Moreover, as aforementioned, the Galerkin decomposition and reduction of the PDE is carried out with the assumption that the domain is rectangular and the radius variation along the crystal is ignored.

In the Galerkin's method, the low dimensional model with twelve dominant modes is used for temperature simulation. Fig.3.6 shows the obtained first three eigenvalues using Galerkin's method compared to the most dominant eigenvalues of the finite element analysis. As it can be seen, the time-varying behaviour of eigenvalues are close enough to represent the model by the Galerkin's method. It can be inferred that refining the mesh size in FEM will decrease the deviation between eigenvalues obtained from these methods.

The estimation is carried out through the estimation of the dominant modes using reduced order model of temperature evolution dynamics. The number of modes to be used in temperature estimation is determined by the accuracy of the estimation and a minimum number of the modes is chosen. The first two dominant modes are used for temperature reconstruction. Hence, using in estimation more than two

Table 3.2: Numerical algorithm for implementation of Galerkin's method on time-varying domain.

$t = t_0$:	$p_i(t_0) = \langle T_{\Omega_{t_0}}(r, z, t_0), \Phi_i(r, z, t_0) \rangle$	Obtain the modes at t_0 on domain Ω_{t_0} by projecting temperature on $\Phi_i(r, z, t_0)$.
	$p^e(t_0 + \Delta t) = p^e(t_0) + (A^e(t_0)p^e(t_0) + B^e(t_0)\tilde{u}_{th.}(t_0))\Delta t$	Evolve the modes in time on domain configuration Ω_{t_0}.
	$T^{aux}_{\Omega_{t_0}}(r, z, t_0 + \Delta t) = \sum_{i=1}^{N} p_i(t_0 + \Delta t)\Phi_i(r, z, t_0)$	Obtain temperature distribution calculated on domain Ω_{t_0} using evolved modes.
	$\mathcal{T} : (r, z) \in \Omega_{t_0} \rightarrow (\hat{r}, \hat{z}) \in \Omega_{t_0+\Delta t}$	Obtain new domain configuration from growth dynamics.
	$T_{\Omega_{t_0+\Delta t}}(r, z, t_0 + \Delta t) = J^{-1} T^{aux}_{\Omega_{t_0}}(r, z, t_0 + \Delta t)$	Map the temperature distribution to new domain configuration $\Omega_{t_0+\Delta t}$.
$t = t_0 + \Delta t$:	$p_i(t_0 + \Delta t) = \langle T_{\Omega_{t_0+\Delta t}}(r, z, t_0 + \Delta t), \Phi_i(r, z, t_0 + \Delta t) \rangle$	Obtain the modes at $t_0 + \Delta t$ on domain configuration $\Omega_{t_0+\Delta t}$ by projecting temperature on $\Phi_i(r, z, t_0 + \Delta t)$

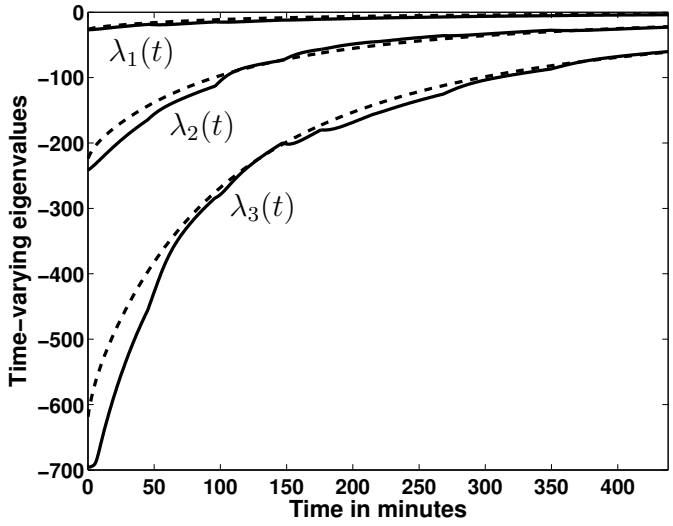

Figure 3.6: Time evolution of the most dominant eigenvalues in Galerkin method (dashed lines) compared to the few slowest eigenvalues of evolution matrix in Finite Element Analysis (solid lines).

modes does not significantly increases the estimation accuracy. The estimated modes (dashed lines) along with the actual modes obtained from reduced order model (solid lines) are shown in Fig.3.7. Further, the estimated temperature at two different points (dash-dotted black lines) are compared to temperatures obtained from the finite element analysis (solid black lines) and Galerkin's method (dashed black lines) are shown in Fig.3.8. As it can be seen, despite the inaccuracy of the reduced order model, estimated temperature asymptotically converges to the actual temperature. The deviation of the Galerkin's method from FEM is due to the present geometric uncertainty in the crystal domain.

The observer performance is evaluated in the case of a model-plant mismatch. The crystal radius used for observer design and the reduced order Galerkin's model are assumed to be different than the finite element numerical model realization. Two cases of -20% and +20% mismatch between radiuses in the observer and the plant are

considered and the temperature estimation results are shown in Fig.3.8. The black lines represent the case with no mismatch while red lines represent +20% mismatch (radius in observer is greater than the actual value) and blue lines represent the -20% mismatch. The reduced order Galerkin model's result and the estimated temperature are shown by dashed and dash-dotted lines, respectively. Fig.3.8 shows the estimation performance for both cases. As it can be seen the estimation is more accurate when a smaller crystal radius is considered in the observer design. This is due to the geometric uncertainty in the crystal shape which is assumed to be rectangular and considering smaller radius for the observer, slightly compensates for this geometric uncertainty and results in a better estimation.

The contour plots of the temperature distribution in the crystal at different time instances are shown in Fig.3.9. Column A shows the 3-D crystal shape along with the crystal radius evolution as the performance of the radius regulation and the temperature distribution. Column B, C and D show the FEM results, estimated temperature and the Galerkin's method simulation results, respectively. At $t = 0$, the temperature distribution in the crystal is unknown and an arbitrary initial condition is assumed for the observer. As it can be seen, the estimated temperature profile (column C) captures the temperature evolution of the FEM model (column B). There is a deviation of the results between FEM and Galerkin's method (column B and D, respectively) which is due to the uncertainties in the modeling, however the estimated temperature distribution shows high degree of agreement with the FEM results.

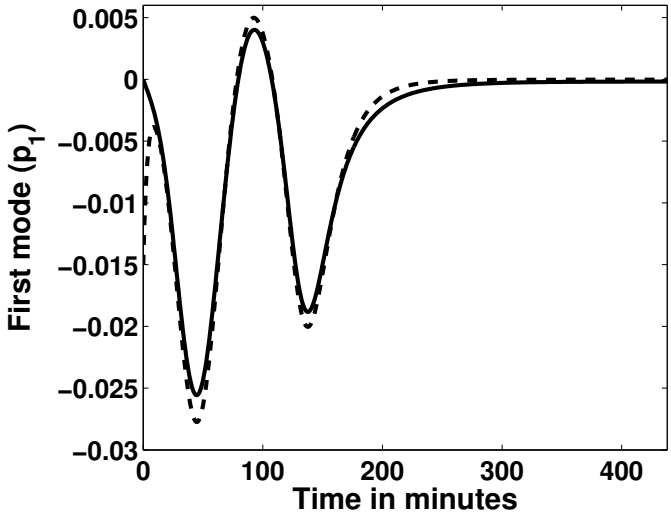

(a)

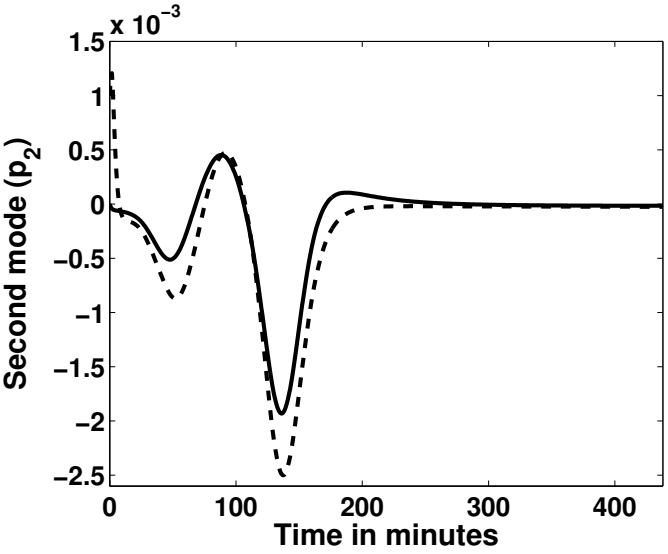

(b)

Figure 3.7: Estimated modes (dashed lines) compared to the actual modes (solid lines) for first two modes of the temperature evolution system.

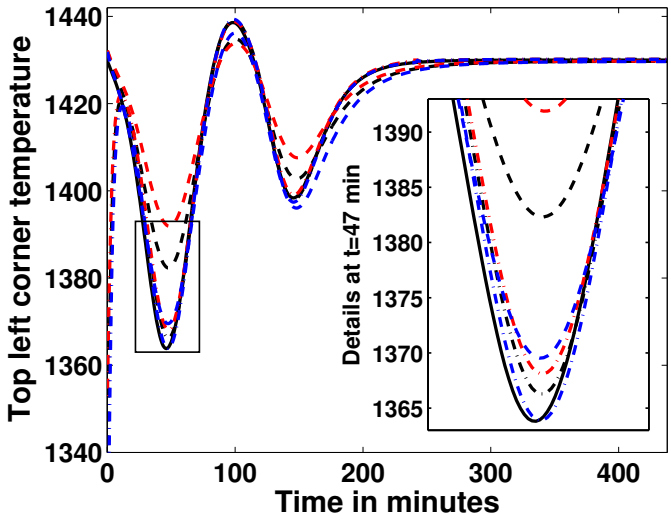

(a)

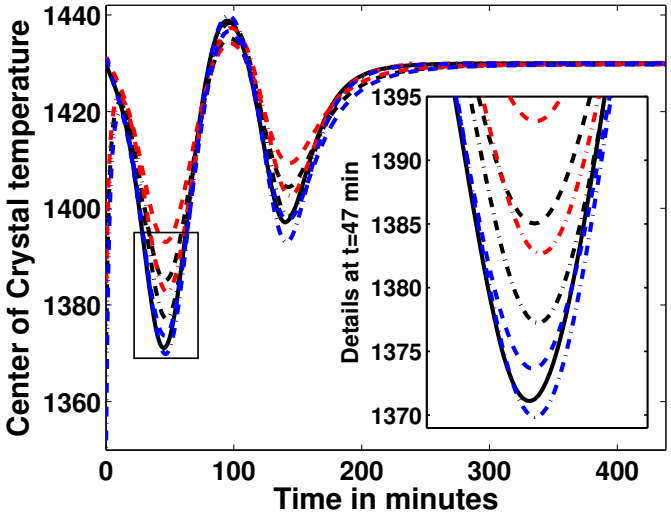

(b)

Figure 3.8: Estimated temperature at crystal boundary (a) and an in-domain point (b) - Solid lines represent the FEM results, open loop simulation results from Galerkin's method are presented by dashed lines, while dash-dotted lines show the estimated temperatures. Black lines represent the case with no mismatch in crystal radius in the FEM and the observer model, blue and red lines demonstrate the case with smaller and larger crystal radius in the observer model than the FEM, respectively.

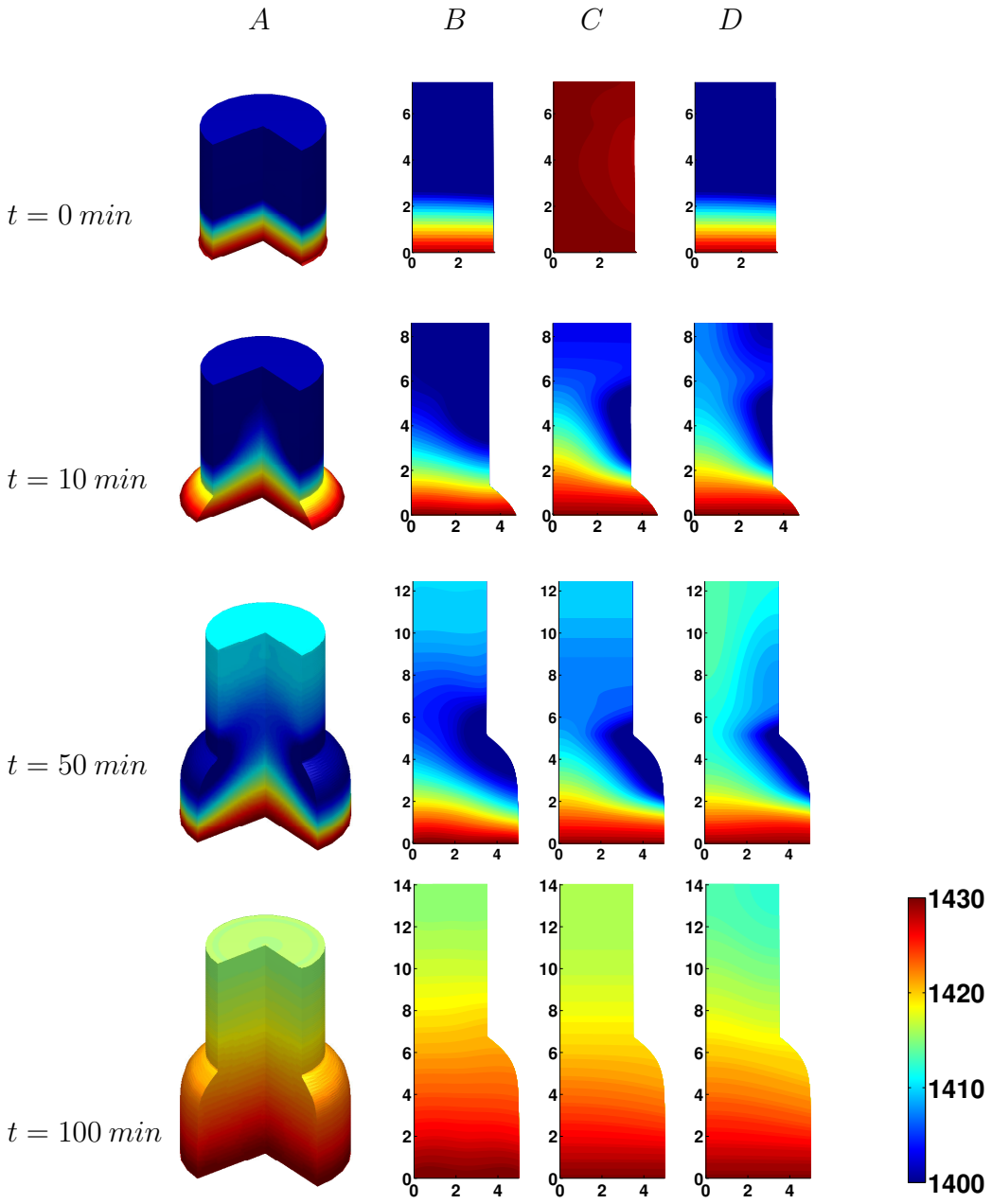

Figure 3.9: Snapshots at different time instances ($t = 0$; 10; 50 and 100 minutes), Column A: 3-D FE simulation of the temperature distribution evolution in the crystal; B: 2-D FEM results; C: Reconstructed temperature distribution; D: Open loop Galerkin's method numerical simulation for comparison with FEM. Note that the initial temperature distribution is not known for the observer at time zero.

3.6 Conclusions

The coupled model of crystal growth and temperature distribution evolution in the Cz crystallization process is provided to describe the radius and temperature evolution in a time-varying domain. The computational framework of the Galerkin's method is implemented for order reduction and consequently for a low dimensional observer synthesis. The parametric uncertainty in the crystal growth dynamics and geometric uncertainty in parabolic PDE of heat conduction are taken into account in the synthesis of the radius regulation and estimation of temperature distribution in the growing crystal. The observer utilizes boundary temperature measurement to reconstruct the crystal temperature distribution over the entire domain and finally the obtained reduced order model and the observer is implemented and validated on a numerically realized finite element model of the Cz crystal growth process. The achieved results show that despite a parametric uncertainty in the crystal growth rate, the geometrical uncertainty in the modelling, time-varying parameters and domain, the reduced order model can be utilized to reconstruct temperature distribution over the entire crystal domain.

Since the temperature gradients during the crystallization process have a significant impact on the grown crystal quality, the reconstructed temperature distribution over the entire crystal domain can be used as a soft sensor for crystal quality monitoring purposes. Moreover, in order to synthesize a temperature regulation or output feedback controller, the on-line knowledge of the temperature distribution is necessary. The developed framework can be utilized as estimation algorithm along with an output tracking control framework to track a desired temperature distribution profile to guarantee the process stability and crystal quality during the crystallization

process.

3.7 Notations

α_0 : capillary angle

α_c : growth angle

Δ : matrix of time-varying effects in eigenvalues

ΔH : latent heat

ϵ : ratio corresponding to uncertainty in crystallization rate

Λ : matrix of eigenvalues

λ_{mn} : eigenvalues of the heat equation

Φ_l : heat flux at the interface in the melt

Φ_s : heat flux at the interface in the solid crystal

Φ_{mn} : eigenfunction of the heat equation

ρ_c : crystal density

ρ_l : liquid silicon density

a : Laplace constant

$b(r, z, t)$: boundary actuation transformation

C_p : heat capacity

C_{growth} : volumetric growth rate

D : bound on the crystallization uncertainty

d : uncertainty in volumetric crystallization rate

$f(z, t)$: actuation profile

F_{ext} : External pulling force

$F_{Y.L.}$: Young-Laplace force

g : gravitational constant

h : total height of crystal from bottom of crucible

h_1 : melt height in crucible

h_2 : total length of

K : control gain

k_0 : $1/Pe$

k_r : relative thermal conductivity

k_s : regional thermal conductivity

l : crystal length

M_c : crystal mass

p : transformed temperature distribution

p^e : extended states of the heat equation

Pe : Peclet number

Q : heater input

R_c : crystal radius as a function of crystal length

R_d : reference crystal radius

$R_{c.i.}$: crystal radius at the interface

$R_{cruc.}$: crucible radius

$u_{mech.}$: mechanical input

$u_{th.}$: thermal input

v_0 : nominal growth velocity

V_c : crystal volume

v_c : average crystal velocity

V_l : liquid volume

V_m : meniscus volume

V_t : total solid and molten silicon volume

V_z : crystal pulling rate

V_{c0} : initial crystal volume

x : temperature distribution

x_1 : crystal length

x_2 : growth velocity

x_3 : crystal volume

z_1 : heater location, bottom

z_2 : heater location, top

3.8 References

Abdollahi, J., Dubljevic, S., 2013. Crystal radius and temperature regulation in czochralski crystallization process, in: American Control Conference (ACC), pp. 1626–1632.

Armaou, A., Christofides, P., 2001a. Crystal temperature control in Czochralski crystal growth process. AIChE Journal 47, 79–106.

Armaou, A., Christofides, P.D., 2001b. Robust control of parabolic PDE systems with time-dependent spatial domains. Automatica 37, 61–69.

Balas, M.J., 1986. Finite-dimensional control of distributed parameter systems by Galerkin approximation of infinite dimensional controllers. Journal of Mathematical Analysis and Applications 114, 17–36.

Bensoussan, A., Prato, G., Delfour, M., Mitter, S., 2007. Representation and Control of Infnite Dimensional Systems. Springer.

Brown, R., 1988. Theory of transport processes in single crystal growth from the melt. AIChE Journal 34, 881–911.

Cao, J., Gao, Y., Chen, Y., Zhang, G., Qiu, M., 2011. Simulation aided hot zone design for faster growth of CZ silicon mono crystals. Rare Metals 30, 155–159.

Curtain, R.F., Zwart, H., 1995. An Introduction to Infinite-Dimensional Linear Systems Theory, Texts In Applied Mathematics. Springer.

Demina, S., Kalaev, V., 2011. 3D unsteady computer modeling of industrial scale Ky and Cz sapphire crystal growth. Journal of Crystal Growth 320, 23–27.

Derby, J., Atherton, L., Gresho, P., 1989. An integrated process model for the growth of oxide crystals by the czochralski method. Journal of Crystal Growth 97, 792 – 826.

Derby, J., Atherton, L., Thomas, P., Brown, R., 1987. Finite-element methods for analysis of the dynamics and control of czochralski crystal growth. Journal of Scientific Computing 2, 297–343.

Derby, J., Brown, R., 1986a. Thermal-capillary analysis of Czochralski and liquid encapsulated Czochralski crystal growth: I. simulation. Journal of Crystal Growth 74, 605–624.

Derby, J., Brown, R., 1986b. Thermal-capillary analysis of Czochralski and liquid encapsulated Czochralski crystal growth: II. processing strategies. Journal of Crystal Growth 75, 227–240.

Derby, J., Brown, R., 1987. On the dynamics of Czochralski crystal growth. Journal of Crystal Growth 83, 137–151.

Duffar, T., 2010. Crystal Growth Processes Based on Capillarity: Czochralski, Floating Zone, Shaping and Crucible Techniques. John Wiley & Sons.

Dunbar, W.B., Petit, N., Rouchon, P., Martin, P., 2003. Boundary control for a nonlinear stefan problem, in: Proceedings of the 42nd IEEE Conference on Decision and Control, pp. 1309–1314.

Fard, M.P., Sagatun, S.I., 2001. Exponential stabilization of a transversely vibrating beam by boundary control via lyapunovs direct method. Journal of Dynamic Systems, Measurement and Control 123, 195–200.

Gevelber, M., 1994a. Dynamics and control of the Czochralski process III. interface dynamics and control requirements. Journal of Crystal Growth 139, 271–285.

Gevelber, M., 1994b. Dynamics and control of the Czochralski process IV. Control structure design for interface shape control and performance evaluation. Journal of Crystal Growth 139, 286–301.

Gevelber, M., Stephanopoulos, G., 1987. Dynamics and control of the Czochralski process. I. modelling and dynamic characterization. Journal of Crystal Growth 84, 647–668.

Gevelber, M., Stephanopoulos, G., Wargo, M., 1988. Dynamics and control of the Czochralski process II. objectives and control structure design. Journal of Crystal Growth 91, 199–217.

Gross, U., Kersten, R., 1972. Automatic crystal pulling with optical diameter control using a laser beam. Journal of Crystal Growth 14, 85–88.

Hagen, G., Mezic, I., 2003. Spillover stabilization in finite-dimensional control and observer design for dissipative evolution equations. SIAM Journal on Control and Optimization 42, 746–768.

Harkort, C., Deutscher, J., 2011. Finite-dimensional observer-based control of linear distributed parameter systems using cascaded output observers. International Journal of Control 84, 107–122.

Irizarry-Rivera, R., Seider, W.D., 1997a. Model-predictive control of the Czochralski crystallization process. part I. conduction-dominated melt. Journal of Crystal Growth 178, 593 – 611.

Irizarry-Rivera, R., Seider, W.D., 1997b. Model-predictive control of the czochralski crystallization process. part ii. reduced-order convection model. Journal of Crystal Growth 178, 612 – 633.

Ito, K., 1990. Finite-dimensional compensators for innite-dimensional systems via Galerkin-type approximation. SIAM Journal of Control and Optimization 28, 1251–1269.

Izadi, M., Dubljevic, S., 2013. Order-reduction of parabolic PDEs with time-varying domain using empirical eigenfunctions. AIChE Journal DOI:10.1002/aic.14152.

Jordan, A., Caruso, R., von Neida, A., 1983. Analysis of the derivative weight-gain signal from measured crystal shape: implications for diameter control of GaAs. Bell System Technical Journal 62, 477–498.

Krstic, M., Smyshlyaev, A., 2008. Boundary Control of PDEs: A Course on Backstepping Designs. SIAM.

Li, X., Xu, C., 2011. Infinite-dimensional Luenberger-like observers for a rotating body-beam system. Systems & Control Letters 60, 138–145.

Liu, W.J., Krstic, M., 2000. Backstepping boundary control of burgers' equation with actuator dynamics. Systems & Control Letters 41, 291–303.

Neubert, M., Winkler, J., 2012. Nonlinear model-based control of the czochralski process III: Proper choice of manipulated variables and controller parameter scheduling. Journal of Crystal Growth 360, 3–11.

Ng, J., Aksikas, I., Dubljevic, S., 2011. Application of optimal boundary control to reaction-diffusion system with time-varying spatial domain, in: American Control Conference (ACC), 2011, pp. 2528–2533.

Ng, J., Aksikas, I., Dubljevic, S., 2013. Control of parabolic PDEs with time-varying spatial domain: Czochralski crystal growth process. International Journal of Control 86, 1467–1478.

Ng, J., Dubljevic, S., 2011. Optimal control of convection-diffusion process with time-varying spatial domain: Czochralski crystal growth. Journal of Process Control 21, 1361–1369.

Ng, J., Dubljevic, S., 2012. Optimal boundary control of a diffusion-convection-reaction PDE model with time-dependent spatial domain: Czochralski crystal growth process. Chemical Engineering Science 67, 111–119.

Ray, W.H., 1981. Advanced process control. McGraw-Hill chemical engineering series, McGraw-Hill.

Reddy, J.N., 2004. An Introduction to Nonlinear Finite Element Analysis. Oxford University Press.

Rudolph, J., Winkler, J., Woittennek, F., . Flatness based approach to a heat conduction problem in a crystal growth process, in: Meurer, T., Graichen, K., Gilles, E.D. (Eds.), Control and Observer Design for Nonlinear Finite and Infinite Dimensional System. Springer Verlag, pp. 387–401. 2005.

Sackinger, P.A., Brown, R.A., Derby, J.J., 1989. A finite element method for analysis of fluid flow, heat transfer and free interfaces in czochralski crystal growth. International Journal for Numerical Methods in Fluids 9, 453–492.

Sinno, T., Brown, R., 1999. Modeling microdefect formation in Czochralski silicon. Journal of Electrochemical Society 146, 2300–2312.

Szabo, G., 1985. Thermal strain during Czochralski crystal growth. Journal of Crystal Growth 73, 131–141.

Thomas, P., Derby, J., Atherton, L., Brown, R., Wargo, M., 1989. Dynamics of liquid-encapsulated czochralski growth of gallium arsenide: Comparing model with experiment. Journal of Crystal Growth 96, 135 – 152.

Vries, D., Keesman, K.J., Zwart, H., 2010. Luenberger boundary observer synthesis for Sturm-Liouville systems. International Journal of Control 83, 1504–1514.

Wang, P., 1990. Stabilization and control of distributed systems with time-dependent spatial domains. Journal of Optimization Theory and Applications 65, 331–362.

Wang, P., 1995. Feedback control of a heat diffusion system with time-dependent spatial domains. Optimal Control Applications and Methods 16, 305–320.

Winkler, J., Neubert, M., Rudolph, J., 2010a. Nonlinear model-based control of the Czochralski process I: motivation, modeling and feedback controller design. Journal of Crystal Growth 312, 1005–1018.

Winkler, J., Neubert, M., Rudolph, J., 2010b. Nonlinear model-based control of the Czochralski process II: reconstruction of crystal radius and growth rate from the weighing signal. Journal of Crystal Growth 312, 1019–1028.

Xu, C.Z., Ligarius, P., Gauthier, J.P., 1995. An observer for infinite-dimensional dissipative bilinear systems. Computers & Mathematics with Applications 29, 13–21.

Chapter 4

Model Predictive Temperature Tracking in Czochralski Crystal Growth Process

4.1 Introduction

Single crystals, due to unique mechanical, physical and electrical properties are common materials in microelectronics, optoelectronics and structurally robust and high temperature resistant applications (Sinno and Brown, 1999; Sinno et al., 2000). The Czochralski (Cz) crystal growth process is the most common mass production process to produce single crystal. In Cz process, the solid crystal is grown from molten material (Si, Ga, etc), starting from a small crystal seed and slowly growing by solidification of material at the melt-crystal interface. Due to the high-tech nature single crystal applications, the quality of the grown crystal is of crucial importance. The crystal quality is defined by physical properties of the produced crystal such as defects density and residual stresses in the crystal. These defects and residual stresses are caused by temperature gradients in the crystal and can be controlled by introducing a controller to limit possibly large temperature gradient fluctuations, see (Gevelber

and Stephanopoulos, 1987).

The Czochralski crystal growth process modelling require a sophisticated model of melt fluid flow, thermal and heat transfer phenomena, solid-liquid interface and pulling dynamics (Demina and Kalaev, 2011; Cao et al., 2011). However, for control purposes a simplified model for the phenomena of interest would suffice and usual assumptions are made to decouple specific processes to achieve a reduced order model as a basis for model based control synthesis. In the recent review on the automation of the Czocharlski crystal growth process (Winkler et al., 2013), both the classical and modern control realizations which are synthesized on the simplified process model description have been explored (Winkler et al., 2010a,b). At present time, one can conclude that a successful controller synthesis relies on the interplay of feedback, feedforward control, the reference trajectory tracking and reconstruction of non directly measurable process states. However, any controller realization is dependent on the quality of the model used in controller synthesis.

In particular, due to a specific feature of the Czochralski crystal growth process, the crystal shape undergoes time-varying changes which introduces moving boundaries to the parabolic partial differential equations (PDE) model of temperature evolution in the crystal growth process. Along this line, there are several works focusing on the model based controller design of parabolic PDE models with time-varying boundary domain, see Armaou and Christofides (2001a,b); Rudolph et al.. For example, Ng and Dubljevic (2012); Ng et al. (2013) studied optimal boundary control of the 2-D temperature model of the Cz crystal growth process with moving boundaries which is coupled with the crystal pulling dynamics. In these contributions, a simplified geometry (e.g. 1-D or 2-D rectangular domain) is used for control synthesis, however in realistic operation of Cz process, the crystal growth starts from a small

three dimensional irregularly shaped seed and grows to a desired radius.

One of the main obstacles in producing high quality large boules of a grown crystal is the presence of thermal stresses during the crystal cooling. The thermal stresses result in crystal cracking and fracture in the crystal during the cooling process. The critical stresses in the crystal depend on the crystal temperature and are usually caused by temperature difference in radial direction (Gevelber and Stephanopoulos, 1987; Gevelber et al., 1988; Fang et al., 2008). Controlling or limiting these stresses are crucial to avoid crystal cracking and to ensure the crystal quality. The conventional method to control these stresses are to adjust the heater temperature in order to maintain the temperature distribution around desired levels, however for larger crystals this method is not successful. In particular, the conventional methods are usually realized as off-line configuration accompanied with large scale simulation studies. The modern control strategies are helpful for on-line temperature distribution control, however limitations associated with distributed temperature measurement realization, the infinite-dimensional nature of the heat transfer process, time-varying crystal boundaries, stringent performance requirements reflected in grown crystal quality and coupled growth and heat transfer dynamics make the control implementation a challenging task. One of the modern control realizations capable of accounting for the aforementioned performance and process characteristics in explicit way is the model predictive control.

Model Predictive Control (MPC) strategies due to their practical and industrially appealing advantages attracted quite a few contributions in the area of Czochralski crystal growth and temperature control. For example, Lee et al. (2005) used the MPC to determine a feedforward trajectory for crystal growth control. Temperature distribution control in solid crystal and melt is also performed by Ng et al. (2013);

Irizarry-Rivera and Seider (1997) where the main approach in these contributions is to use a reduced order model of the complex dynamical system to apply the MPC and ensure that the desired objectives are satisfied. In Irizarry-Rivera and Seider (1997) work, the lumped models are considered for both the pulling dynamics and bulk heat transfer and then two different MPC are coupled to control the radius and pulling velocity. Although utilizing a more sophisticated model of the process would be more accurate and performance recommended, the complexity and the computational efforts associated with more detailed models must be weighted against ability of these algorithms to be implemented on-line in real-time setting.

The Czochralski crystal growth is a batch slow process (3-5 cm/hr growth rate) and one of the strategies to ensure the efficiency of process is to force the process to track a reliable predefined reference trajectory. Using the crystal growth model, the states and inputs evolution can be determined to achieve the maximum rate of crystal cooling. The optimal trajectory can be calculated taking into account all constraints associated with temperature and gradient distributions along with constraints on available input. However, due to infinite-dimensional nature of the process (e.g. PDE model), the trajectory optimization of the process needs to be realized on a reduced order model with enough accuracy to satisfy stringent production requirements. After an optimal trajectory is obtained, it is used in the model predictive control framework to drive the process towards a desired control objective.

In this chapter, a framework is provided for reference temperature profile tracking in the Czochralski crystal growth process. A predefined reference crystal shape evolution is used to calculate the optimal temperature trajectory. Dynamical coupling among the thermal and pulling of crystal model provide a basis for combined finite and infinite dimensional system setting through the parabolic PDE and ODE model. The

moving boundary finite element model (FEM) of the conduction-convection thermal phenomena within the grown reference crystal shape is used to determine the optimal temperature distribution trajectory. Then the MPC is designed to work on the coupled crystal growth and temperature dynamics to track both the reference crystal shape and desired temperature distribution. The constraints on the temperature distribution are derived from the conditions on critical thermal stresses and implemented in the MPC reference tracking framework. In this chapter, we explore the predetermining optimal trajectory evolution, realizability for practical implementation and handling of constraints within the control and realizable online real time optimization framework. We demonstrate that tracking the predetermined optimal reference trajectory is a reliable way to maximize cooling efficiency which can be applied to different settings to achieve a desired goal of minimizing important thermal stresses during the crystallization process.

The organization of the chapter is as following: after the Introduction section, a brief descriptions of the growth model, heat transfer model and thermal stresses are provided in Section 4.2. In the following sections the optimization and the MPC controller realizations are presented and followed by adequate numerical results and discussion.

4.2 Heat Transfer model on Moving boundary Domain

The crystal growth process model, that we considered in this chapter, consists of coupled crystal growth and heat transfer dynamics. The crystal growth model dynamics depicts crystal radius and length evolution. The time evolution of the heat transfer model boundaries is determined from the crystal shape (radius and length).

The crystal shape is also influenced by temperature distribution. Using a robust controller with respect to uncertainty in crystal growth rate can reduce the problem to a one-way coupling model realization such that the influence of the temperature distribution on the crystal growth dynamics is considered as a parametric uncertainty in the growth rate.

4.2.1 Crystal growth model

The schematic of the crystal pulling dynamics along with the notations are presented in Fig.4.1. The dynamic model of crystal growth is derived assuming horizontal melt-solid interface (see Abdollahi et al. (2014)). The planar interface assumption is relaxed in developing the finite element model of the crystal growth. The crystal growth model is given by (Abdollahi et al., 2014):

$$\begin{aligned}
\dot{x}_1(t) &= x_2(t) \\
\dot{x}_2(t) &= \frac{2}{\rho_c x_3(t)}[F_{ext}(t) - \rho_c \pi C_{growth}(\frac{x_2(t)}{2} - \frac{C_{growth}}{R^2_{cruc.}})] \\
\dot{x}_3(t) &= \pi C_{growth}
\end{aligned} \tag{4.1}$$

and the crystal radius, $r(t)$, as the output is given as:

$$R_{c.i.}(t) = \sqrt{\frac{C_{growth}}{x_2(t)}} = \sqrt{\frac{C_{growth}}{\dot{l}(t)}} \tag{4.2}$$

where $x_1(t) = l(t)$, $x_2(t) = \dot{l}(t)$, $x_3(t) = V_c(t)$ and $R_{c.i.}(t)$ are the crystal length, growth velocity, the crystal volume and the crystal radius, respectively. F_{ext}, C_{growth}, $R_{cruc.}$ and ρ_c are the puling force, volumetric crystal growth rate, crucible radius and the crystal density, respectively (see Fig.4.1). The control objective is to regulate

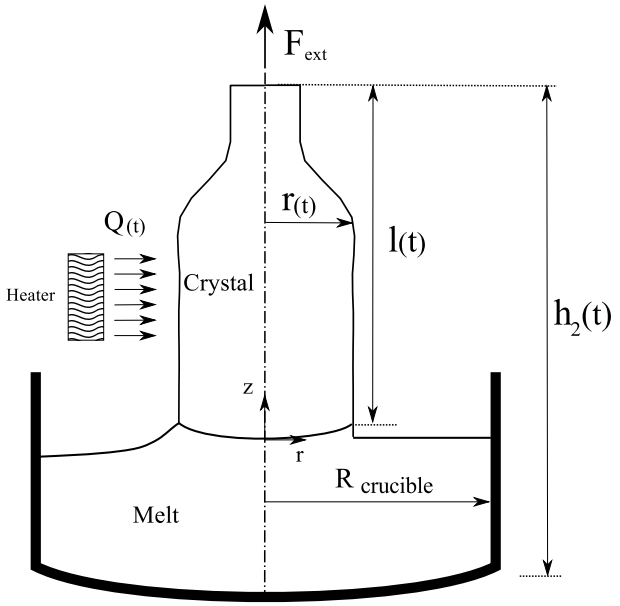

Figure 4.1: Schematic of the Cz crystal growth process with the realistic geometry of the process given in the left figure side, and geometric simplifications and parameters given in the right figure side.

the crystal radius at a desired value, R_d , despite the parametric uncertainty. The controller is designed using input-output linearization of the crystal growth model, given by:

$$F_{ext}(t) = \rho\pi C_{growth}^2(\frac{1}{2R_{c.i.}^2(t)} - \frac{1}{R_{cruc.}^2}) + K\rho\pi C_{growth}^2(t + V_{c0}/\pi C)\frac{R_{c.i.}(t) - R_d}{R_{c.i.}^3(t)} \quad (4.3)$$

where K is the controller gain which is determined to stabilize the crystal radius at desired value considering the parametric uncertainty in the crystal growth rate $C_{nominal} - d(t) \leq C_{growth} \leq C_{nominal} + d(t)$. The control gain, K, is given as:

$$K > \frac{\pi}{2V_{c0}C_{growth}^2} D(C_{growth} + D)(2C_{growth} + D) \quad (4.4)$$

where D is the upper bound for disturbance $d(t)$ and is assumed to have a lower and upper limit, $-C_{growth} < d(t) < D$. The lower limit corresponds to the case of crystallization not occurring and the upper bound, which represents fast crystallization, can be arbitrarily chosen.

The crystal radius is regulated despite the uncertainty in the crystal growth rate and since the growth rate is affected by temperature distribution in the crystal, the robustness of the control law allows the radius control synthesis to be decoupled from the thermal phenomena that can adversely affect the crystallization rate and the radius growth. This is an important point in the coupled thermal and pulling of the crystal modelling used for the control purposes, since the bidirectional coupling can be effectively reduced by the robust feedback linearizing control to one-directional coupling from the mechanical to the thermal model. In the ensuing section we provide a thermal PDE model which domain dynamics is driven by the time-varying evolution of the $x_1(t)$-state from Eq.4.1 and $r(t)$ from Eq.4.2.

4.2.2 Heat transfer model

In the Czochralski process, the heat transfer within the solid crystal is described by the conduction-convection PDE model given by Eq.4.5 where convective terms are manifested by the boundaries growth velocity. The model along with the boundary conditions (Fig.4.2) are given as follows (Abdollahi et al., 2014; Derby and Brown, 1987):

$$\frac{\partial x}{\partial t} = \frac{1}{r}\frac{\partial}{\partial r}\left(k_0 r \frac{\partial x}{\partial r}\right) + k_0 \frac{\partial^2 x}{\partial z^2} - V_z(t)\frac{\partial x}{\partial z} \tag{4.5}$$

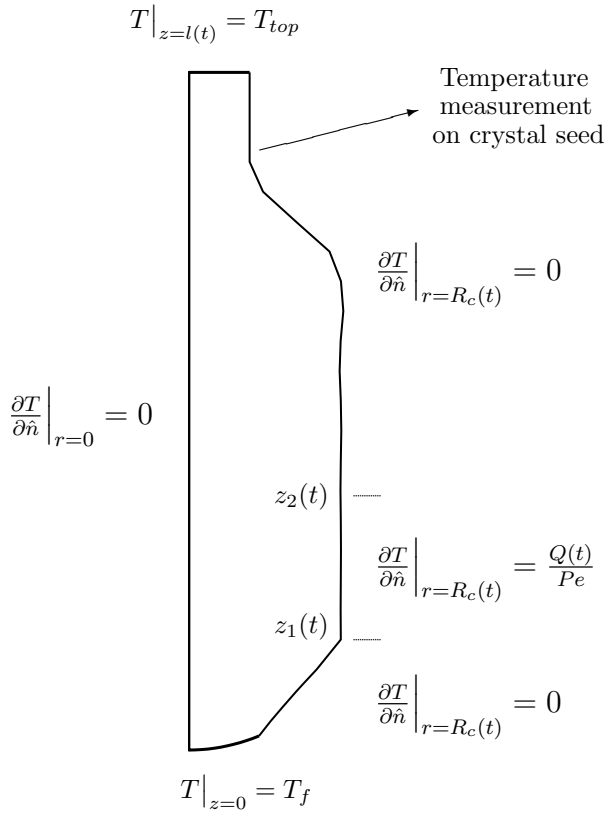

Figure 4.2: Boundary conditions, actuation interval and measurement point.

$$x\Big|_{z=0} = 0\,; \qquad x\Big|_{z=l(t)} = x_{top}\,; \qquad \frac{\partial x}{\partial r}\Big|_{r=0} = 0 \tag{4.6}$$

$$\frac{\partial x}{\partial \hat{n}}\Big|_{r=R_c(z),\, z<z_1(t)} = 0\,; \; \frac{\partial x}{\partial \hat{n}}\Big|_{r=R_c(z),\, z>z_2(t)} = 0\,; \; \frac{\partial x}{\partial \hat{n}}\Big|_{r=R_c(z),\, z_1(t)<z<z_2(t)} = \frac{Q(t)}{Pe} \tag{4.7}$$

where $x(r, z, t)$ is the scaled temperature within the crystal, $k_0 = k_r/Pe$ and $V_z(t)$ is the bulk movement velocity along the axial direction. For detailed description of the model, see Abdollahi et al. (2014).

In the Czochralski process, due to high operating temperature, the crystal loses heat at high rate mainly through radiation. This heat loss results in very fast crystal cooling and consequently results in thermal stresses and dislocation or crystal cracking. In order to model the global thermal behaviour of the process, it is required to incorporate all the coupled phenomena like conduction-convection in the crystal

and in the melt, the heat transfer in the meniscus and radiation between all surfaces along with the crystal growth dynamics and fluid flow. A comprehensive model of the process would be successful in simulation studies but for the control purpose, a simpler model of the process is required. In order to have closer thermal behaviour to real operating conditions, Dirichlet boundary condition is considered at the top of the crystal and it is considered to be equal to $T_{top} = 850\,^{\circ}C$ (taken from the experimental results of Sinno et al. (2000)).

4.2.3 Thermal stresses in crystal

Due to high temperature during the crystal growth process, thermal stresses do occur and are present during the cool down process. These stresses are translated to strains which in principle may result in the crystal cracking. Avoiding these stresses during the crystal production will guarantee reliability of the process quality of the crystal (Fang et al., 2008). Temperature gradients are also known to be one of important factors in creating dislocations in the crystal. Decreasing the thermal gradients will result in lower stresses and consequently reduce dislocations in the crystal. Obtaining exact stresses in the crystal during the crystallization process requires modelling the coupled thermal, growth and meniscus dynamics, however there are some conservative criteria on temperature gradients to avoid stresses exceeding the critical value.

Thermal stresses in the crystal can be obtained with the assumption of plain strain in the crystal to define the aforementioned criteria for temperature gradients (Gevelber, 1994). The stresses are known to be at their maximum values at the crystal centre and the crystal surface. Assuming plain strain and a simple meniscus geometry, Gevelber (1994) provided these stresses as temperature dependent functionals given by:

$$\sigma_{r,norm} = \begin{cases} -\frac{5}{48}\frac{\partial T}{\partial r}R_i & \text{at} \quad r = 0 \\ 0 & \text{at} \quad r = R_i \end{cases} \tag{4.8}$$

$$\sigma_{z,norm} = \begin{cases} -\frac{10}{48}\frac{\partial T}{\partial r}R_i & \text{at} \quad r = 0 \\ \frac{7}{24}\frac{\partial T}{\partial r}R_i & \text{at} \quad r = R_i \end{cases} \tag{4.9}$$

$$\sigma_{\phi,norm} = \begin{cases} -\frac{5}{48}\frac{\partial T}{\partial r}R_i & \text{at} \quad r = 0 \\ \frac{7}{24}\frac{\partial T}{\partial r}R_i & \text{at} \quad r = R_i \end{cases} \tag{4.10}$$

where R_i denotes the point along the radius coordinate. The maximum stress is obtained in the growth direction and the stresses are the largest at the crystal surface and they should be less than critical resolved shear stress (σ_{CRSS}). For Silicon crystal, the critical stress is $\sigma_{CRSS} = 5.55 \times 10^6 dyn/cm^2$ and this condition is reduced to (Gevelber, 1994):

$$\left|\frac{\partial T}{\partial r}\right| R_i \begin{cases} \leq 10.3K \quad \text{for} \quad r = R \\ \leq 28.8K \quad \text{for} \quad r = 0 \end{cases} \tag{4.11}$$

Since the maximum stress occurs at the crystal surface, the temperature gradients should be minimum at the crystal surface. The constraints on the temperature gradients can be considered in order to minimize thermal stresses.

To study and utilize the thermal stresses evolution in the control algorithm, the thermal stresses are solved for the growing silicon crystal. Since the silicon crystal has cubic atomic lattice structure, the thermal stress analysis is performed using axisymmetric thermoelastic stress model for anisotropic materials provided by Fainberg and Leister (1996); Chen et al. (2008). The governing equations for the momentum

balance for axisymmetric geometry is given by:

$$\frac{1}{r}\frac{\partial}{\partial r}(r\sigma_{rr}) + \frac{\partial}{\partial z}(\sigma_{rz}) - \frac{\sigma_{\phi\phi}}{r} = 0 \tag{4.12}$$

$$\frac{1}{r}\frac{\partial}{\partial r}(r\sigma_{rz}) + \frac{\partial}{\partial z}(\sigma_{zz}) = 0 \tag{4.13}$$

where σ_{rr} , σ_{zz} and $\sigma_{\phi\phi}$ are normal stresses in the radial, axial and tagential directions, respectively and σ_{rz} is the shear stress. The stress-strain relation for anisotropic thermoelastic material is given by:

$$\begin{bmatrix} \sigma_{rr} \\ \sigma_{\phi\phi} \\ \sigma_{zz} \\ \sigma_{rz} \end{bmatrix} = \begin{bmatrix} c_{11} & c_{12} & c_{13} & 0 \\ c_{12} & c_{22} & c_{23} & 0 \\ c_{13} & c_{23} & c_{33} & 0 \\ 0 & 0 & 0 & c_{44} \end{bmatrix} \begin{bmatrix} \epsilon_{rr} - \beta_1(T - T_{ref}) \\ \epsilon_{\phi\phi} - \beta_2(T - T_{ref}) \\ \epsilon_{zz} - \beta_3(T - T_{ref}) \\ \epsilon_{rz} \end{bmatrix} \tag{4.14}$$

where β_i is the thermal expansion coefficient in i direction, c_{ij} is the elastic coefficient. T and T_{ref} are the temperature distribution and reference temperature, respectively. The elastic coefficients for cubic crystal lattices reduce to three independent coefficients and all the other coefficients can be expressed in terms of independent coefficients as follows: $c_{11} = c_{22} = c_{33} = 165.77GPa$, $c_{12} = c_{13} = c_{23} = 63.93GPa$, $c_{44} = 79.62GPa$. The expansion coefficient is constant for all directions, $\beta_{11} = \beta_{22} = \beta_{33} = 4.5 \times 10^{-6}K^{-1}$ (Chen et al., 2008). The strain-displacement relations are given by:

$$\epsilon_{rr} = \frac{\partial u}{\partial r}, \quad \epsilon_{\phi\phi} = \frac{u}{r}, \quad \epsilon_{zz} = \frac{\partial v}{\partial z}, \quad \epsilon_{rz} = \frac{\partial u}{\partial z} + \frac{\partial v}{\partial r} \tag{4.15}$$

where u and v are displacement components in the radial and axial directions, respectively. Traction free boundary conditions is assumed for crystal surface, $t^n = \sigma.n$,

where t^n is the traction force normal to the surface and n is the surface normal unit vector. For the axisymmetric axis, the boundary condition is applied on the displacements, $v = 0$ and $\frac{\partial u}{\partial n} = 0$, where n is the unit vector normal to the axisymmetric axis.

The thermal stresses has important role in creating dislocations through causing slip in the crystal structure. It is well known that slip occurs in a plane that resolved shear stress (σ_{RSS}) on that plane is greater than the critical resolved shear stress (σ_{CRSS}). It has been previously shown that slip occurs on $\{111\}$ plane and $[1\bar{1}0]$ direction (shown in Fig.4.3). Assuming that growth happens at [001] direction, in the cubical crystal lattice, there are total of 12 slip directions on four planes. It is shown that these 12 resolved stresses can be expressed as five independent stresses given in Table 4.1.

The maximum absolute value of the resolved shear stresses occur at different tangential angles. These angles are shown in Table 4.1. The maximum values of these stresses are used in model predictive control utilization as constraints to minimize dislocation generation.

Table 4.1: Five independent resolved shear stresses and the angle of maximum stress

Independent resolved shear stress	Maximum occurs at ϕ
$\sigma_1 = \frac{\sqrt{6}}{6}\bar{\sigma}_r cos2\phi$	$0, \pi$
$\sigma_2 = \frac{\sqrt{6}}{6}[\bar{\sigma}_z - \bar{\sigma}_r \frac{2}{\sqrt{2}} sin\phi sin(\phi + \frac{\pi}{4})]$	$\frac{3\pi}{8}, \frac{7\pi}{8}$
$\sigma_3 = \frac{\sqrt{6}}{6}[\bar{\sigma}_z - \bar{\sigma}_r \frac{2}{\sqrt{2}} sin\phi sin(\phi - \frac{\pi}{4})]$	$\frac{\pi}{8}, \frac{5\pi}{8}$
$\sigma_4 = -\frac{\sqrt{6}}{6}[\bar{\sigma}_z - \bar{\sigma}_r \frac{2}{\sqrt{2}} cos\phi sin(\phi + \frac{\pi}{4})]$	$\frac{\pi}{8}, \frac{5\pi}{8}$
$\sigma_5 = -\frac{\sqrt{6}}{6}[\bar{\sigma}_z + \bar{\sigma}_r \frac{2}{\sqrt{2}} cos\phi sin(\phi - \frac{\pi}{4})]$	$\frac{3\pi}{8}, \frac{7\pi}{8}$

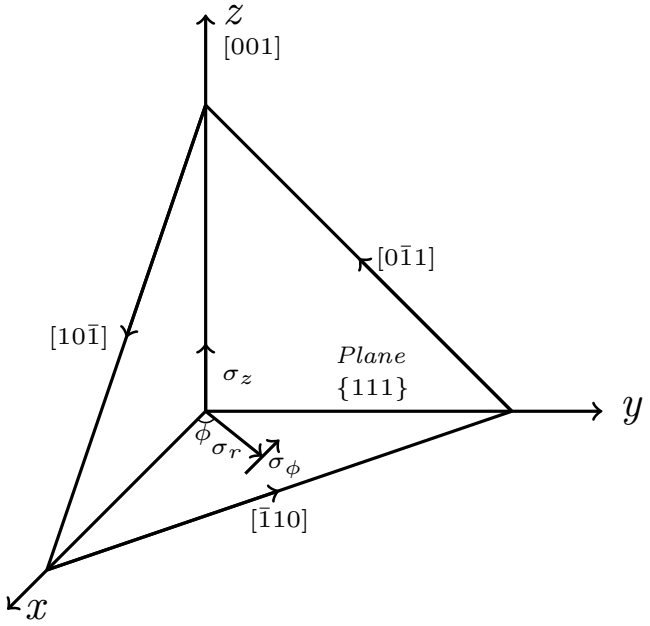

Figure 4.3: Representaion of stress transformation in slip plane and direction

4.3 Optimization and Temperature Reference Tracking

The conduction-convection heat transfer model provided in Section 2.2 is used for process optimization and control. Since the crystal shape is not known at the beginning of the process, the reference crystal shape (reference crystal radius and length) is used for trajectory planning and optimization. The heater input $Q(t)$ is determined such that the maximum cooling achieved and the constraints on the input and the temperature gradients close to interface not violated. Hence, optimization on the reference crystal shape is plausible since the radius control law is robust with respect to uncertainty in growth rate which results from temperature distribution within the crystal. A low dimensional finite element model of the crystal as the dynamic model along with quadratic programming are used to determine the heater inputs optimizing the objective function and satisfying the constraints. The optimization and control

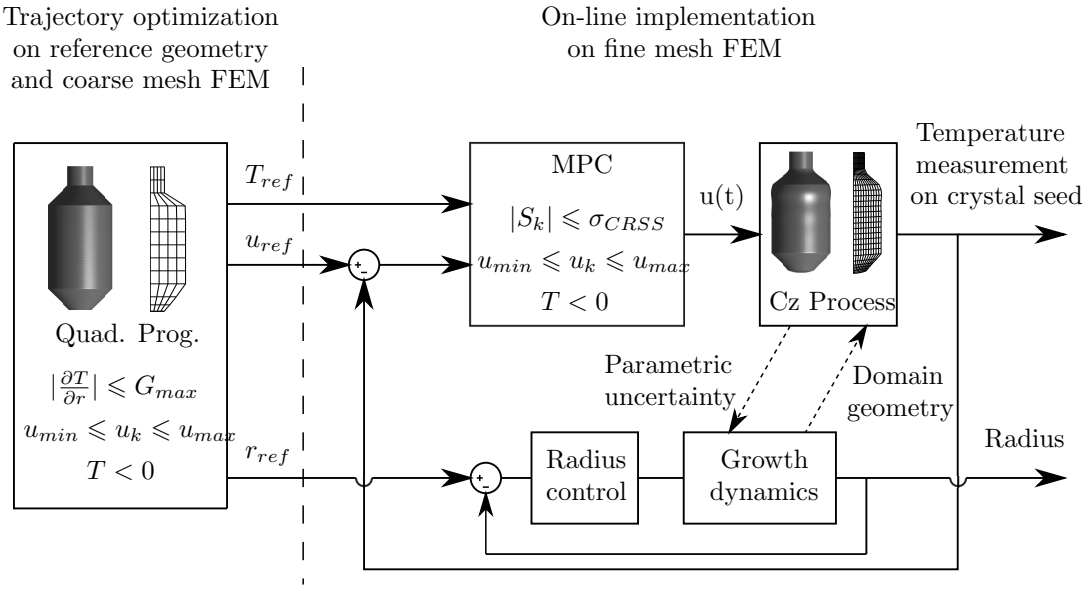

Figure 4.4: Trajectory optimization and temperature distribution control algorithm along with thee coupling between crystal growth and temperature dynamics.

framework used in this chapter is shown in Fig.4.4. The presence of non-trivial crystal shape, moving boundaries and partial actuation in one boundary makes available options for model reduction and control of the process limited. In this chapter, we directly use the finite element model (FEM) of the process for optimization and control synthesis, since the direct use of the FEM model of heat transfer in non-cylindrical crystal domain is more accurate than the reduced order models, moreover, the temperature field in this case can be easily translated into thermal stress in the crystal.

The FEM model of the conduction-convective PDE given by Eqs.4.5-4.7 is obtained and is written as:

$$\begin{aligned} X_{k+1} &= A_k X_k + B_k u_k + B c_k \\ Y_k &= C_k X_k \end{aligned} \tag{4.16}$$

where X_k is the vector of temperature field at nodes of FEM model, A_k, B_k and Bc_k are the matrices obtained from FEM. The system output, Y_k, is the temperature gradients at nodes of interest. Due to the moving boundaries and time varying term in the PDE, the dynamical system given by Eq.4.16 is time-varying.

Knowing the reference crystal shape, the finite element method is used to optimize the temperature distribution evolution for the batch process time. The optimal inputs are obtained such that the maximum cooling takes place without violating the constraints on temperature gradients. The most important gradients are those close to melt-crystal interface and since the radial gradients at the boundary are zero (boundary condition), the gradients inside the crystal are taken into account. In order to obtain an optimal trajectory, the following optimization problem is solved to maximize cooling of the crystal by keeping the temperature gradients within the desired level.

$$\min_{u1,\ldots,u_{N_p}} J = \sum_{k=1}^{N_p} X_k^T Q X_k + u_k^T R u_k \tag{4.17}$$

subject to:

$$X_{k+1} = A_k X_k + B_k u_k + B c_k \tag{4.18}$$

$$u_{min} \leqslant u_k \leqslant u_{max} \tag{4.19}$$

$$|Y_k| \leqslant G_{max} \tag{4.20}$$

where X_k and Y_k are the nodal temperature and temperature gradients at time k, respectively and N_p is the number of intervals that used to span time horizon of the whole process. In order to solve the optimization problem, it can be formulated as a

large-scale quadratic program when the evolution matrices are known. The reference crystal shape evolution is utilized to generate FEM matrices for entire process time and consequently these matrices are used to formulate the quadratic program.

Knowing the optimal reference trajectory, model predictive reference tracking control is used to track the reference trajectory by measuring crystal temperature at the crystal surface. Model predictive control uses the finite element model of the process to predict future behaviour of the process and optimize the input such that the control action keep the process close to the reference trajectory. For reference temperature tracking, the model predictive reference tracking is defined as:

$$\min_{u_0 \cdots u_{N_c-1}} \Phi = \sum_{k=1}^{N_c} (y_k^r - C_k' X_k)^T Q' (y_k^r - C_k' X_k) + \sum_{j=0}^{N_c-1} (u_k - u_k^r)^T R' (u_k - u_k^r) \tag{4.21}$$

subject to:

$$X_{k+1} = A_k X_k + B_k u_k + B c_k \tag{4.22}$$

$$y_k = C' X_k \tag{4.23}$$

$$u_{min} \leqslant u_k \leqslant u_{max} \tag{4.24}$$

$$|S_k| \leqslant \sigma_{CRSS} \tag{4.25}$$

where y_k^r and u_k^r are the reference trajectory and reference inputs at time instance k, obtained from optimization problem (Eqs.4.17-4.20) and $y_k = C' X_k$ is the temperature measurement at the crystal surface. S_k is the vector of resolved shear stresses, σ_{RSS}, calculated by solving FEM model of thermal stresses (Eqs.4.12-4.15 and the

equation provided in Table 4.1) and σ_{CRSS} is the critical resolved shear stress of silicon. Since the relation between thermal stresses, displacements and temperature distribution are linear, the resolved shear stresses in the crystal after solving by FEM can be written as:

$$S_k = A'_k X_k \tag{4.26}$$

The trajectory obtained from the finite element model (Eq.4.16) is used as reference trajectory. Then MPC reference tracking controller is constructed using the online crystal shape (not reference geometry) to track the temperature reference. The temperature gradient constraints are present in the MPC formulation to avoid high gradients in the crystal. The integrated control and optimization is shown in Fig.1. There are two steps, first to calculate optimal inputs along with optimal temperature trajectories taking into account all the present constraints. Then by optimal trajectory and the refined finite element model on the tracked crystal shape, reference temperature tracking is performed. Since the finite element model used for MPC is different than the model used for optimization (different crystal shape and nonplanar interface), the constraints need to be present.

4.4 Numerical Simulation Results

The reference temperature tracking provided in this chapter is based on the FEM model of the Czochralski crystal growth process. The temperature distribution evolution optimization is performed on a pre-defined reference crystal shape. Then the temperature tracking is provided using the optimal trajectory obtained on the reference crystal shape and the model predictive reference temperature tracking is implemented on the high fidelity FEM model of the temperature evolution on the realistic

crystal shape in the presence of disturbances in the model (see Fig.4.4).

Two finite element model of the process is used. The first is a low dimensional model with DOF of 80 (5×16 two-dimensional linear 4-node elements) for off-line optimization. This finite element model is constructed on the reference crystal geometry with planar interface and utilized for off-line optimization. The second finite element model has 348 DOF (12×29 two-dimensional linear 4-node elements) which is constructed on the realistic crystal geometry with non-planar interface and is utilized as the process model to calculate the temperature distribution and thermal stresses over the crystal domain to verify the proposed control synthesis. The finite element model for off-line optimization is derived based on the reference crystal shape without considering the crystal radius control while the the FEM for on-line implementation is based on the realtime evolution of the crystal geometry. Note that the spatial domain of the crystal is known from growth dynamics and therefore the Arbitrary Lagrangian Eulerian (ALE) method (Reddy, 2004) is used to discretize the spatial domain of the crystal. First-order implicit time integration with the time step $dt = 0.005$ is used to obtain the evolution of the time-varying system.

The control synthesis, introduced in Section 4.2, is used to track the reference crystal radius. The robustness of control law with respect to the parametric uncertainty in crystal growth leads to a decoupled growth dynamics from the heat transfer model. This decoupled model can be used independently to control the crystal shape, however due to the present uncertainty, the tracked crystal geometry is slightly different than the reference shape. The reference crystal radius as a function of crystal length along with 3-D representation of the reference and tracked crystal geometry are shown in Fig.4.5. The tracking performance of controller is shown as dash-dotted line. The reference crystal geometry (left hand side) is known and used as the crystal

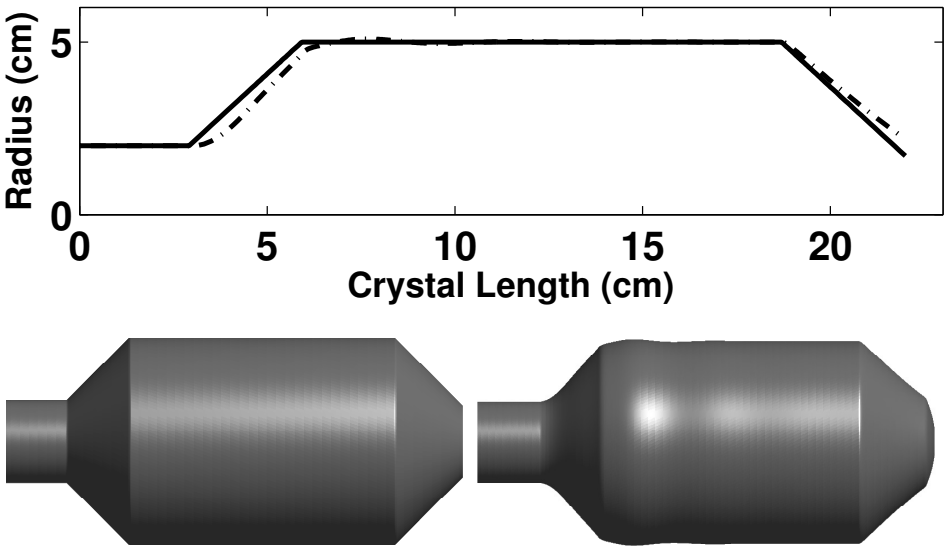

Figure 4.5: The reference crystal shape (solid line) and the tracked crystal radius (dash-dotted line) - The 3-D reference crystal shape along with the tracked 3-D crystal

geometry for temperature distribution evolution optimization and trajectory planning. The obtained inputs and trajectories are implemented on the realistic crystal shape (righ hand side) crystal geometry.

Since the desired reference crystal shape evolution is known, the time-varying crystal mesh can be extracted from the reference crystal shape for the whole process time. Using the known time-varying mesh, the system dynamics is represented by FE model (Eqs.4.16). The temperature distribution is assumed to be at equilibrium at the beginning of the process (temperature distribution initial condition) and the quadratic programming (QP) is used to optimize the inputs and the temperature distribution evolution for the whole process. In order to implement the QP, the total process time is considered to be 3.5 hours with average crystal growth of 5 cm/hours. The dynamic model is discritized using sampling time of 26 seconds which results in 500 manipulating variables in QP framework to be optimized. A FE model with

DOF of 70 is used for optimization which results in 35000 equality constraints along with more than 35000 inequality constraints on nodal temperatures in QP ($T < 0$, $\frac{\partial T}{\partial r} < G_{max}$ and $\frac{\partial T}{\partial z} < G_{max}$).

The MPC is implemented on the more realistic FE model of the process to show the performance of the controller. The planar melt-crystal interface assumption is relaxed and approximated by a second order polynomial in the Cz process model (Chen et al., 1997) to examine the performance on more realistic crystal geometry. The optimal input along with the tracked temperature are shown in Fig.4.6. As it can be seen the MPC tracks the reference trajectory with higher accuracy at the beginning of the process. However the tracking efficiency decreases (maximum deviation of 2%) as the crystal grows and the distance between the actuation and the point of interest increases. The presented tracking performance is in presence of model disturbance of random noise with the covariance of 10% of the maximum temperature. In absence of disturbances the MPC follows the reference with deviation less than 0.1%.

During the process, as the crystal grows, more molten material solidifies and new material points are created in the crystal. These points are created at the solid-melt interface at the melting point temperature (T_f) and then start moving with crystal. The annealing profile of these points at different heights are shown in Fig.4.7. As the growth process starts, the material at the interface starts to solidify and its temperature drops down, however the controller interrupts the temperature drop and by heating the crystal, the temperature increases to avoid occurrence of large gradients.

Temperature distribution evolution and normal stresses' snapshots for different time instances are shown in Fig.4.8. The resolved shear stresses that are calculated from transformation of normal stresses in different planes and directions are shown for same time instances in Fig.4.9. Fig.4.10 shows the evolution of maximum resolved

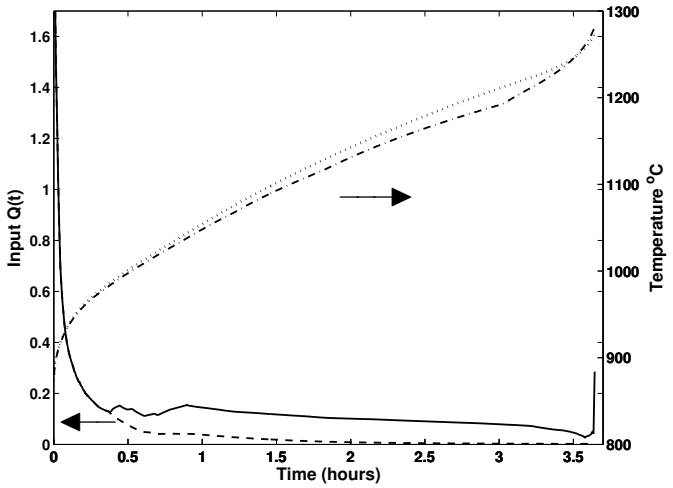

Figure 4.6: Reference input and temperature located on the surface of the crystal seed along with the input and the tracked temperature in presence of disturbances. Solid and dash-dotted lines are the reference trajectories while dashed and dotted lines are the input and the tracked temperature, respectively.

shear stress on the crystal interface. As it can be seen, however the constraints on σ_{RSS} is active only at the beginning of the process, the constraints on the maximum σ_{RSS} is satisfied (see Fig.4.9-4.10). The off-line optimization which is performed by posing constraints on temperature gradients instead of stresses themselves, despite simplifications, is an efficient way to limit the resolved shear stresses. Normal stresses (and consequently, resolved shear stresses) are higher at points far from the solid-melt interface, however due to higher critical resolved shear stress at lower temperatures, higher σ_{RSS} at points with lower temperature will not generate dislocations. As the stresses are the direct result of temperature gradients, the heater actuation flattens the temperature distribution at points closer to the interface which results in lower gradients in this region and with less gradient, the normal and resolved stresses are bounded at points close to interface.

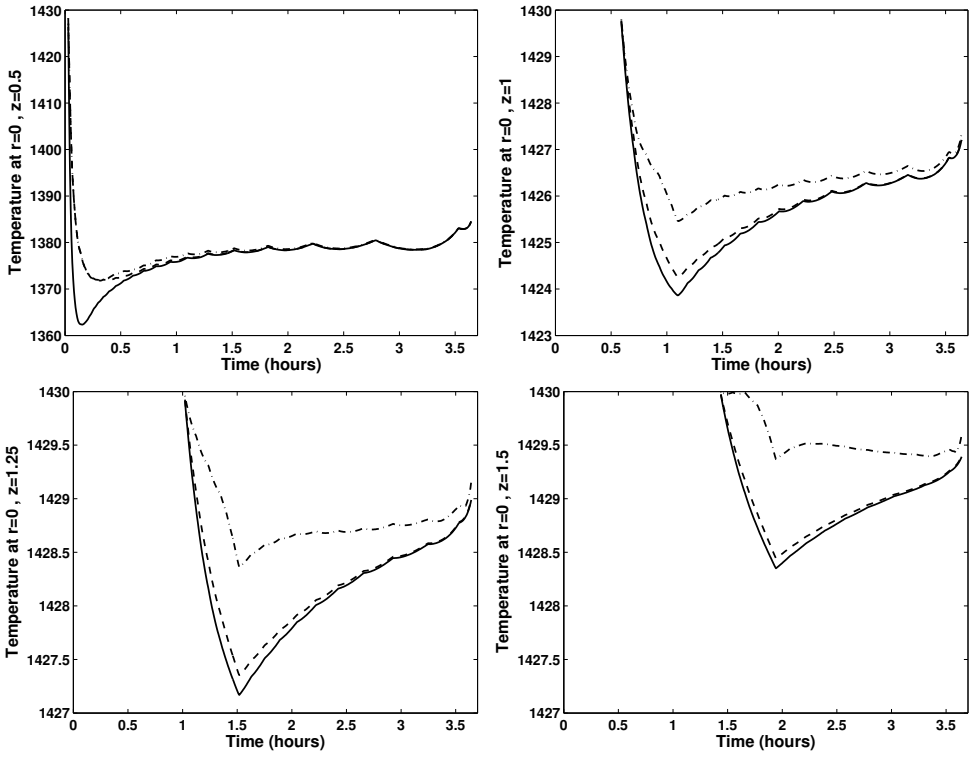

Figure 4.7: Annealing profile for different points at centre of crystal - Solid line: reference; Dashed line: tracked temperature without disturbance; Dash-dotted line: In presence of disturbance. Note, when the point is created, the temperature starts from the melting point and then due to heater action the temperature increases to avoid large gradients in crystal.

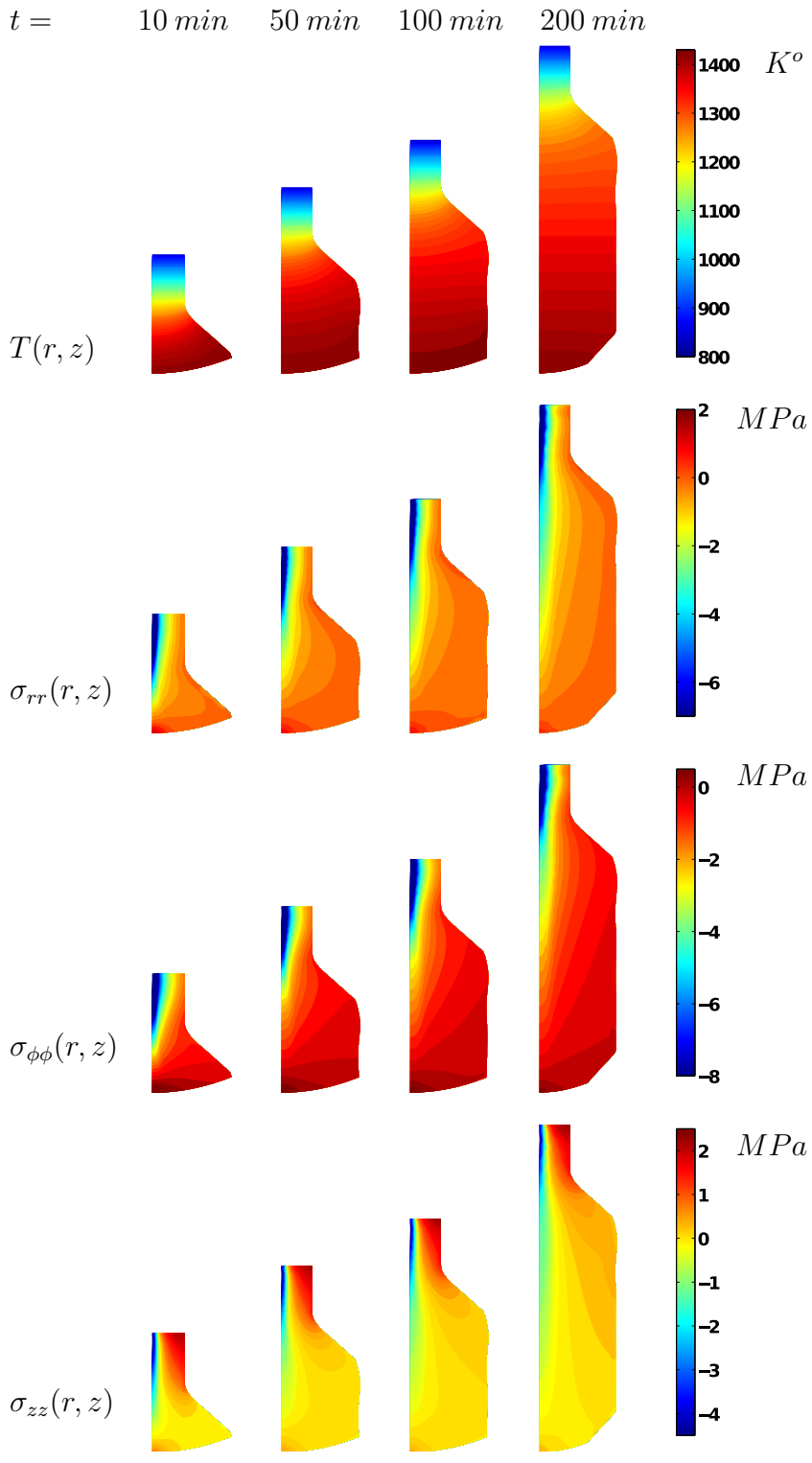

Figure 4.8: Temperature and gradients distribution in the crystal at different time instances - A: temperature distribution; B: Radial gradients; C: longitudinal gradients.

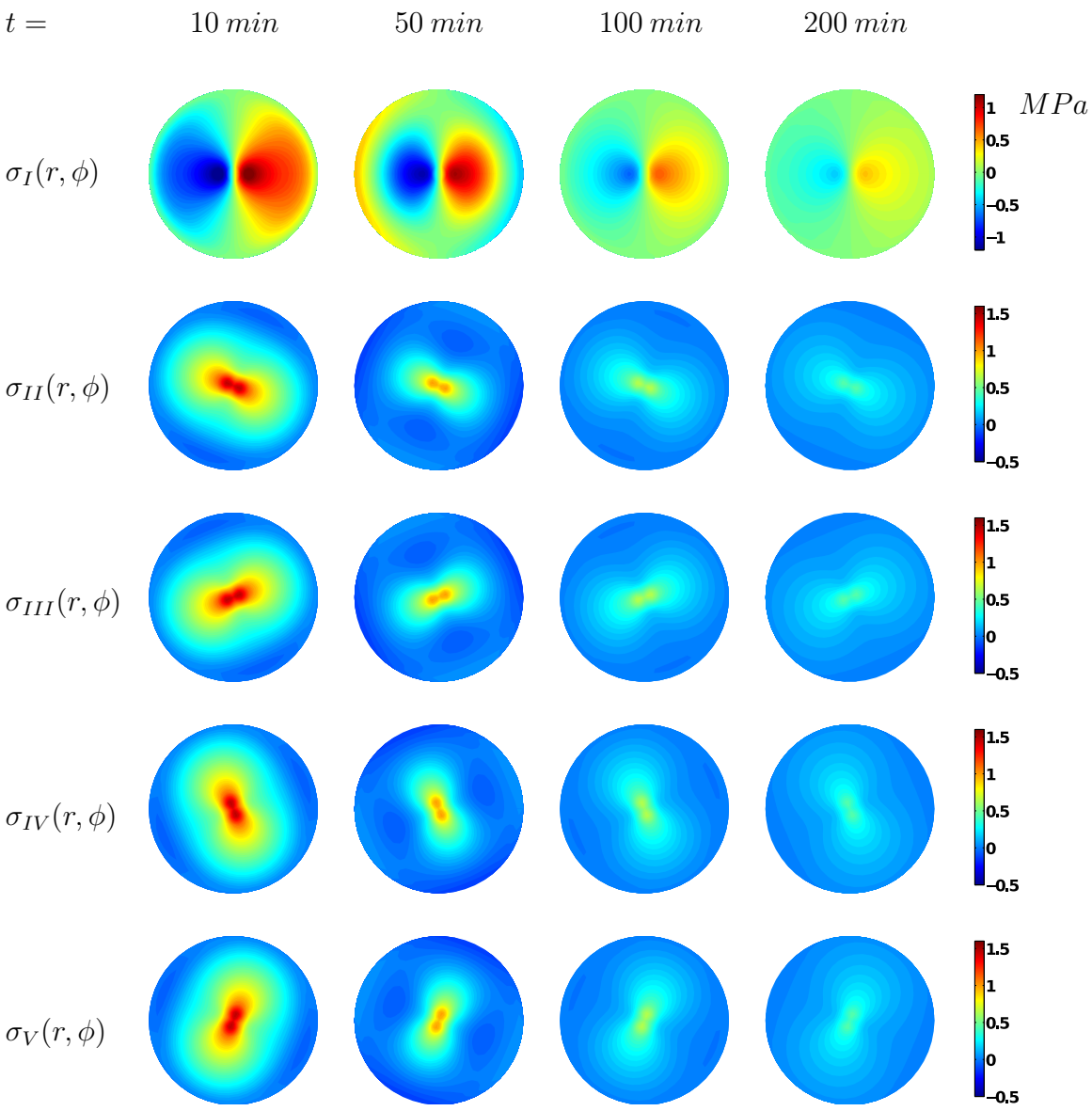

Figure 4.9: Temperature and gradients distribution in the crystal at different time instances - A: temperature distribution; B: Radial gradients; C: longitudinal gradients.

4.5 Summary

The reference temperature distribution tracking problem is considered in this chapter. Temperature tracking is performed by tracking a desired point temperature evolution along with satisfying the present constraints. The optimal temperature trajectory is obtained using quadratic programming and then the MPC is implemented to control the coupled crystal growth and conduction-convection heat transfer model. The provided approach in this chapter uses a simplified model of heat transfer in the Czochralski crystal growth process that preserves the main effect of temperature dynamics and the thermal behaviour of the Czochralski process, however, the approach can be extended to more comprehensive model by including the heat radiation, the heater/actuator dynamics and also the heat transfer in fluid and meniscus in both the optimization and implementation steps.

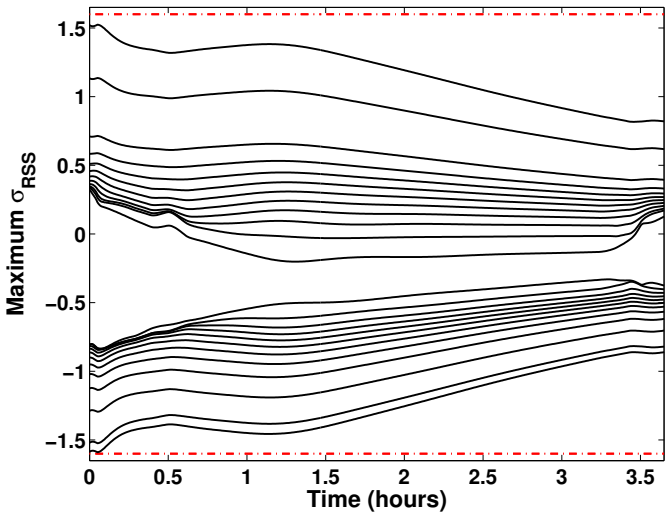

Figure 4.10: Maximum resolved shear stresses at tangential angles provided in Table 4.1 for nodes close to the solid-melt interface

4.6 References

Abdollahi, J., Izadi, M., Dubljevic, S., 2014. Temperature distribution reconstruction in czochralski crystal growth process. AIChE Journal DOI 10.1002/aic.14486.

Armaou, A., Christofides, P., 2001a. Crystal temperature control in Czochralski crystal growth process. AIChE Journal 47, 79–106.

Armaou, A., Christofides, P.D., 2001b. Robust control of parabolic PDE systems with time-dependent spatial domains. Automatica 37, 61–69.

Cao, J., Gao, Y., Chen, Y., Zhang, G., Qiu, M., 2011. Simulation aided hot zone design for faster growth of CZ silicon mono crystals. Rare Metals 30, 155–159.

Chen, T., Wu, H., Weng, C.I., 1997. The effect of interface shape on anisotropic thermal stress of bulk single crystal during czochralski growth. Journal of Crystal Growth 173, 367–379.

Chen, X., Nakano, S., Liu, L., Kakimoto, K., 2008. Study on thermal stress in a silicon ingot during a unidirectional solidification process. Journal of Crystal Growth 310, 4330 – 4335.

Demina, S., Kalaev, V., 2011. 3D unsteady computer modeling of industrial scale Ky and Cz sapphire crystal growth. Journal of Crystal Growth 320, 23–27.

Derby, J., Brown, R., 1987. On the dynamics of Czochralski crystal growth. Journal of Crystal Growth 83, 137–151.

Fainberg, J., Leister, H.J., 1996. Finite volume multigrid solver for thermo-elastic stress analysis in anisotropic materials. Computer Methods in Applied Mechanics and Engineering 137, 167 – 174.

Fang, H., Qiu, S., Zheng, L., Schaffers, K., Tassano, J., Caird, J., Zhang, H., 2008. Optimization of the cooling profile to achieve crack-free Yb:S-FAP crystals. Journal of Crystal Growth 310, 3825 – 3832.

Gevelber, M., 1994. Dynamics and control of the Czochralski process III. interface dynamics and control requirements. Journal of Crystal Growth 139, 271–285.

Gevelber, M., Stephanopoulos, G., 1987. Dynamics and control of the Czochralski process. I. modelling and dynamic characterization. Journal of Crystal Growth 84, 647–668.

Gevelber, M., Stephanopoulos, G., Wargo, M., 1988. Dynamics and control of the Czochralski process II. objectives and control structure design. Journal of Crystal Growth 91, 199–217.

Irizarry-Rivera, R., Seider, W.D., 1997. Model-predictive control of the Czochralski crystallization process. part I. conduction-dominated melt. Journal of Crystal Growth 178, 593 – 611.

Lee, K., Lee, D., Park, J., Lee, M., 2005. MPC based feedforward trajectory for pulling speed tracking control in the commercial Czochralski crystallization process. International Journal of Control, Automation and Systems 3, 252–257.

Ng, J., Aksikas, I., Dubljevic, S., 2013. Control of parabolic PDEs with time-varying spatial domain: Czochralski crystal growth process. International Journal of Control 86, 1467–1478.

Ng, J., Dubljevic, S., 2012. Optimal boundary control of a diffusion-convection-reaction PDE model with time-dependent spatial domain: Czochralski crystal growth process. Chemical Engineering Science 67, 111–119.

Reddy, J.N., 2004. An Introduction to Nonlinear Finite Element Analysis. Oxford University Press.

Rudolph, J., Winkler, J., Woittennek, F., . Flatness based approach to a heat conduction problem in a crystal growth process, in: Meurer, T., Graichen, K., Gilles, E.D. (Eds.), Control and Observer Design for Nonlinear Finite and Infinite Dimensional System. Springer Verlag, pp. 387–401. 2005.

Sinno, T., Brown, R., 1999. Modeling microdefect formation in Czochralski silicon. Journal of Electrochemical Society 146, 2300–2312.

Sinno, T., Dornberger, E., von Ammon, W., Brown, R., Dupret, F., 2000. Defect engineering of Czochralski single-crystal silicon. Materials Science and Engineering: R: Reports 28, 149 – 198.

Winkler, J., Neubert, M., Rudolph, J., 2010a. Nonlinear model-based control of the Czochralski process I: motivation, modeling and feedback controller design. Journal of Crystal Growth 312, 1005–1018.

Winkler, J., Neubert, M., Rudolph, J., 2010b. Nonlinear model-based control of the Czochralski process II: reconstruction of crystal radius and growth rate from the weighing signal. Journal of Crystal Growth 312, 1019–1028.

Winkler, J., Neubert, M., Rudolph, J., 2013. A review of the automation of the czochralski process. Acta Physica Polonica A: Special Anniversary Issues: Professor Jan Czochralski 124, 181–192.

Chapter 5

Conclusions and Future work

5.1 Conclusions

In time-varying processes, a reliable way of control and estimation is to utilize the time-varying effects within regulation and estimation synthesis. In particular, in spatially distributed parameter systems with moving domain, knowing the states evolution during entire processing time, provides a foundation for optimal control/estimation strategies. Namely, once the trajectory optimization is performed to determine a optimal trajectory for the process, the model predictive control is utilized as tracking control strategy to maintain the actual trajectory as close as possible to the optimal desired trajectory.

Trajectory optimization for the time-varying nonlinear and distributed parameter systems usually results in a complex optimization problem. The optimization problem is formulated in a quadratic/nonlinear programming framework by discretizing the process model and considering the whole process dynamic as equality constraints. In order to solve the optimization problem, interior-point optimization method is used by IPOPT software and MATLAB for microalgae bioreactor and Czochralski crystallization process, respectively.

State estimation is provided for both processes. For microalgae bioreactor, moving horizon estimator is used to estimated nitrogen concentration, this estimation along with other measurable state are used for model predictive control implementation. In Czochralski crystal growth process, a distributed parameter observer is developed to reconstruct the spatial temperature distribution over the crystal domain. The computational framework of Galerkin's method is utilized for model reduction and few dominant modes are estimated using Luenberger observer to reconstruct the temperature distribution.

In batch processes, different initial conditions, different disturbances and measurement noises can affect the product quality of different runs of a batch process. Introducing a reference trajectory along with a trajectory tracking control can minimize this effects and provide a reliable operation performance for different batch runs. The reference trajectory optimized for maximum lipid production is used for tracking MPC for microalgae bioreactor and it is shown that the controller performs with high efficiency in presence of the noises. For the Czochralski crystal growth process, the trajectory optimized in order to maintain the thermally induced stresses below the critical value. The performance of the controller is examined by implementing on a high fidelity finite element model of the process.

5.2 Future Work

The mathematical model of lipid production in the microalgae bioreactor is an experimentally identified model. The model parameters are identified using experimental data which is performed for a certain range. The results provided for optimization and control of microalgae bioreactor could be experimentally validated. The obtained

results from the experiment then can be used for tuning the parameters in the model to obtain a more accurate model for the range of data collected. Repeating this procedure will result in more reliable model as well as experimentally validated reference trajectory.

In Chapter 4, a controller is developed for Cz process. The model predictive temperature tracking controller is a full state feedback controller, however, in realistic implementation of the controller, the temperature distribution is not measurable and only few measurements can be realized. It is of practical value to combine and evaluate the observer and controller that is suggested in Chapters 3-4 and construct a output feedback controller.

As it is stated, a simplified model of the Czochralski process used in this work. For example, the dynamic of heat transfer by radiation is neglected and considered as the input to the system, the boundary conditions are simplified to no flux boundary conditions and the model is constructed by axisymmetric assumption. In order to have a more realistic model, these assumptions (or some of them) can be relaxed and the controller performance can be examined in presence of these more realistic conditions.

Bibliography

Abdollahi, J., Dubljevic, S., 2012. Lipid production optimization and optimal control of heterotrophic microalgae fed-batch bioreactor. Chemical Engineering Sciencel 84, 619–627.

Abdollahi, J., Dubljevic, S., 2013. Crystal radius and temperature regulation in czochralski crystallization process, in: American Control Conference (ACC), pp. 1626–1632.

Abdollahi, J., Izadi, M., Dubljevic, S., 2014. Temperature distribution reconstruction in czochralski crystal growth process. AIChE Journal DOI 10.1002/aic.14486.

Alcaraz-Gonzlez, V., Salazar-Pea, R., Gonzlez-lvarez, V., Gouz, J., Steyer, J., 2005. A tunable multivariable nonlinear robust observer for biological systems. Comptes Rendus - Biologies 328, 317–325.

Alvarez-Vzquez, L.J., Fernndez, F.J., Martnez, A., 2010. Optimal management of a bioreactor for eutrophicated water treatment: A numerical approach. Journal of Scientific Computing 43, 67–91.

Armaou, A., Christofides, P., 2001a. Crystal temperature control in Czochralski crystal growth process. AIChE Journal 47, 79–106.

Armaou, A., Christofides, P.D., 2001b. Robust control of parabolic PDE systems with time-dependent spatial domains. Automatica 37, 61–69.

Balas, M.J., 1986. Finite-dimensional control of distributed parameter systems by Galerkin approximation of infinite dimensional controllers. Journal of Mathematical Analysis and Applications 114, 17–36.

Bastin, G., Dochain, D., 1990. On-line estimation and adaptive control of bioreactors. Process measurement and control, Elsevier.

Bensoussan, A., Prato, G., Delfour, M., Mitter, S., 2007. Representation and Control of Infnite Dimensional Systems. Springer.

Biegler, L., 2010. Nonlinear Programming: Concepts, Algorithms, and Applications to Chemical Processes. Mos-siam Series on Optimization, Society for Industrial and Applied Mathematics.

Brown, R., 1988. Theory of transport processes in single crystal growth from the melt. AIChE Journal 34, 881–911.

Cao, J., Gao, Y., Chen, Y., Zhang, G., Qiu, M., 2011. Simulation aided hot zone design for faster growth of CZ silicon mono crystals. Rare Metals 30, 155–159.

Chen, T., Wu, H., Weng, C.I., 1997. The effect of interface shape on anisotropic thermal stress of bulk single crystal during czochralski growth. Journal of Crystal Growth 173, 367–379.

Chen, X., Nakano, S., Liu, L., Kakimoto, K., 2008. Study on thermal stress in a silicon ingot during a unidirectional solidification process. Journal of Crystal Growth 310, 4330 – 4335.

Chisti, Y., 2007. Biodiesel from microalgae. Biotechnology Advances 25, 294–306.

Curtain, R.F., Zwart, H., 1995. An Introduction to Infinite-Dimensional Linear Systems Theory, Texts In Applied Mathematics. Springer.

De la Hoz Siegler, H., Ben-Zvi, A., Burrell, R.E., Mccaffrey, W.C., 2011. The dynamics of heterotrophic algal cultures. Bioresource technology 102, 5764–5774.

De la Hoz Siegler, H., McCaffrey, W.C., Burrell, R.E., Ben-Zvi, A., 2012. Optimization of microalgal productivity using an adaptive, non-linear model based strategy. Bioresource technology 104, 537–546.

Demina, S., Kalaev, V., 2011. 3D unsteady computer modeling of industrial scale Ky and Cz sapphire crystal growth. Journal of Crystal Growth 320, 23–27.

Derby, J., Atherton, L., Gresho, P., 1989. An integrated process model for the growth of oxide crystals by the czochralski method. Journal of Crystal Growth 97, 792 – 826.

Derby, J., Atherton, L., Thomas, P., Brown, R., 1987. Finite-element methods for analysis of the dynamics and control of czochralski crystal growth. Journal of Scientific Computing 2, 297–343.

Derby, J., Brown, R., 1986a. Thermal-capillary analysis of Czochralski and liquid encapsulated Czochralski crystal growth: I. simulation. Journal of Crystal Growth 74, 605–624.

Derby, J., Brown, R., 1986b. Thermal-capillary analysis of Czochralski and liquid encapsulated Czochralski crystal growth: II. processing strategies. Journal of Crystal Growth 75, 227–240.

Derby, J., Brown, R., 1987. On the dynamics of Czochralski crystal growth. Journal of Crystal Growth 83, 137–151.

Doucha, J., Lvansky, K., 2012. Production of high-density chlorella culture grown in fermenters. Journal of Applied Phycology 24, 35–43.

Duffar, T., 2010. Crystal Growth Processes Based on Capillarity: Czochralski, Floating Zone, Shaping and Crucible Techniques. John Wiley & Sons.

Dunbar, W.B., Petit, N., Rouchon, P., Martin, P., 2003. Boundary control for a nonlinear stefan problem, in: Proceedings of the 42nd IEEE Conference on Decision and Control, pp. 1309–1314.

El Bahja, H., Vega, P., Bakka, O., Mesquine, F., 2009. Non linear gpc of a nutrient removal biological plant, in: ETFA 2009 - 2009 IEEE Conference on Emerging Technologies and Factory Automation.

Estrada, V., Parodi, E.R., Diaz, M.S., 2009. Addressing the control problem of algae growth in water reservoirs with advanced dynamic optimization approaches. Computers and Chemical Engineering 33, 2063–2074.

Fainberg, J., Leister, H.J., 1996. Finite volume multigrid solver for thermo-elastic stress analysis in anisotropic materials. Computer Methods in Applied Mechanics and Engineering 137, 167 – 174.

Fang, H., Qiu, S., Zheng, L., Schaffers, K., Tassano, J., Caird, J., Zhang, H., 2008. Optimization of the cooling profile to achieve crack-free Yb:S-FAP crystals. Journal of Crystal Growth 310, 3825 – 3832.

Fard, M.P., Sagatun, S.I., 2001. Exponential stabilization of a transversely vibrating beam by boundary control via lyapunovs direct method. Journal of Dynamic Systems, Measurement and Control 123, 195–200.

Farza, M., Busawon, K., Hammouri, H., 1998. Simple nonlinear observers for on-line estimation of kinetic rates in bioreactors. Automatica 34, 301–318.

Farza, M., Hammouri, H., Othman, S., Busawon, K., 1997. Nonlinear observers for parameter estimation in bioprocesses. Chemical Engineering Science 52, 4251–4267.

Gevelber, M., 1994a. Dynamics and control of the Czochralski process III. interface dynamics and control requirements. Journal of Crystal Growth 139, 271–285.

Gevelber, M., 1994b. Dynamics and control of the Czochralski process IV. Control structure design for interface shape control and performance evaluation. Journal of Crystal Growth 139, 286–301.

Gevelber, M., Stephanopoulos, G., 1987. Dynamics and control of the Czochralski process. I. modelling and dynamic characterization. Journal of Crystal Growth 84, 647–668.

Gevelber, M., Stephanopoulos, G., Wargo, M., 1988. Dynamics and control of the Czochralski process II. objectives and control structure design. Journal of Crystal Growth 91, 199–217.

Gonzalez, J., Fernandez, G., Aguilar, R., Barron, M., Alvarez-Ramirez, J., 2001. Sliding mode observer-based control for a class of bioreactors. Chemical Engineering Journal 83, 25–32.

Gross, U., Kersten, R., 1972. Automatic crystal pulling with optical diameter control using a laser beam. Journal of Crystal Growth 14, 85–88.

Hagen, G., Mezic, I., 2003. Spillover stabilization in finite-dimensional control and observer design for dissipative evolution equations. SIAM Journal on Control and Optimization 42, 746–768.

Harkort, C., Deutscher, J., 2011. Finite-dimensional observer-based control of linear distributed parameter systems using cascaded output observers. International Journal of Control 84, 107–122.

Hoffert, M.I., Caldeira, K., Benford, G., Criswell, D.R., Green, C., Herzog, H., Jain, A.K., Kheshgi, H.S., Lackner, K.S., Lewis, J.S., Lightfoot, H.D., Manheimer, W., Mankins, J.C., Mauel, M.E., Perkins, L.J., Schlesinger, M.E., Volk, T., Wigley, T.M.L., 2002. Engineering: Advanced technology paths to global climate stability: Energy for a greenhouse planet. Science 298, 981–987.

Hsieh, C., Wu, W., 2009. Cultivation of microalgae for oil production with a cultivation strategy of urea limitation. Bioresource technology 100, 3921–3926.

Instrument Society of America, 1995. Batch control. Part 1, models and terminology. ISA, Research Triangle Park.

Irizarry-Rivera, R., Seider, W.D., 1997a. Model-predictive control of the Czochralski crystallization process. part I. conduction-dominated melt. Journal of Crystal Growth 178, 593 – 611.

Irizarry-Rivera, R., Seider, W.D., 1997b. Model-predictive control of the Czochralski crystallization process. part I. conduction-dominated melt. Journal of Crystal Growth 178, 593 – 611.

Irizarry-Rivera, R., Seider, W.D., 1997c. Model-predictive control of the czochralski crystallization process. part ii. reduced-order convection model. Journal of Crystal Growth 178, 612 – 633.

Ito, K., 1990. Finite-dimensional compensators for innite-dimensional systems via Galerkin-type approximation. SIAM Journal of Control and Optimization 28, 1251–1269.

Izadi, M., Dubljevic, S., 2013. Order-reduction of parabolic PDEs with time-varying domain using empirical eigenfunctions. AIChE Journal DOI:10.1002/aic.14152.

Jordan, A., Caruso, R., von Neida, A., 1983. Analysis of the derivative weight-gain signal from measured crystal shape: implications for diameter control of GaAs. Bell System Technical Journal 62, 477–498.

Khan, S.A., Rashmi, Hussain, M.Z., Prasad, S., Banerjee, U.C., 2009. Prospects of biodiesel production from microalgae in India. Renewable and Sustainable Energy Reviews 13, 2361–2372.

Krstic, M., Smyshlyaev, A., 2008. Boundary Control of PDEs: A Course on Backstepping Designs. SIAM.

Lee, K., Lee, D., Park, J., Lee, M., 2005. MPC based feedforward trajectory for pulling speed tracking control in the commercial Czochralski crystallization process. International Journal of Control, Automation and Systems 3, 252–257.

Li, X., Xu, C., 2011. Infinite-dimensional Luenberger-like observers for a rotating body-beam system. Systems & Control Letters 60, 138–145.

Liu, W.J., Krstic, M., 2000. Backstepping boundary control of burgers' equation with actuator dynamics. Systems & Control Letters 41, 291–303.

Mailleret, L., Bernard, O., Steyer, J., 2004. Nonlinear adaptive control for bioreactors with unknown kinetics. Automatica 40, 1379–1385.

Muske, K.R., Rawlings, J.B., 1993a. Model predictive control with linear models. AIChE Journal 39, 262–287.

Muske, K.R., Rawlings, J.B., 1993b. Receding horizon recursive state estimation, in: American Control Conference, pp. 900–904.

Nadadoor, V.R., De la Hoz Siegler, H., Shah, S.L., McCaffrey, W.C., Ben-Zvi, A., 2012. Online sensor for monitoring a microalgal bioreactor system using support vector regression. Chemometrics and Intelligent Laboratory Systems 110, 38–48.

Neubert, M., Winkler, J., 2012. Nonlinear model-based control of the czochralski process III: Proper choice of manipulated variables and controller parameter scheduling. Journal of Crystal Growth 360, 3–11.

Ng, J., Aksikas, I., Dubljevic, S., 2011. Application of optimal boundary control to reaction-diffusion system with time-varying spatial domain, in: American Control Conference (ACC), 2011, pp. 2528–2533.

Ng, J., Aksikas, I., Dubljevic, S., 2013. Control of parabolic PDEs with time-varying spatial domain: Czochralski crystal growth process. International Journal of Control 86, 1467–1478.

Ng, J., Dubljevic, S., 2011. Optimal control of convection-diffusion process with time-varying spatial domain: Czochralski crystal growth. Journal of Process Control 21, 1361–1369.

Ng, J., Dubljevic, S., 2012. Optimal boundary control of a diffusion-convection-reaction PDE model with time-dependent spatial domain: Czochralski crystal growth process. Chemical Engineering Science 67, 111–119.

Patil, V., Tran, K., Giselrd, H.R., 2008. Towards sustainable production of biofuels from microalgae. International Journal of Molecular Sciences 9, 1188–1195.

Ray, W.H., 1981. Advanced process control. McGraw-Hill chemical engineering series, McGraw-Hill.

Reddy, J.N., 2004. An Introduction to Nonlinear Finite Element Analysis. Oxford University Press.

Rudolph, J., Winkler, J., Woittennek, F., . Flatness based approach to a heat conduction problem in a crystal growth process, in: Meurer, T., Graichen, K., Gilles, E.D. (Eds.), Control and Observer Design for Nonlinear Finite and Infinite Dimensional System. Springer Verlag, pp. 387–401. 2005.

Sackinger, P.A., Brown, R.A., Derby, J.J., 1989. A finite element method for analysis of fluid flow, heat transfer and free interfaces in czochralski crystal growth. International Journal for Numerical Methods in Fluids 9, 453–492.

Selisteanu, D., Petre, E., Rasvan, V.B., 2007. Sliding mode and adaptive sliding-mode control of a class of nonlinear bioprocesses. International Journal of Adaptive Control and Signal Processing 21, 795–822.

Sendrescu, D., Popescu, D., Petre, E., Bobasu, E., Selisteanu, D., 2011. Nonlinear model predictive control of a lipase production bioprocess, in: Proceedings of the 2011 12th International Carpathian Control Conference, ICCC'2011, pp. 337–341.

Sinno, T., Brown, R., 1999a. Modeling microdefect formation in Czochralski silicon. Journal of Electrochemical Society 146, 2300–2312.

Sinno, T., Brown, R., 1999b. Modeling microdefect formation in Czochralski silicon. Journal of Electrochemical Society 146, 2300–2312.

Sinno, T., Dornberger, E., von Ammon, W., Brown, R., Dupret, F., 2000. Defect engineering of Czochralski single-crystal silicon. Materials Science and Engineering: R: Reports 28, 149 – 198.

Szabo, G., 1985. Thermal strain during Czochralski crystal growth. Journal of Crystal Growth 73, 131–141.

Tebbani, S., Dumur, D., Hafidi, G., vande Wouwer, A., 2010. Nonlinear predictive control of fed-batch cultures of escherichia coli. Chemical Engineering and Technology 33, 1112–1124.

Thomas, P., Derby, J., Atherton, L., Brown, R., Wargo, M., 1989. Dynamics of liquid-encapsulated czochralski growth of gallium arsenide: Comparing model with experiment. Journal of Crystal Growth 96, 135 – 152.

Vries, D., Keesman, K.J., Zwart, H., 2010. Luenberger boundary observer synthesis for Sturm-Liouville systems. International Journal of Control 83, 1504–1514.

Wachter, A., Biegler, L.T., 2000. Failure of global convergence for a class of interior point methods for nonlinear programming. Mathematical Programming 88, 565–574.

Wachter, A., Biegler, L.T., 2006. On the implementation of an interior-point filter line-search algorithm for large-scale nonlinear programming. Mathematical Programming 106, 25–57.